

# Mixing

The physical operation of mixing can determine the success of bioprocesses. In fermentations, single- and multiple-phase mixing occurs in fluids with a range of rheologies. Mixing controls the access of cells to dissolved nutrients and oxygen, and plays a critical role in controlling the culture temperature. The equipment used for mixing has a significant effect on agitation efficiency, power requirements, and operating costs. A consequence of mixing operations is the development of hydrodynamic forces in the fluid. These forces are responsible for important processes in fermenters such as bubble break-up and dispersion; however, cell damage can also occur and must be avoided. Problems with mixing are a major cause of productivity loss after commercial scale-up of bioprocesses.

This chapter draws on material introduced in Chapter 7 about fluid properties and flow behaviour. In turn, as mixing underpins effective heat and mass transfer in bioprocesses, this chapter provides the foundations for detailed treatment of these subjects in Chapters 9 and 10.

## 8.1 FUNCTIONS OF MIXING

Mixing is a physical operation that reduces nonuniformities in fluid by eliminating gradients of concentration, temperature, and other properties. Mixing is accomplished by interchanging material between different locations to produce a mingling of components. If a system is perfectly mixed, there is a random, homogeneous distribution of system properties. Mixing is used in bioprocesses to:

- Blend soluble components of liquid media such as sugars
- Disperse gases such as air through liquids in the form of small bubbles
- Maintain suspension of solid particles such as cells and cell aggregates
- Where necessary, disperse immiscible liquids to form an emulsion or suspension of fine droplets
- Promote heat transfer to or from liquids

Mixing is one of the most important operations in bioprocessing. To create an optimal environment for cell culture, bioreactors must provide the cells with access to all

substrates, including oxygen in aerobic cultures. It is not enough to just fill the fermenter with nutrient-rich medium; unless the culture is mixed, zones of nutrient depletion will develop as the cells rapidly consume the materials they need within their local environment. This problem is heightened if mixing does not maintain a uniform suspension of biomass; substrate concentrations can quickly drop to zero within layers of settled cells. We rely on good mixing to distribute any material added during the fermentation, such as fresh medium to feed the cells or concentrated acid or alkali to control the culture pH. If these materials are not mixed rapidly throughout the reactor, their concentration can build up to toxic levels near the feed point with deleterious consequences for the cells in that region. Another important function of mixing is heat transfer. Bioreactors must be capable of transferring heat to or from the broth rapidly enough so that the desired temperature is maintained. Cooling water is used to take up excess heat from fermentations; the rate of heat transfer from the broth to the cooling water depends on mixing conditions.

Mixing can be achieved in many different ways. In this chapter we will concentrate on the most common mixing technique in bioprocessing: mechanical agitation using an impeller.

## 8.2 MIXING EQUIPMENT

Mixing is carried out most often in cylindrical stirred tanks, such as that shown in [Figure 8.1](#). *Baffles*, which are vertical strips of metal mounted against the wall of the tank, are installed to reduce gross vortexing and swirling of the liquid. Mixing is achieved using an *impeller* mounted on a centrally located *stirrer shaft*. The stirrer shaft is driven rapidly by the *stirrer motor*; the effect of the rotating impeller is to pump the liquid and create a regular flow pattern. Liquid is forced away from the impeller, circulates through the vessel, and periodically returns to the impeller region. In gassed stirred tanks such as bioreactors used for aerobic culture, gas is introduced into the vessel by means of a *sparger* located beneath the impeller.

The equipment chosen for mixing operations exerts a significant influence on the outcome of the process. Aspects of this equipment are outlined in the following sections. The operating characteristics of different impellers are described in detail in [Section 8.4](#).

### 8.2.1 Vessel Geometry and Liquid Height

The shape of the base of stirred tanks affects the efficiency of mixing. Several base shapes are shown in [Figure 8.2](#). If possible, the base should be rounded at the edges rather than flat; this eliminates sharp corners and pockets into which fluid currents may not penetrate, and discourages the formation of stagnant zones. The energy required to suspend solids in stirred tanks is sensitive to the shape of the vessel base: depending on the type of impeller and the flow pattern generated, the modified geometries shown in [Figure 8.2\(b\) through \(e\)](#) can be used to enhance particle suspension compared with the flat-bottom tank of [Figure 8.2\(a\)](#). In contrast, sloping sides or a conical base such as that shown in

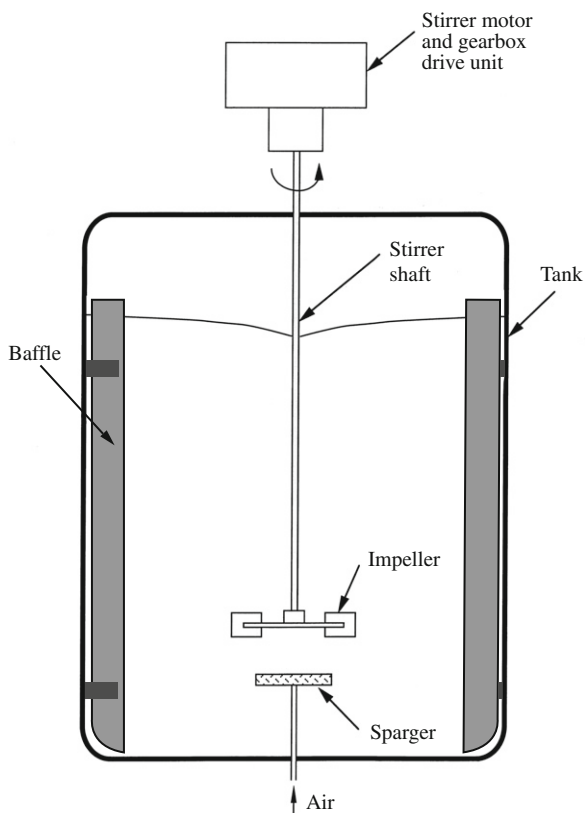


**FIGURE 8.1** Typical configuration of a stirred tank.

Figure 8.2(f) promotes settling of solids and should be avoided if solids suspension is required.

Other geometric specifications for stirred tanks are shown in Figure 8.3. For efficient mixing with a single impeller of diameter  $D_i$  equal to a 1/4 to 1/2 the tank diameter  $D_T$ , the height of liquid in the tank  $H_L$  should be no more than 1.0 to 1.25  $D_T$ . Because the intensity of mixing decreases quickly as fluid moves away from the impeller zone, large volumes of liquid in the upper parts of the vessel distant from the impeller are difficult to mix and should be avoided.

Another aspect of vessel geometry influencing mixing efficiency is the clearance  $C_i$  between the impeller and the lowest point of the tank floor (Figure 8.3). This clearance affects solids suspension, gas bubble dispersion, and hydrodynamic stability. In most practical stirring operations,  $C_i$  is within the range 1/6 to 1/2 the tank diameter.

### 8.2.2 Baffles

Baffles are standard equipment in stirred tanks. They assist mixing and create turbulence in the fluid by breaking up the circular flow generated by rotation of the impeller.

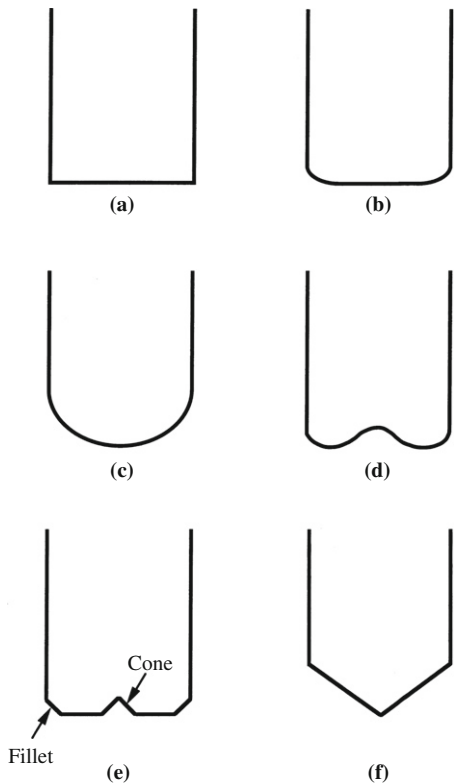


**FIGURE 8.2** Different profiles for the base of stirred vessels: (a) flat; (b) dished; (c) round; (d) contoured; (e) cone-and-fillet; (f) conical.

Baffles are attached to the inside vertical walls of the tank by means of welded brackets. Four equally spaced baffles are usually sufficient to prevent liquid swirling and vortex formation. The optimum baffle width  $W_{BF}$  depends on the impeller design and fluid viscosity, but is of the order 1/10 to 1/12 the tank diameter. For clean, low-viscosity liquids, baffles are attached perpendicular to the wall as illustrated in Figure 8.4(a). Alternatively, as shown in Figures 8.4(b) and (c), baffles may be mounted away from the wall with clearance  $C_{BF} \approx 1/50 D_T$ , or set at an angle. These arrangements prevent the development of stagnant zones and sedimentation along the inner edge of the baffle during mixing of viscous fluids or fluids containing suspended cells or particles.

### 8.2.3 Sparger

There exists a large variety of sparger designs. These include simple open pipes, perforated tubes, porous diffusers, and complex two-phase injector devices. *Point spargers*, such as open pipe spargers, release bubbles at only one location in the vessel. Other sparger designs such as *ring spargers* have multiple gas outlets so that bubbles are released simultaneously from various locations. Bubbles leaving the sparger usually fall within a relatively narrow size range depending on the sparger type. However, as the bubbles rise

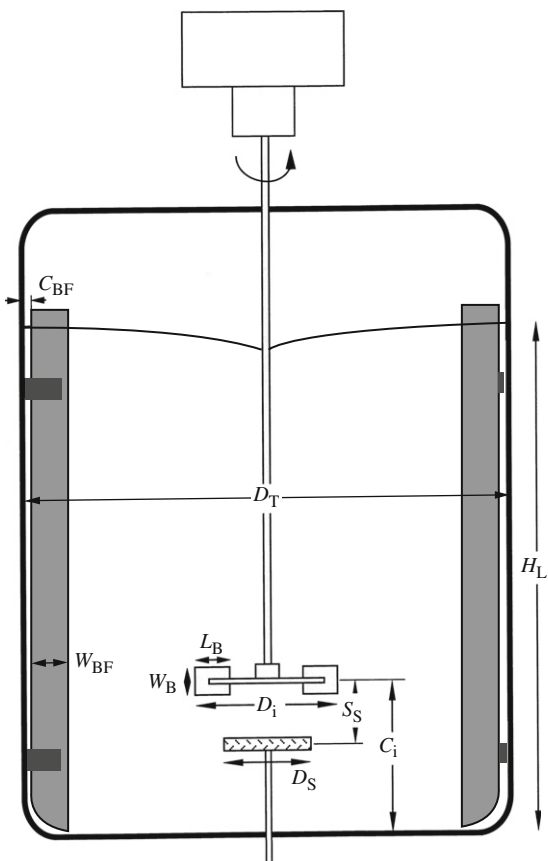


FIGURE 8.3 Some geometric specifications for a stirred tank.

$C_{BF}$  = baffle clearance  
 $C_i$  = impeller clearance  
 $D_i$  = impeller diameter  
 $D_S$  = sparger diameter  
 $D_T$  = tank diameter  
 $H_L$  = liquid height  
 $L_B$  = blade length  
 $S_S$  = sparger separation  
 $W_B$  = blade width  
 $W_{BF}$  = baffle width

from the sparger into the impeller zone, they are subjected to very high shear forces from operation of the stirrer that cause bubble break-up. The resulting small bubbles are flung out by the impeller into the bulk liquid for dispersion throughout the vessel. Although the type of sparger used has a relatively minor influence on the mixing process in most stirred tanks, the diameter  $D_S$  of large ring spargers and the separation  $S_S$  between the sparger and impeller (Figure 8.3) can have an important influence on the efficiency of gas dispersion.

#### 8.2.4 Stirrer Shaft

The primary function of the stirrer shaft is to transmit *torque* from the stirrer motor to the impeller. Torque is the tendency of a force to cause an object to rotate. The magnitude

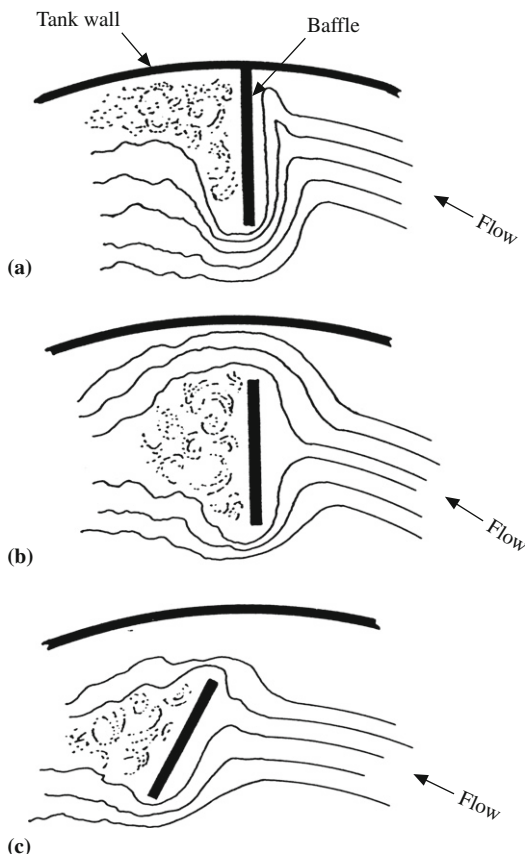


**FIGURE 8.4** Baffle arrangements: (a) baffles attached to the wall for low-viscosity liquids; (b) baffles set away from the wall for moderate-viscosity liquids; (c) baffles set away from the wall and at an angle for high-viscosity liquids.

From F.A. Holland and F.S. Chapman, 1966, Liquid Mixing and Processing in Stirred Tanks, Reinhold, New York.

of the torque around the shaft axis is related to the power required for operation of the impeller. The stirrer shaft also performs other mechanical functions: it resists the bending forces created by the impeller, it limits any lateral deflections, and it supports the impeller weight. These functions must all be achieved without excessive vibration.

In typical mixing operations, the impeller is attached to a vertical stirrer shaft that passes from the motor through the top of the vessel. However, when headplate access is at a premium because of other devices and instruments located on top of the tank, or if a shorter shaft is required to alleviate mechanical stresses (e.g., when mixing viscous fluids), the stirrer shaft may be designed to enter through the base of the vessel. The vessel configuration for a bottom-entering stirrer is shown in Figure 8.5. The main disadvantage of bottom-entering stirrers is the increased risk of fluid leaks due to failure or wear of the seals between the rotating stirrer shaft and the vessel floor.

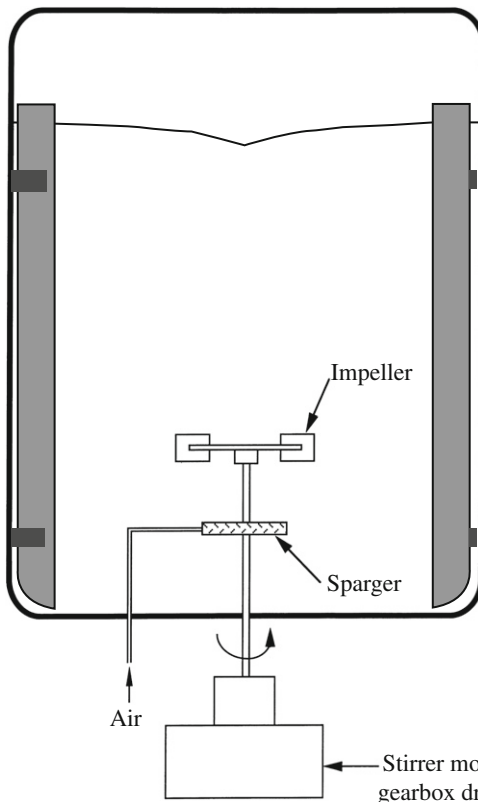
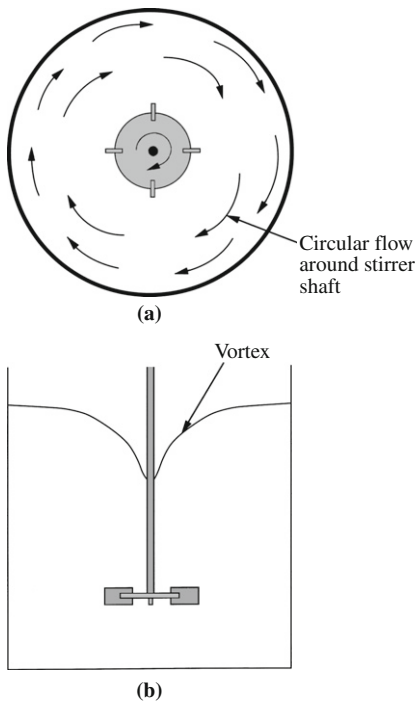


FIGURE 8.5 Stirred tank configuration for a bottom-entry stirrer.

### 8.3 FLOW PATTERNS IN STIRRED TANKS

The liquid flow pattern established in stirred tanks depends on the impeller design, the size and geometry of the vessel, and the properties of the fluid. There are three directional elements to the flow: *rotational flow* (i.e., around the stirrer shaft), *radial flow* (i.e., from the central axis out to the sides of the tank and back again), and *axial flow* (i.e., up and down the height of the vessel). An effective mixer will cause motion in all three directions; however, radial and axial flows generated at the impeller are primarily responsible for bulk mixing. Impellers are broadly classified as *radial-flow impellers* or *axial-flow impellers* depending on the direction of the flow leaving the impeller; some impellers have both radial- and axial-flow characteristics. When gas is sparged into the tank, two-phase flow patterns are created. The characteristics of this flow depend mainly on the stirrer speed, the gas flow rate, and the fluid properties.



**FIGURE 8.6** (a) Circular flow in an unbaffled stirred tank viewed from above. (b) Vortex formation during circular flow.

### 8.3.1 Rotational Flow

Because stirring is rotational in action, all impellers generate circular flow of liquid around the stirrer shaft as illustrated in Figure 8.6(a). However, simple rotational flow is disadvantageous for mixing and should be avoided as much as possible. In circular flow, liquid moves in a streamline fashion and there is little top-to-bottom mixing between different heights in the vessel. Circular flow also leads to vortex development as shown in Figure 8.6(b). At high impeller speeds, the vortex may reach down to the impeller so that gas from the surrounding atmosphere is drawn into the liquid. This is undesirable as it produces very high mechanical stresses in the stirrer shaft, bearings, and seals. Attenuating circular flow has a high priority in design of mixing systems. It is usually minimised by installing baffles to interrupt the rotational flow pattern and create turbulence in the fluid.

### 8.3.2 Radial Flow

Radial or horizontal flow is generated by impellers with blades aligned parallel to the stirrer shaft. A typical liquid circulation pattern set up by a high-speed radial-flow impeller is shown in Figure 8.7. Liquid is driven radially from the impeller towards the walls of the tank where it divides into two streams, one flowing up to the top of the tank and the other flowing down to the bottom. These streams eventually reach the central axis of the tank and are drawn back to the impeller. Radial-flow impellers also set up circular flow that must be reduced by baffles.

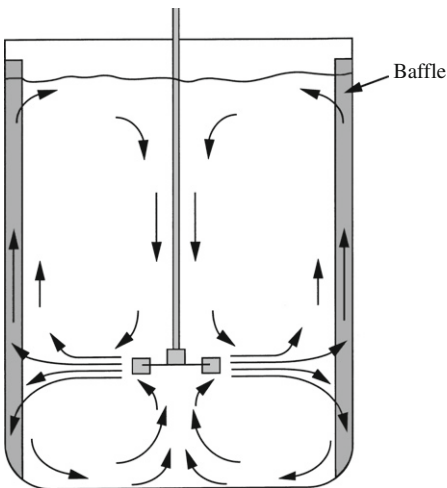


**FIGURE 8.7** Flow pattern produced by a radial-flow impeller in a baffled tank.

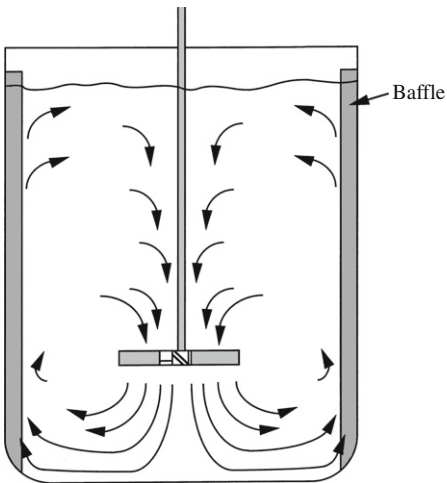


**FIGURE 8.8** Flow pattern produced by an axial-flow impeller in a baffled tank.

### 8.3.3 Axial Flow

Axial flow is necessary for top-to-bottom mixing in stirred tanks. Axial flow is generated by impellers with inclined or pitched blades that make an angle of less than  $90^\circ$  with the plane of rotation. Axial flow is particularly useful when strong vertical currents are required. For example, if the fluid contains solids, a strong downward flow of liquid leaving the impeller will discourage settling at the bottom of the tank. The type of flow pattern set up by a typical axial-flow impeller is illustrated in [Figure 8.8](#). Fluid leaving the impeller is driven at a downward angle until it is deflected from the floor of the vessel. It then spreads out over the floor and flows up along the walls before being drawn back to the impeller. As rotational flow is also generated by axial-flow impellers, baffles are required.

Axial-flow impellers are most commonly operated to generate downward flow of fluid leaving the impeller blades, as illustrated in [Figure 8.8](#). However, if the direction of impeller rotation is reversed, axial-flow impellers may be applied for upward pumping, but this mode of operation is not often used.

### 8.3.4 Gas Flow Patterns

Sparging stirred tanks with gas creates two-phase flow patterns of bubbles in liquid. Different bubble distributions develop depending on the relative rates of gas flow and stirring. At high gassing rates or low stirrer speeds, the impeller is surrounded by gas and is unable to pump effectively, indicating that the gas-handling capacity of the impeller has been exceeded. This condition is called *impeller flooding*. Flooding should be avoided because an impeller blanketed by gas no longer contacts the liquid properly, resulting in poor mixing and gas dispersion. As the stirrer speed is increased or the gas flow rate reduced, the impeller blades start to process the gas and bubbles are dispersed towards the walls of the tank. This condition is known as *impeller loading*. At even higher stirrer speeds or lower gas flow rates, *complete gas dispersion* is achieved below as well as above the impeller. Complete gas dispersion with homogeneous distribution of gas to all parts of the vessel is the desirable operating condition.

As the stirrer speed is raised above that required to prevent impeller flooding, *gas recirculation* occurs. As well as rising upwards from the sparger to the liquid surface, gas bubbles are increasingly recirculated around the tank via the impeller. The extent of gas recirculation depends on the type of impeller and the stirrer speed, but can become very high. Under these conditions, the total flow rate of gas entering the impeller region at any given time is significantly greater than that supplied directly from the sparger.

Different impellers vary considerably in their ability to handle high gas flow rates without flooding. A parameter giving a rough indication of the tendency of impellers to flood is the impeller *solidity ratio*. The solidity ratio is equal to the projected blade area divided by the area of the circle swept out by the impeller during rotation. This is illustrated in [Figure 8.9](#) for an axial-flow impeller with a relatively low solidity ratio. Impellers with low

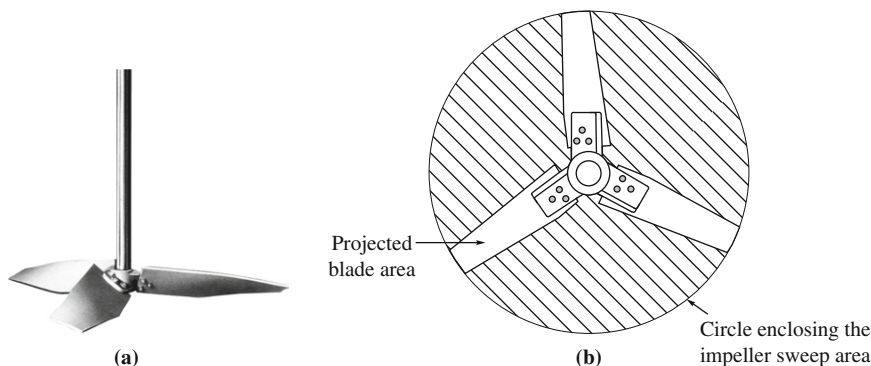


**FIGURE 8.9** Illustration of the solidity ratio for an axial-flow impeller.

- (a) Low-solidity-ratio Lightnin A310 hydrofoil impeller. *Photograph provided courtesy of Lightnin Mixers, Australia.*
- (b) Diagram showing the projected blade area and impeller sweep area. *Adapted from J.Y. Oldshue, 1989, Fluid mixing in 1989. Chem. Eng. Prog. 85(5), 33–42.*

solidity ratio tend to flood at lower gas velocities than impellers with high solidity ratio operated at the same stirrer speed. Impellers with solidity ratios greater than 90% have been developed for improved gas handling.

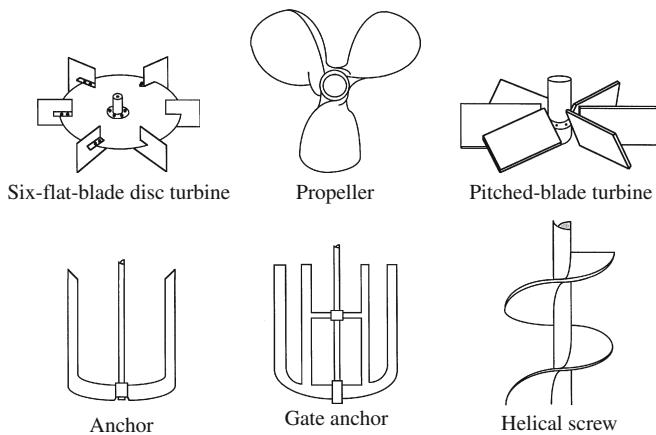
## 8.4 IMPELLERS

Many different types of impeller are available for mixing applications. A small selection is illustrated in [Figure 8.10](#). The choice of impeller depends on several factors, including the liquid viscosity, the need for turbulent shear flows (e.g., for bubble break-up and gas dispersion), and whether strong liquid currents are required. The recommended viscosity ranges for a number of common impellers are indicated in [Figure 8.11](#). Impellers can also be classified broadly depending on whether they produce high levels of turbulence, or whether they have a strong pumping capacity for generation of large-scale flow currents. Both functions are required for good mixing but they usually do not work together. The characteristics of several impellers in terms of their turbulence- and flow-generating properties are indicated in [Figure 8.12](#).

Typically, mixing in fermenters is carried out using *turbines* or *propellers*. These impellers are described in detail in [Sections 8.4.1 through 8.4.4](#). Turbines and propellers are *remote-clearance impellers*; this means they have diameters of 1/4 to 2/3 the tank diameter, thus allowing considerable clearance between the rotating impeller and the vessel walls. They are operated at relatively high speeds to generate impeller tip velocities of the order of  $3 \text{ m s}^{-1}$ . As indicated in [Figure 8.11](#), turbines and propellers are recommended for mixing liquids with viscosities between 1 and about  $10^4$  centipoise, which includes most fermentation broths. From [Figure 8.12](#), compared with the broad variety of other stirring devices available, turbines and propellers generate moderate-to-high levels of turbulence while retaining significant pumping capacity.

When remote-clearance agitators are applied in low-viscosity fluids, a turbulent region of high shear and rapid mixing is generated near the impeller. This high-shear region is responsible for bubble break-up in sparged systems. Because the mixing process should

**FIGURE 8.10** Selected impeller designs.



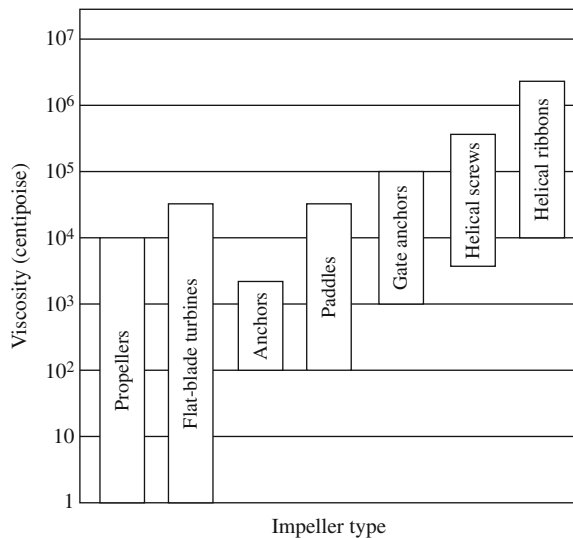


FIGURE 8.11 Viscosity ranges for different impellers.

From F.A. Holland and F.S. Chapman, 1966, Liquid Mixing and Processing in Stirred Tanks, Reinhold, New York.

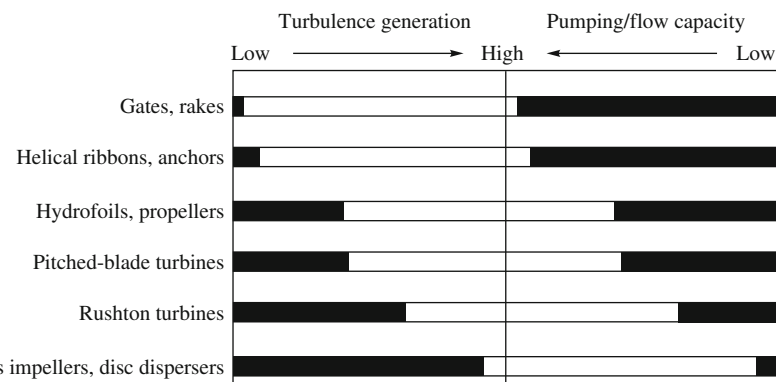


FIGURE 8.12 Characteristics of different impellers for generation of turbulence and liquid pumping.

involve fluid from all parts of the vessel, the impeller must also generate circulatory currents with sufficient velocity to carry material from the impeller to the furthermost regions of the tank and back again. In viscous fluids, it is often impossible for mechanical or economic reasons to rotate the impeller fast enough to generate turbulence; instead, impellers for viscous mixing are designed to provide maximum bulk movement or turnover of material. As indicated in Figures 8.11 and 8.12, impellers with high flow capacity suitable for mixing high-viscosity fluids include *gate*, *anchor*, and *helical stirrers*. Examples of these impellers are shown in Figure 8.10. All are large agitators installed with small wall clearance (around 1%–5% of the tank diameter) and operated at low stirrer speeds (5–20 rpm) to generate bulk fluid currents. For viscous fluids or when high shear rates must be avoided, slow-speed, low-turbulence, high-flow impellers are preferred to

high-speed, high-turbulence, low-flow impellers. Although gate, anchor, and helical stirrers are not often applied for mixing in bioreactors because they do not disperse air bubbles adequately for oxygen supply to the cells, they may be used for other applications in bioprocessing such as blending viscous slurries, pastes, or gums.

Several impellers used in industrial fermentations are described in the following sections.

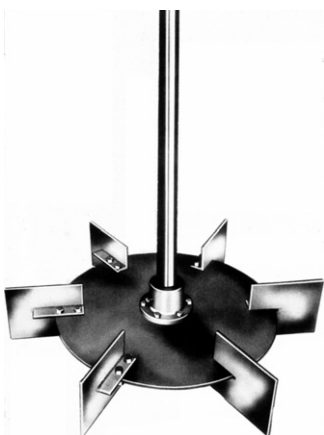
#### 8.4.1 Rushton Turbine

The most frequently used impeller in the fermentation industry is the six-flat-blade disc-mounted turbine shown in [Figures 8.10](#) and [8.13](#). This impeller is also known as the *Rushton turbine*. The Rushton turbine has been the impeller of choice for fermentations since the 1950s, largely because it has been well studied and characterised, and because it is very effective for gas dispersion. Although Rushton turbines of diameter one-third the tank diameter have long been used as standard hardware for aerobic fermentations, in recent years it has been recognised that larger impellers of size up to one-half the tank diameter provide considerable benefits for improved mixing and gas distribution.

##### **Without Gassing**

A typical mean velocity vector plot for a Rushton turbine is shown in [Figure 8.14](#). In velocity vector plots, the length and direction of the arrows indicate the magnitude and direction of the velocities at discrete locations in the fluid. The velocities in [Figure 8.14](#) were measured using laser Doppler velocimetry—see Section 7.9.3 (Laser Doppler Velocimetry subsection). [Figure 8.14](#) represents the mean liquid flow pattern; as described in Section 7.9.1 (Mean and Fluctuating Velocities subsection), turbulent flow in agitated tanks is characterised by highly chaotic secondary fluid motion and fluctuating velocity fields that disappear when instantaneous flow velocities are averaged over time.

FIGURE 8.13 Rushton turbine.



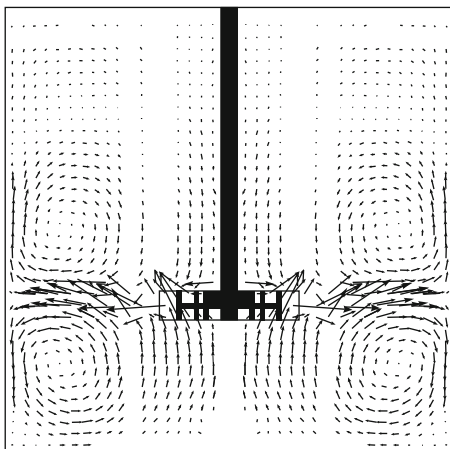


**FIGURE 8.14** Typical mean velocity vector plot for a Rushton turbine. The velocities were measured using laser Doppler velocimetry.

Adapted from M. Schäfer, M. Höfken, and F. Durst, 1997, Detailed LDV measurements for visualization of the flow field within a stirred-tank reactor equipped with a Rushton turbine. Trans. IChemE 75A, 729–736.

As indicated in Figure 8.14, the Rushton turbine is a radial-flow impeller. It generates a jet of high-speed flow directed radially outwards from the impeller; this jet entrains the surrounding fluid to form the impeller discharge stream. The discharge stream slows down as it approaches the tank wall and splits into two sections to create upper and lower circulatory flows. These circulatory currents traverse the remainder of the tank before returning directly to the impeller or becoming entrained again in the impeller outflow. The bulk flow in the vessel therefore comprises two large ring vortices, one above and one below the impeller. For impeller off-bottom clearances of less than one-half the liquid height, liquid velocities in the lower ring vortex are somewhat stronger than those in the upper circulatory stream, which traverses a greater distance into the upper reaches of the vessel during each circuit. Under these conditions, the return axial flow from beneath the impeller can be sufficiently strong to affect the radial discharge pattern, with the result that the outflow issuing from the impeller blades can be inclined slightly upwards instead of purely horizontal, as illustrated in Figure 8.14.

Compared with other types of turbine, Rushton impellers have a low pumping or circulatory capacity per unit power consumed. This is due mainly to a relatively high power requirement, as described in Section 8.5.1. The pumping capacity of impellers is discussed further in Section 8.7.

Operation of the Rushton turbine is characterised by the formation of *two high-speed roll and trailing vortices* in the liquid behind the horizontal edges of each flat blade of the impeller, as shown in Figure 8.15. These vortices play a critical role in determining the performance of the impeller. Most of the mixing in stirred vessels takes place near the vortices issuing from the impeller blades. As discussed further in the next section, the trailing vortex system is responsible for gas dispersion in aerated vessels. It is also the most important flow mechanism for turbulence generation. Steep velocity gradients are associated with trailing vortices; however, as the vortices move out from the blades they lose their identities and break down, thus providing a major source of turbulence in the fluid. The formation of trailing vortices affects the distribution of power dissipation in stirred tanks, which has consequences for phenomena such as cell damage in bioreactors. Fluid entrained by the vortices comprises much of the radial discharge stream generated by Rushton turbines.

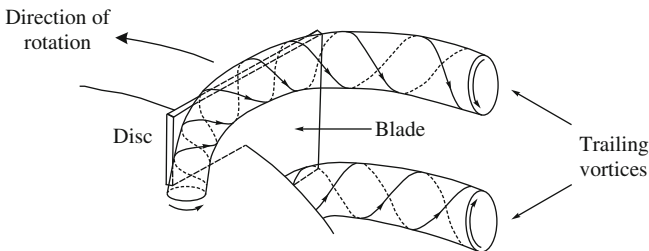


**FIGURE 8.15** Roll and trailing vortices generated behind the blade of a Rushton turbine.

From K. van't Riet and J.M. Smith, 1975, *The trailing vortex system produced by Rushton turbine agitators*. Chem. Eng. Sci. 30, 1093–1105.

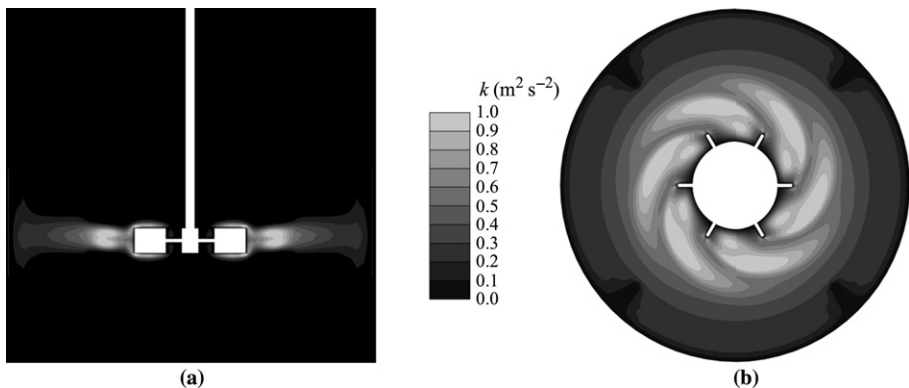


**FIGURE 8.16** Distribution of  $k$ , the turbulence kinetic energy per unit mass of fluid, in a tank stirred by a Rushton turbine. The data were determined using computational fluid dynamics (CFD) modelling. (a) Distribution of  $k$  in the vertical plane; (b) distribution of  $k$  in the horizontal plane at impeller height, with the impeller rotating clockwise.

Adapted from K. Ng, N.J. Fentiman, K.C. Lee, and M. Yianneskis, 1998, *Assessment of sliding mesh CFD predictions and LDA measurements of the flow in a tank stirred by a Rushton impeller*. Trans. IChemE 76A, 737–747. Images provided courtesy of M. Yianneskis, King's College, London.

Even if the impeller Reynolds number  $Re_i$  (Section 7.2.3) is high, indicating that flow is in the turbulent regime, the turbulence intensity in stirred vessels is far from uniform or randomly distributed. Figure 8.16 shows the distribution of turbulence kinetic energy per unit mass of fluid,  $k$  (Section 7.9.2, Turbulence Kinetic Energy subsection), in the vertical and horizontal planes of a tank stirred with a Rushton turbine. As illustrated in Figure 8.16(a), the highest values of  $k$  occur in the outwardly flowing liquid jet leaving the impeller blades: in this zone,  $k$  is at least an order of magnitude greater than in the remainder of the vessel. Figure 8.16(b) shows the turbulence kinetic energy distribution in the horizontal plane of the tank at the height of the impeller. The six plumes of elevated kinetic energy stretching out from the blades identify the trailing vortices generated by the impeller and indicate the extent of their radial spread. The vortices and associated turbulence dominate the horizontal plane of fluid near the impeller; however, these high levels of turbulence kinetic energy are not transmitted very far above or below the impeller, as indicated in Figure 8.16(a).

The distribution of the rate of dissipation of turbulence kinetic energy per unit mass,  $\varepsilon$  (Section 7.9.2, Rate of Dissipation of Turbulence Kinetic Energy subsection), in a tank

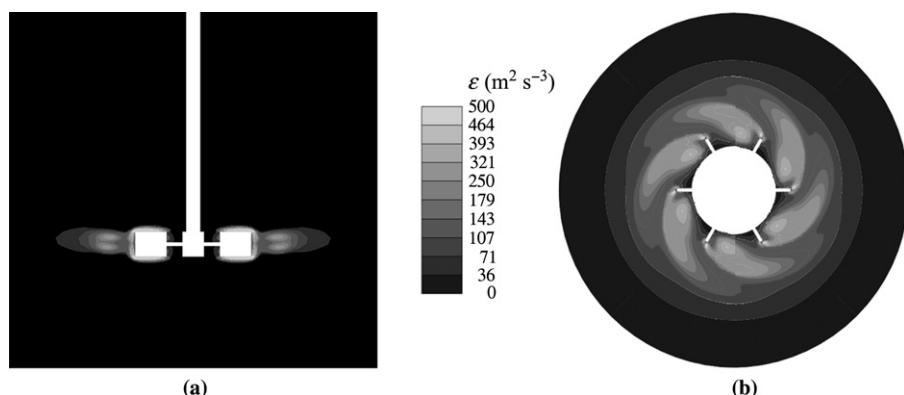


**FIGURE 8.17** Distribution of  $\varepsilon$ , the rate of dissipation of turbulence kinetic energy per unit mass, in a tank stirred by a Rushton turbine. The data were determined using computational fluid dynamics (CFD) modelling. (a) Distribution of  $\varepsilon$  in the vertical plane; (b) distribution of  $\varepsilon$  in the horizontal plane at impeller height, with the impeller rotating clockwise.

Adapted from K. Ng and M. Yianneskis, 2000, *Observations on the distribution of energy dissipation in stirred vessels*. Trans. IChemE 78A, 334–341. Images provided courtesy of M. Yianneskis, King's College, London.

stirred by a Rushton turbine is shown in Figure 8.17. The results are qualitatively similar to those for  $k$  in Figure 8.16. The values of  $\varepsilon$  are highest near the blades and in the region dominated by the trailing vortices; in most of the rest of the vessel,  $\varepsilon$  is 1 to 2 orders of magnitude lower. The intense turbulence generated by the trailing vortices is contained within a relatively small region and dissipates quickly away from the impeller.

### With Gassing

Rushton turbines are very effective for gas dispersion. To some extent, this can be attributed to the way the rotating disc on the turbine captures gas released below the impeller and channels it into the regions of high turbulence near the blades. Rushton turbines are often chosen for their gas-handling capacity, as they can be operated with relatively high gas flow rates without impeller flooding.

Typical gas flow patterns generated by a Rushton turbine in a low-viscosity fluid are shown in Figure 8.18. At high gassing rates or low stirrer speeds, the impeller is blanketed by gas, indicating impeller flooding. Under these conditions, as shown in Figure 8.18(a), the flow pattern is dominated by buoyant gas–liquid flow up the middle of the vessel. At higher stirrer speeds or lower gas flow rates, the impeller is loaded as gas is captured behind the impeller blades and dispersed towards the vessel walls, as indicated in Figure 8.18(b). Further increase in stirrer speed or reduction of the gas flow rate produces complete gas dispersion, as illustrated in Figure 8.18(c).

Photographs demonstrating the transition from impeller flooding to complete gas dispersion in a transparent tank stirred by a Rushton turbine are shown in Figure 8.19. In these experiments, the volumetric gas flow rate was held constant as the stirrer speed was increased from 100 rpm to 400 rpm. At the two lowest stirrer speeds in Figure 8.19(a)

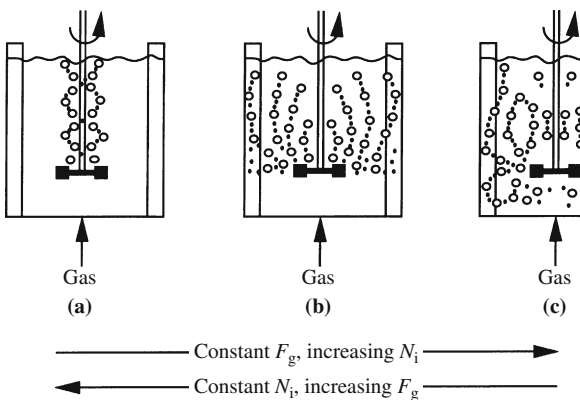


**FIGURE 8.18** Patterns of gas distribution in an aerated tank stirred with a Rushton turbine as a function of the impeller speed  $N_i$  and gas flow rate  $F_g$ . (a) Impeller flooding; (b) impeller loading; (c) complete gas dispersion.

Adapted from A.W. Nienow, M. Konno, and W. Bujalski, 1986, Studies on three-phase mixing: a review and recent results. *Chem. Eng. Res. Des.* 64, 35–42.

and (b), the impeller remains flooded as the stirrer is surrounded by gas and there is little outward dispersion of bubbles towards the vessel wall. Liquid motion is weak as blanketing by the gas prevents the impeller from pumping effectively. As indicated in Figure 8.19(c), at higher stirrer speeds the impeller becomes loaded and gas is distributed throughout the upper part of the vessel above the stirrer. Further increases in stirrer speed allow complete dispersion of bubbles below as well as above the impeller, as shown in Figure 8.19(d).

Correlations have been developed for predicting the operating conditions under which impeller loading and complete gas dispersion are achieved using Rushton turbines. These relationships are expressed using two dimensionless variables, the *gas flow number*  $Fl_g$ :

$$Fl_g = \frac{F_g}{N_i D_i^3} \quad (8.1)$$

and the *Froude number*  $Fr$ :

$$Fr = \frac{N_i^2 D_i}{g} \quad (8.2)$$

where  $F_g$  is the volumetric gas flow rate,  $N_i$  is stirrer speed,  $D_i$  is impeller diameter, and  $g$  is gravitational acceleration. Conceptually,  $Fl_g$  is the ratio of the gas flow rate to the pumping capacity of the impeller;  $Fr$  is the ratio of inertial to gravitational or buoyancy forces. Conditions at the flooding–loading transition for Rushton turbines are represented by the following equation [1]:

$$Fl_g = 30 \left( \frac{D_i}{D_T} \right)^{3.5} Fr \quad \text{at the flooding–loading transition} \quad (8.3)$$

The conditions for complete dispersion of gas by Rushton turbines are represented by another equation [1]:

$$Fl_g = 0.2 \left( \frac{D_i}{D_T} \right)^{0.5} Fr^{0.5} \quad \text{for complete gas dispersion} \quad (8.4)$$

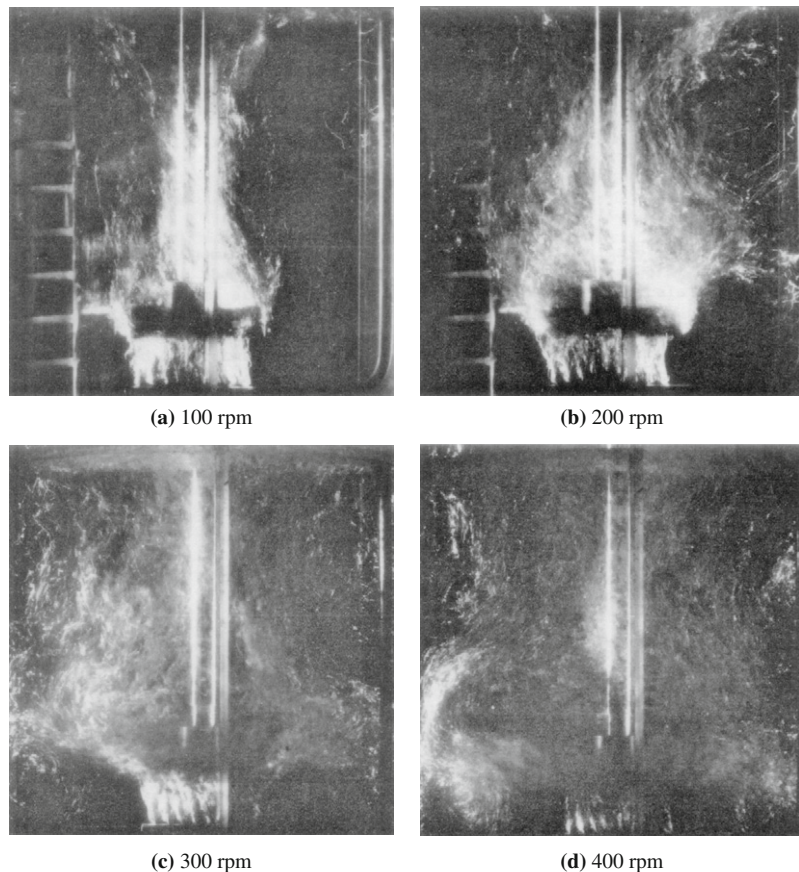


**FIGURE 8.19** Gas–liquid flow patterns in a tank stirred by a Rushton turbine. The sparger positioned below the impeller is a horizontal steel tube with eight holes on its upper surface.  
*From K.L. Man, 1985, A study of local heat-transfer coefficients in mechanically agitated gas–liquid vessels. In: Mixing, Proc. 5th Eur. Conf. on Mixing, Würzburg, Germany, pp. 221–231, BHRA: The Fluid Engineering Centre, Cranfield, U.K.*

**Equations (8.3) and (8.4)** apply to low-viscosity fluids and were determined using a variety of point and ring (diameter  $< D_i$ ) spargers. The flooding–loading transition is not affected by the impeller off-bottom clearance; however complete gas dispersion is, and [Eq. \(8.4\)](#) was developed for an impeller clearance of a one-quarter the liquid height.

**Equations (8.1) through (8.4)** demonstrate the strong dependence of gas-handling capacity on the impeller diameter. The volumetric gas flow rate  $F_g$  for loading is proportional to  $D_i^{7.5}$ ;  $F_g$  for complete gas dispersion is proportional to  $D_i^4$ . This means that for a 10% increase in  $D_i$ , the gas flow rate that can be handled without flooding increases by about 100%, while the gas flow rate for complete dispersion increases by about 50%. The dependence on stirrer speed is not as strong: a 10% increase in  $N_i$  increases  $F_g$  for flooding and complete gas dispersion by about 30% and 20%, respectively.

## EXAMPLE 8.1 GAS HANDLING WITH A RUSHTON TURBINE

A fermenter of diameter and liquid height 1.4 m is fitted with a Rushton impeller of diameter 0.5 m and off-bottom clearance 0.35 m operated at 75 rpm. The fermentation broth is sparged with air at a volumetric flow rate of  $0.28 \text{ m}^3 \text{ min}^{-1}$ . Half-way through the culture some bearings in the stirrer drive begin to fail and the stirrer speed must be reduced to a maximum of 45 rpm for the remainder of the process.

- (a) Under normal operating conditions, is the gas completely dispersed?
- (b) After the stirrer speed is reduced, is the impeller flooded or loaded?

**Solution**

(a)  $N_i = 75 \text{ min}^{-1} \cdot \left| \frac{1 \text{ min}}{60 \text{ s}} \right| = 1.25 \text{ s}^{-1}$

From Eq. (2.16),  $g = 9.81 \text{ m s}^{-2}$ . Under normal operating conditions, from Eq. (8.2):

$$Fr = \frac{(1.25 \text{ s}^{-1})^2 \cdot 0.5 \text{ m}}{9.81 \text{ m s}^{-2}} = 0.0796$$

Applying Eq. (8.4) for complete gas dispersion:

$$Fl_g = 0.2 \left( \frac{0.5 \text{ m}}{1.4 \text{ m}} \right)^{0.5} (0.0796)^{0.5} = 0.0337$$

Therefore, from Eq. (8.1):

$$F_g = Fl_g N_i D_i^3 = 0.0337 (1.25 \text{ s}^{-1}) (0.5 \text{ m})^3 = 0.00527 \text{ m}^3 \text{ s}^{-1} = 0.32 \text{ m}^3 \text{ min}^{-1}$$

As the air flow rate that can be completely dispersed by the impeller ( $0.32 \text{ m}^3 \text{ min}^{-1}$ ) is greater than the operating flow rate ( $0.28 \text{ m}^3 \text{ min}^{-1}$ ), we can conclude that the air provided is completely dispersed under normal operating conditions.

- (b) After the stirrer speed reduction:

$$N_i = 45 \text{ min}^{-1} \cdot \left| \frac{1 \text{ min}}{60 \text{ s}} \right| = 0.75 \text{ s}^{-1}$$

From Eq. (8.2):

$$Fr = \frac{(0.75 \text{ s}^{-1})^2 \cdot 0.5 \text{ m}}{9.81 \text{ m s}^{-2}} = 0.0287$$

Applying Eq. (8.3) for the flooding-loading transition:

$$Fl_g = 30 \left( \frac{0.5 \text{ m}}{1.4 \text{ m}} \right)^{3.5} 0.0287 = 0.0234$$

Therefore, from Eq. (8.1):

$$F_g = Fl_g N_i D_i^3 = 0.0234 (0.75 \text{ s}^{-1}) (0.5 \text{ m})^3 = 0.00219 \text{ m}^3 \text{ s}^{-1} = 0.13 \text{ m}^3 \text{ min}^{-1}$$

At the reduced stirrer speed, the maximum air flow rate that can be handled without impeller flooding is  $0.13 \text{ m}^3 \text{ min}^{-1}$ . As the operating air flow rate ( $0.28 \text{ m}^3 \text{ min}^{-1}$ ) is greater than this, the impeller is flooded.

Gas dispersion by Rushton turbines is related directly to the trailing vortices that develop behind the impeller blades (refer to [Figure 8.15](#)). Rolling or rotation of each vortex results in centrifugal acceleration of the liquid and a reduction in pressure along the vortex axis. When the liquid is sparged with gas, the gas accumulates readily in these low-pressure regions, producing *ventilated cavities* behind the blades. A photograph of ventilated cavities behind the blades of a Rushton turbine is shown in [Figure 8.20](#). Bubble dispersion occurs primarily at the outer tails of the cavities, where small bubbles are shed to balance the rate of gas flow into the cavities from under the disc.

The effectiveness of gas dispersion in stirred vessels is controlled by the size and structure of the ventilated cavities behind the impeller blades. The types of cavity formed with Rushton turbines in low-viscosity fluids have been well documented and are illustrated in [Figure 8.21](#). With increasing gas flow rate  $F_g$  at constant stirrer speed  $N_i$ , vortex cavities at each of the blades give rise to clinging cavities, after which there is a transition to a very stable '3–3' structure characterised by large cavities behind three of the blades and smaller cavities behind the remaining alternate three blades. If the gas flow rate is increased beyond the gas-handling capacity of the impeller, six equal-sized ragged cavities are formed; these cavities are unstable and oscillate violently. The formation of ragged cavities occurs at the point represented in [Figure 8.18](#) as the transition from [Figure 8.18\(b\) to \(a\)](#): at these high gas flow rates, the impeller ceases to function effectively and is flooded. No particular change in cavity structure has been associated with the transition shown in [Figure 8.18](#) from loading (b) to complete gas dispersion (c). Cavity formation in fluids with viscosity greater than about 20 centipoise is more complex than that represented in [Figure 8.21](#); cavities of different shape and greater stability are produced. Cavities in



**FIGURE 8.20** Gas cavities that are formed behind the blades of a 7.6-cm Rushton turbine in water. The impeller was rotated counterclockwise; the camera was located below the impeller and ring sparger.

From W. Bruijn, K. van't Riet, and J.M. Smith, 1974, Power consumption with aerated Rushton turbines. Trans. IChemE 52, 88–104.

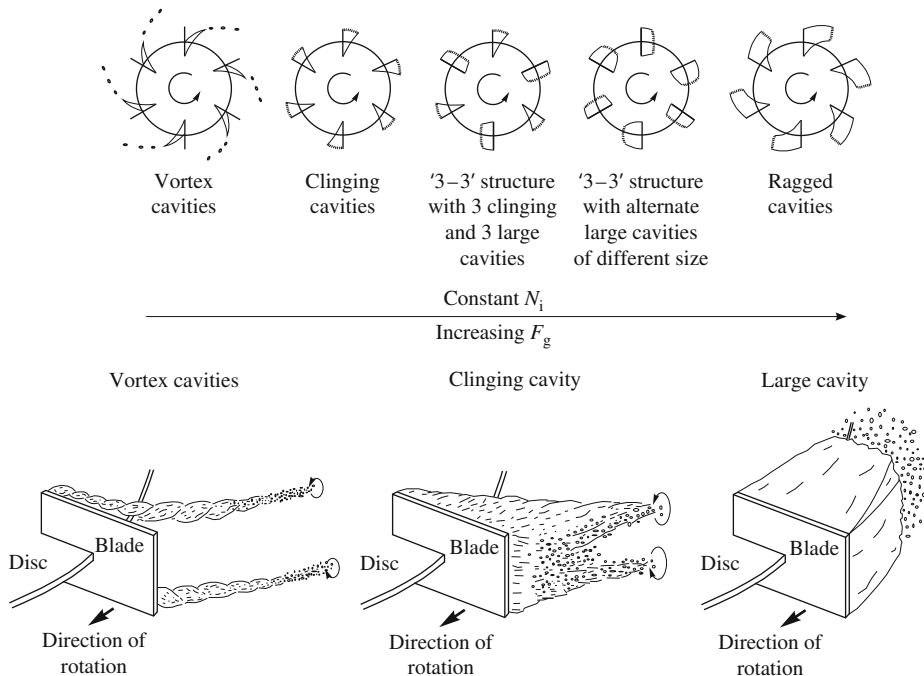


**FIGURE 8.21** Changes in ventilated cavity structure for a Rushton turbine at constant stirrer speed  $N_i$  and increasing gas flow rate  $F_g$ .

Adapted from J.M. Smith and M.M.C.G. Warmoeskerken, 1985, *The dispersion of gases in liquids with turbines*. In: *Mixing*, Proc. 5th Eur. Conf. on Mixing, Würzburg, Germany, pp. 115–126, BHRA: The Fluid Engineering Centre, Cranfield, U.K.

viscous fluids may be so stable that they persist behind the impeller blades for several hours even after the gas supply is stopped [2].

### Solids Suspension

Rushton turbines are effective for solids suspension, including in three-phase (solid–liquid–gas) systems. Suspension of solids is generally improved by reducing the impeller off-bottom clearance, but this can cause flow instabilities when the system is aerated. For three-phase mixing, an impeller clearance of a 1/4 the tank diameter has been recommended for Rushton turbines, as this allows effective solids suspension, gas dispersion under the impeller, and adequate agitation in the upper parts of the vessel [3].

### 8.4.2 Propellers

A typical three-blade marine-type propeller is illustrated in Figure 8.22. The slope of the individual blades varies continuously from the outer tip to the inner hub. The *pitch* of a propeller is a measure of the angle of the propeller blades. It refers to the properties of the propeller as a segment of a screw: pitch is the advance per revolution, or the distance that

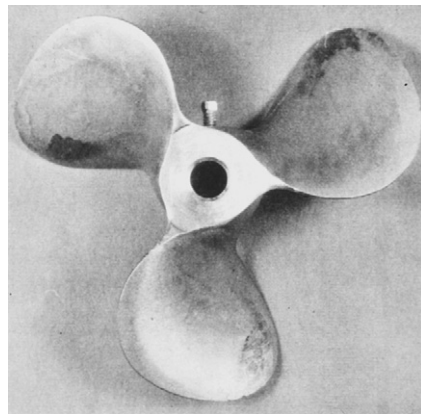


FIGURE 8.22 Propeller.

liquid is displaced along the impeller axis during one full turn. Propellers with square pitch, that is, pitch equal to the impeller diameter, are often used.

Propellers are axial-flow impellers. They may be operated for either downward or upward pumping of the fluid; downward pumping is more common. Propellers have high flow capacity and produce mean flow patterns similar to that shown in [Figure 8.8](#). They are used with low-to-medium viscosity fluids and are usually installed with diameter around one-third the tank diameter. With gassing, propellers operated at high speed can generate flow and torque instabilities. However, propellers are very effective for suspending solids, outperforming Rushton turbines in that respect.

#### 8.4.3 Pitched-Blade Turbines

Pitched-blade turbines have flat inclined blades, as shown in [Figure 8.10](#). Although commonly referred to as axial-flow impellers, pitched-blade turbines generate discharge streams with significant radial as well as axial velocity components. Pitched-blade turbines produce strong liquid flows and have a much higher pumping efficiency than Rushton turbines, making them very effective for blending applications. With gassing, ventilated cavities form behind the blades as a result of underpressure in the trailing vortices in much the same way as for Rushton turbines. However, for pitched-blade turbines, there is only one vortex per blade.

Pitched-blade turbines can be operated in either downward or upward pumping modes, downward being the more common.

##### **Downward Pumping**

[Figure 8.8](#) shows the liquid flow pattern typical of downward-pumping pitched-blade turbines. Performance of these impellers is sensitive to several aspects of tank geometry, such as the impeller off-bottom clearance and the sparger size and location. This sensitivity is greater than is found normally with Rushton turbines. Depending on the impeller off-bottom clearance, secondary circulation loops may develop in the lower regions of the tank in addition to the primary flow pattern shown in [Figure 8.8](#). Because the strength of these secondary currents determines the angle of fluid discharge from the impeller, which

in turn determines whether the primary circulation currents reach the vessel floor, the flows set up by downward-pumping turbines can be considerably more complex than that shown in [Figure 8.8 \[4\]](#). Unlike with Rushton turbines, the fluid currents generated by pitched-blade turbines are not compartmentalised into upper and lower circulatory loops. However, because the flow velocity becomes progressively weaker away from the impeller, the primary circulation currents generated by downward-pumping turbines may not reach the upper parts of the tank, even when the liquid height does not exceed the tank diameter [\[5\]](#).

The distribution of turbulence kinetic energy per unit mass of fluid,  $k$  (Section 7.9.2, Turbulence Kinetic Energy subsection), in a tank stirred with a downward-pumping pitched-blade turbine is shown in [Figure 8.23](#). Turbulence kinetic energy is not distributed uniformly throughout the tank. The highest values of  $k$  are concentrated near the impeller where the turbulence is most intense. As the discharge streams move downwards away from the impeller blades, the turbulence kinetic energy decreases accordingly. Levels of turbulence kinetic energy in the remainder of the tank away from the impeller are up to an order of magnitude lower than the maximum values measured.

With gassing, downward-pumping turbines are prone to flooding, especially if the impeller diameter and solidity ratio are small. The hydrodynamic changes that occur as the stirrer speed is increased at constant gas flow rate are similar to but more complex than those represented in [Figure 8.18](#) for a Rushton turbine; for example, asymmetrical flow patterns may be generated. At low stirrer speeds when the impeller is flooded, liquid circulation is weak and the flow is dominated by gas bubbling up the stirrer shaft. With increasing stirrer speed, streaming ventilated cavities form behind the impeller blades and bubbles breaking away from the cavities are dispersed downwards; however, the large flow of bubbles up the centre of the vessel remains the primary flow pattern. Further increases in speed allow the pumping action of the impeller to dominate, so that gas is vigorously dispersed throughout the vessel. However, this condition is unstable; the flow

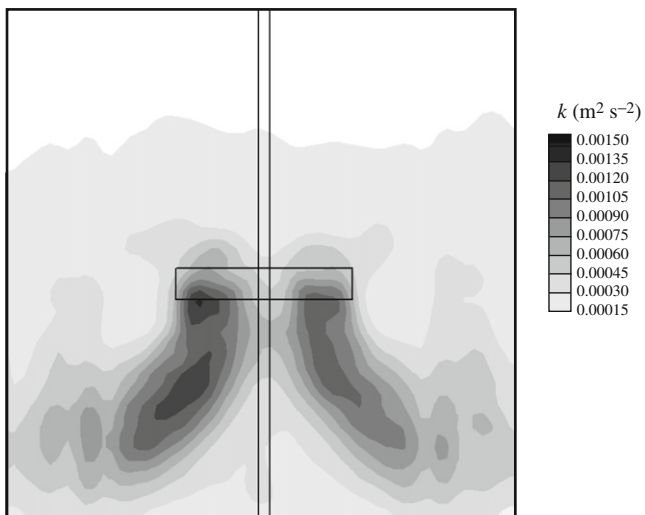


**FIGURE 8.23** Distribution of  $k$ , the turbulence kinetic energy per unit mass of fluid, in a tank stirred by a downward-pumping pitched-blade turbine located near the centre of the tank. The data were measured using particle image velocimetry. From J. Sheng, H. Meng, and R.O. Fox, 1998, Validation of CFD simulations of a stirred tank using particle image velocimetry data. *Can. J. Chem. Eng.* 76, 611–625. Image provided courtesy of the authors.

pattern periodically reverts to a nondispersed state and large flow oscillations and torque and power instabilities can occur. Eventually, at high enough stirrer speeds, large gas-filled cavities are formed behind the impeller blades, the instabilities disappear, and the gas remains fully dispersed. Because instability and flow oscillations prior to stable gas dispersion can lead to mechanical problems including vessel vibration, operation in this regime is not recommended. Thus, in contrast with Rushton impellers, for downward-pumping pitched-blade turbines there is no practical range of operating conditions between flooding and complete gas dispersion. As neither flow instability nor incomplete gas dispersion is desirable, the impeller should always be operated at speeds high enough to fully distribute the gas.

The instabilities associated with downward-pumping turbines are generally thought to occur because of the inherent opposition of flow directions generated by the impeller and by the gas; that is, fluid driven downward by the impeller is opposed by bubble flow rising up from the sparger. As shown in Figure 8.24, two flow regimes have been identified for downward-pumping impellers. *Direct loading*, which occurs at low stirrer speeds or high gas flow rates, is characterised by gas entering the impeller region directly from the sparger. In contrast, during *indirect loading* at high stirrer speeds or low gas flows, gas approaching the impeller is swept away by the downward thrust of liquid from the stirrer and only enters the impeller region by recirculation. Flow instabilities are associated with the transition from direct to indirect loading, and coincide with the formation of large gas-filled cavities behind the impeller blades. Problems with instability are greater for impellers with four blades rather than six, and when small impeller-to-tank diameter ratios are used.

Sparger geometry and position have significant effects on the performance of downward-pumping impellers. The use of point spargers increases the likelihood of flow instabilities with gassing. Although pitched-blade impellers are more prone to flooding than Rushton turbines, their gas-handling ability can be improved by replacing point spargers with ring spargers of diameter about 0.8 times the impeller diameter, and optimising the separation between the sparger and impeller [6, 7].

At low gassing rates, suspension of solids is achieved by downward-pumping agitators with very high energy efficiency. However, severe loss of suspension capacity can occur

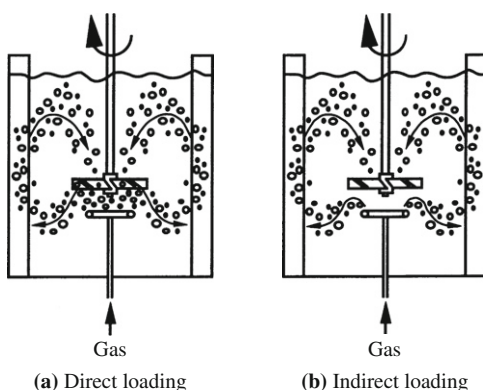


**FIGURE 8.24** Direct and indirect gas loading regimes for a downward-pumping pitched-blade turbine.

From M.M.C.G. Warmoeskerken, J. Speur, and J.M. Smith, 1984, Gas–liquid dispersion with pitched blade turbines. Chem. Eng. Commun. 25, 11–29.

with gassing, especially when there are flow instabilities associated with the direct–indirect loading transition.

### ***Upward Pumping***

Many of the problems associated with downward-pumping pitched-blade impellers under gassed conditions can be avoided by reversing the direction of rotation so that the impeller pumps upwards. The upward flow generated is then cocurrent with that of the sparged gas, and the resulting flow patterns are inherently more stable than with downward pumping. Yet, the use of turbine impellers in upward-pumping mode is much less common than downward-pumping operation.

The gas–liquid flow patterns developed by upward-pumping turbines are very different from those produced during downward flow operation. At low stirrer speeds, there is negligible gas dispersion, the impeller is flooded, and there are no gas cavities behind the blades. As the impeller speed is increased, there is a change from flooding to loading as more and more gas is dispersed towards the vessel walls. With loading, streaming vortex gas cavities are formed behind the impeller blades. Clinging cavities develop with further increases in stirrer speed and gas bubbles start to be dispersed below the impeller. At even higher speeds, large clinging cavities are formed and bubbles shed from the tails of these cavities are dispersed throughout the vessel. No significant flow instabilities occur with upward-pumping turbines. Compared with downward-pumping impellers, complete gas dispersion is achieved at lower stirrer speeds and with less energy consumption, and more gas can be handled before flooding occurs.

Because upward-pumping impellers generate relatively small velocities beneath the impeller, the energy required for solids suspension is significantly greater than for downward-pumping impellers. However, an advantage in aerated systems is that both the agitation speed and power required for solids suspension are almost independent of the gassing rate [8].

#### **8.4.4 Alternative Impeller Designs**

So far, we have considered the characteristics of several traditional impellers that have been used in the chemical and bioprocessing industries for many decades. More recently, a variety of new agitator configurations has been developed commercially. These modern impellers have a range of technical features aimed at improving mixing in stirred tanks.

##### ***Curved-Blade Disc Turbines***

Curved-blade disc turbines such as that shown in Figure 8.25 generate primarily radial flow, similar to the Rushton turbine. However, changing the shape of the blades has a significant effect on the impeller power requirements and gas-handling characteristics. Rotation with the concave side forward greatly discourages the development of trailing vortices behind the blades; therefore, with sparging, no large ventilated cavities form on the convex surfaces. A major advantage is that the impeller is more difficult to flood, being able to handle gas flow rates several times higher than those that cause flooding of Rushton turbines [9].

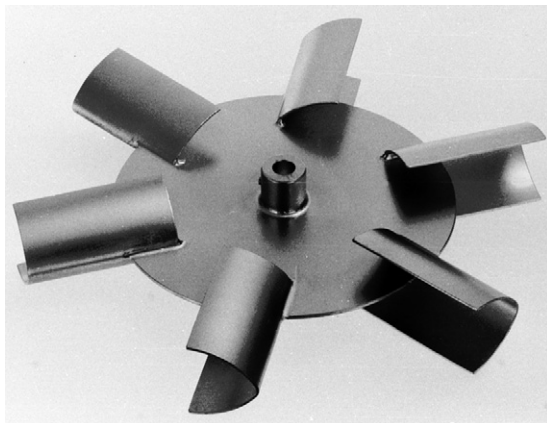
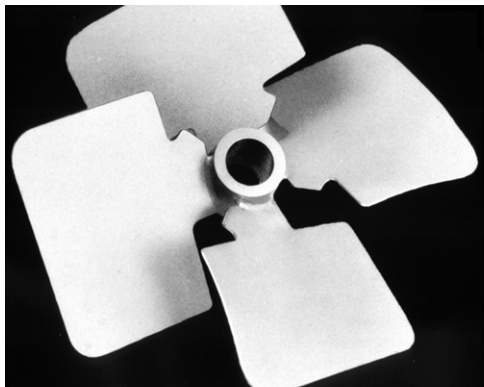


**FIGURE 8.25** Scaba 6SRGT six-curved-blade disc turbine.

*Photograph courtesy of Scaba AB, Sweden.*



(a)



(b)

**FIGURE 8.26** (a) Lightnin A315 hydrofoil impeller.

*Photograph courtesy of Lightnin Mixers, Australia.*

(b) Prochem Maxflo T hydrofoil impeller.

*Photograph courtesy of Chemineer Inc., Dayton, OH.*

### **Hydrofoil Impellers**

Two different hydrofoil impellers are shown in Figure 8.26. The blade angle and width are varied along the length of hydrofoil blades, and the leading edges are rounded like an airplane wing to reduce form drag and generate a positive lift. The shape of hydrofoil impellers allows for effective pumping and bulk mixing with strong axial velocities and low power consumption. Most hydrofoils are operated for downward pumping, but upward flow is also possible. A typical mean velocity vector plot for a downward-pumping hydrofoil impeller is shown in Figure 8.27. Downward-flowing currents with very strong axial velocity components leave the impeller. Fluid in these currents sweeps the vessel floor in an outward radial direction, then moves up alongside the vessel walls before returning back to the impeller. Liquid velocities in regions of the tank above the main circulation loops are considerably lower than below the impeller.

With aeration, downward-pumping hydrofoil impellers exhibit many of the hydrodynamic properties of downward-pumping pitched-blade turbines. They remain more prone to flooding than Rushton turbines, even when the impeller solidity ratio is large. The types

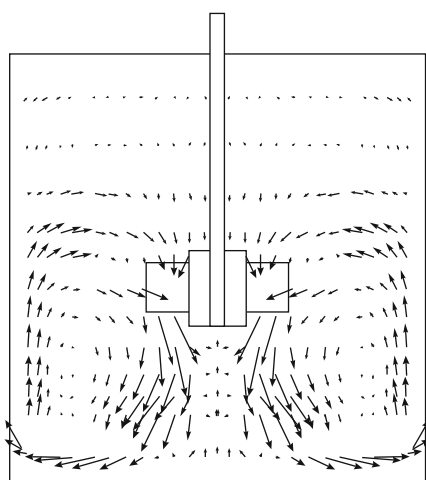


**FIGURE 8.27** Mean velocity vector plot for a Prochem Maxflo T hydrofoil impeller. The velocities were measured using laser Doppler velocimetry.

Adapted from Z. Jaworski, A.W. Nienow, and K.N. Dyster, 1996, An LDA study of the turbulent flow field in a baffled vessel agitated by an axial, down-pumping hydrofoil impeller. Can. J. Chem. Eng. 74, 3–15.

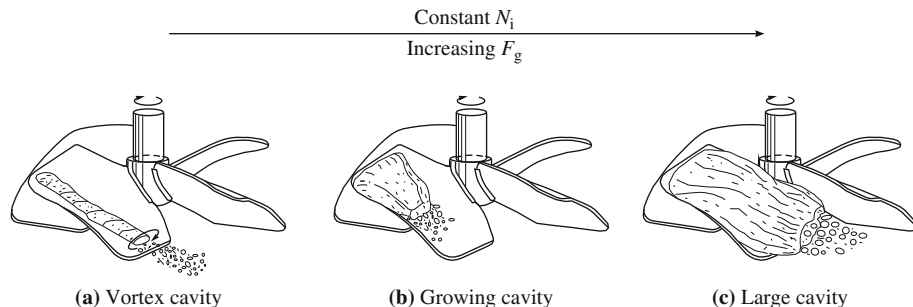


**FIGURE 8.28** Changes in ventilated cavity structure for a Lightnin A315 hydrofoil impeller at constant stirrer speed  $N_i$  and increasing gas flow rate  $F_g$ .

Adapted from A. Bakker and H.E.A. van den Akker, 1994, Gas–liquid contacting with axial flow impellers. Trans. IChemE 72A, 573–582.

of ventilated cavity formed behind the blades of a downward-pumping hydrofoil impeller in low-viscosity fluid are illustrated in Figure 8.28. The cavities in Figure 8.28(a) and (b) occur during indirect loading (Section 8.4.3, Downward Pumping subsection); at relatively low gas flow rates, only recirculating gas reaches the impeller to form vortex or growing cavities. With increasing gas flow, the growing cavities can exhibit various types of instability. At higher gassing rates when the impeller is no longer capable of deflecting the rising gas flow, direct loading occurs as gas enters the impeller region directly from the sparger to produce large cavities as shown in Figure 8.28(c). Further increases in gas flow lead to impeller flooding.

The flow instabilities generated in gassed systems by downward-pumping hydrofoil impellers can be eliminated using wide-blade, upward-pumping hydrofoils. These impellers also have high gas-handling capacity and a limited tendency to flood at low stirrer speeds.

## 8.5 STIRRER POWER REQUIREMENTS

Electrical power is used to drive impellers in stirred vessels. The average power consumption per unit volume for industrial bioreactors ranges from  $10 \text{ kW m}^{-3}$  for small vessels (approx.  $0.1 \text{ m}^3$ ) to  $1$  to  $2 \text{ kW m}^{-3}$  for large vessels (approx.  $100 \text{ m}^3$ ). Friction in the stirrer motor gearbox and seals reduces the energy transmitted to the fluid; therefore, the electrical power consumed by stirrer motors is always greater than the mixing power by an amount depending on the efficiency of the drive. Energy costs for operation of stirrers in bioreactors are a major ongoing financial commitment and an important consideration in process economics.

The power required to achieve a given stirrer speed depends on the magnitude of the frictional forces and form drag that resist rotation of the impeller. Friction and form drag give rise to torque on the stirrer shaft; experimentally, the power input for stirring can be determined from measurements of the induced torque  $M$ :

$$P = 2\pi N_i M \quad (8.5)$$

where  $P$  is power and  $N_i$  is the stirrer speed.

General guidelines for estimating the power requirements in stirred tanks are outlined in the following sections.

### 8.5.1 Ungassed Newtonian Fluids

The power required to mix nonaerated fluids depends on the stirrer speed, the impeller shape and size, the tank geometry, and the density and viscosity of the fluid. The relationship between these variables is usually expressed in terms of dimensionless numbers such as the impeller Reynolds number  $Re_i$ :

$$Re_i = \frac{N_i D_i^2 \rho}{\mu} \quad (7.2)$$

and the power number  $N_P$ :

$$N_P = \frac{P}{\rho N_i^3 D_i^5} \quad (8.6)$$

In Eqs. (7.2) and (8.6),  $N_i$  is stirrer speed,  $D_i$  is impeller diameter,  $\rho$  is fluid density,  $\mu$  is fluid viscosity, and  $P$  is power. The power number  $N_P$  can be considered analogous to a drag coefficient for the stirrer system.

The relationship between  $Re_i$  and  $N_P$  has been determined experimentally for a range of impeller and tank configurations. The results for five impeller designs—Rushton turbine, downward-pumping pitched-blade turbine, marine propeller, anchor, and helical ribbon—are shown in Figures 8.29 and 8.30. Once the value of  $N_P$  is known, the power is calculated from Eq. (8.6) as:

$$P = N_P \rho N_i^3 D_i^5 \quad (8.7)$$

For a given impeller, the general relationship between power number and Reynolds number depends on the flow regime in the tank. The following three flow regimes can be identified in Figures 8.29 and 8.30.

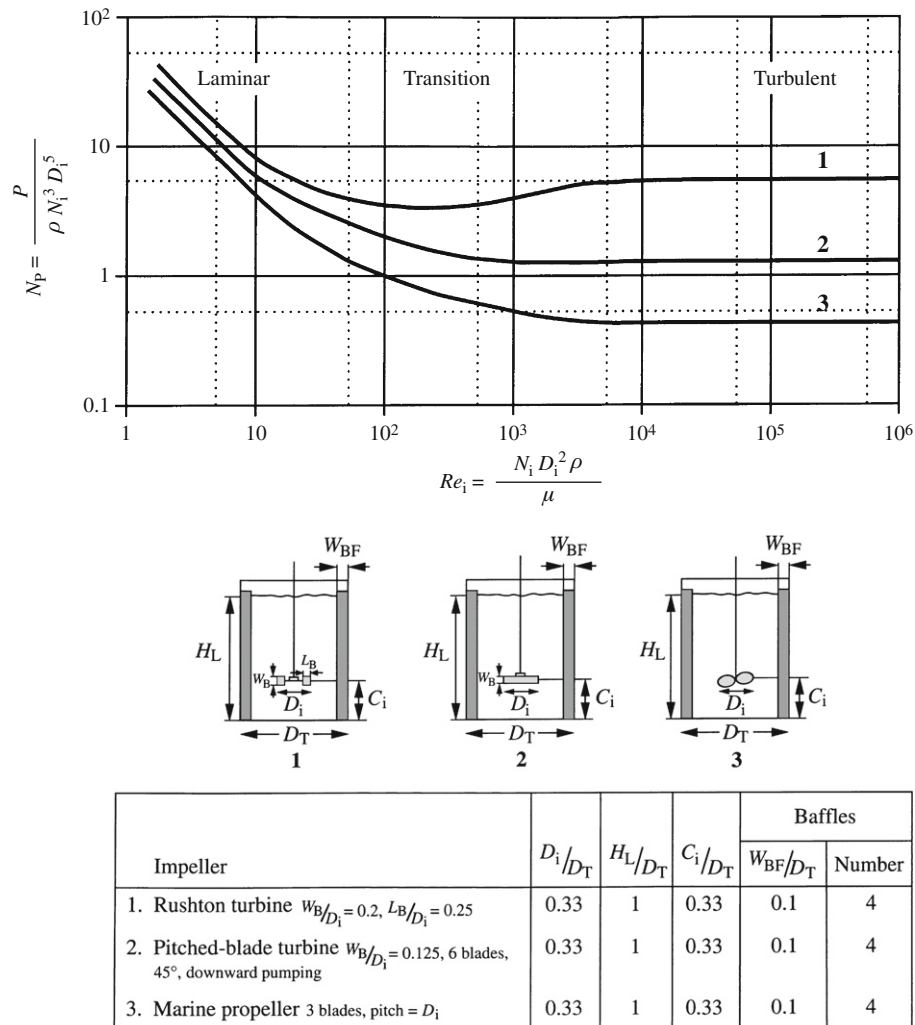


FIGURE 8.29 Correlations between the Reynolds number and power number for Rushton turbines, downward-pumping pitched-blade turbines, and marine propellers in fluids without gassing.  
Data from J.H. Rushton, E.W. Costich, and H.J. Everett, 1950, *Power characteristics of mixing impellers. Parts I and II*. Chem. Eng. Prog. 46, 395–404, 467–476; and R.L. Bates, P.L. Fonds, and R.R. Corpstein, 1963, *An examination of some geometric parameters of impeller power*. Ind. Eng. Chem. Process Des. Dev. 2, 310–314.

1. **Laminar regime.** The laminar regime corresponds to  $Re_i < 10$  for many impellers, including turbines and propellers. For stirrers with small wall-clearance such as anchor and helical ribbon mixers, laminar flow persists until  $Re_i = 100$  or greater. In the laminar regime:

$$N_p \propto \frac{1}{Re_i} \quad \text{or} \quad P = k_1 \mu N_i^2 D_i^3 \quad (8.8)$$

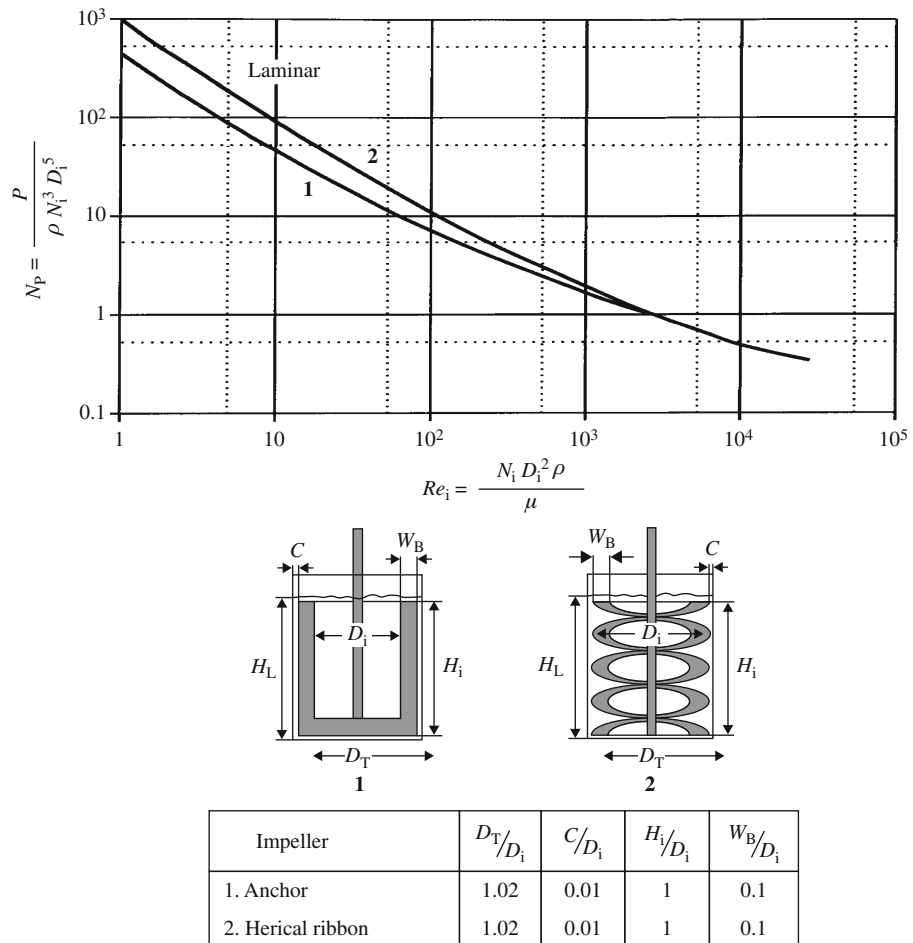


FIGURE 8.30 Correlations between the Reynolds number and power number for anchor and helical ribbon impellers in fluids without gassing.

From M. Zlokarnik and H. Judat, 1988, *Stirring*. In: W. Gerhartz, Ed., Ullmann's Encyclopedia of Industrial Chemistry, 5th ed., vol. B2, pp. 25-1–25-33, VCH, Weinheim, Germany.

where  $k_1$  is a proportionality constant. Values of  $k_1$  for the impellers represented in Figures 8.29 and 8.30 are listed in Table 8.1 [10, 11]. The power required for laminar flow is independent of the density of the fluid but directly proportional to the fluid viscosity.

2. *Turbulent regime*. The power number is independent of the Reynolds number in turbulent flow. Therefore:

$$P = N'_P \rho N_i^3 D_i^5 \quad (8.9)$$

where  $N'_P$  is the constant value of the power number in the turbulent regime. Approximate values of  $N'_P$  for the impellers in Figures 8.29 and 8.30 are listed in

**TABLE 8.1** Values of the Constants in Eqs. (8.8) and (8.9) for the Stirred Tank Geometries Defined in Figures 8.29 and 8.30

| Impeller type         | $k_1 (Re_i = 1)$ | $N'_P (Re_i = 10^5)$ |
|-----------------------|------------------|----------------------|
| Rushton turbine       | 70               | 5.0                  |
| Pitched-blade turbine | 50               | 1.3                  |
| Marine propeller      | 40               | 0.35                 |
| Anchor                | 420              | 0.35                 |
| Helical ribbon        | 1000             | 0.35                 |

**Table 8.1 [10, 11].**  $N'_P$  for Rushton turbines is significantly higher than for most other impellers, indicating that the Rushton turbine has strong form drag, generates high levels of torque, and transmits more power at the same operating speed than other designs. Values of  $N'_P$  for a selection of other impellers and system geometries are listed in Table 8.2. Depending on the number of blades and solidity ratio, hydrofoil impellers have relatively low  $N'_P$ ; this reflects their aerodynamic blade design, which effectively minimises form drag.

As indicated in Eq. (8.9), the power required for turbulent flow is independent of the viscosity of the fluid but proportional to the density. The turbulent regime is fully developed at  $Re_i > 10^4$  for most small impellers in baffled vessels. For the same impellers in vessels without baffles, the power curves are somewhat different from those shown in Figure 8.29. Without baffles, turbulence may not be fully developed until  $Re_i > 10^5$ ; the value of  $N'_P$  is also reduced to as little as 10 to 50% of that with baffles [18, 19].

3. *Transition regime.* Between laminar and turbulent flow lies the transition region. Although the viscosity of fermentation broths is not usually sufficient for stirrers in industrial bioreactors to operate in the laminar regime, many broths become sufficiently viscous to give Reynolds numbers in the transition region. Both density and viscosity affect the power requirements in this regime. There is usually a gradual transition from laminar to fully developed turbulent flow in stirred tanks; the Reynolds-number range for transition depends on the system geometry.

Equations (8.8) and (8.9) express the strong dependence of power consumption on stirrer diameter and, to a lesser extent, stirrer speed. Small changes in impeller size have a large effect on power requirements, as would be expected from dependency on impeller diameter raised to the third or fifth power. In the turbulent regime, a 10% increase in impeller diameter increases the power requirements by more than 60%; a 10% increase in stirrer speed raises the power required by over 30%.

Friction and form drag, and therefore the power required for stirring, are sensitive to the detailed geometry of the impeller and configuration of the tank. The curves of Figures 8.29 and 8.30 and the values of  $N'_P$  in Tables 8.1 and 8.2 refer to the particular geometries specified and are subject to change if the number, size, or position of the baffles, the number, length, width, pitch, or angle of the impeller blades, the liquid height,

**TABLE 8.2** Values of the Turbulent Ungassed Power Number  $N'_P$  for a Selection of Impellers and System Geometries

| Impeller                                       | System geometry       | $N'_P$ | Reference |
|--|-----------------------|--------|-----------|
| <b>Rushton turbine</b>                         | Flat-bottom tank      | 5.9    | [12, 13]  |
| $D_i/D_T = 0.50$                               | $H_L/D_T = 1.0$       |        |           |
| $W_B/D_i = 0.20$                               | Number of baffles = 4 |        |           |
| $L_B/D_i = 0.25$                               | $W_{BF}/D_T = 0.1$    |        |           |
|  | $C_i/D_T = 0.25$      |        |           |
| <b>Pitched-blade turbine</b>                   | Flat-bottom tank      | 1.8    | [14]      |
| Downward pumping                               | $H_L/D_T = 1.0$       |        |           |
| 6 blades, $45^\circ$                           | Number of baffles = 4 |        |           |
| $D_i/D_T = 0.40$                               | $W_{BF}/D_T = 0.1$    |        |           |
|  | $C_i/D_T = 0.25$      |        |           |
| <b>Pitched-blade turbine</b>                   | Flat-bottom tank      | 1.6    | [13]      |
| Downward pumping                               | $H_L/D_T = 1.0$       |        |           |
| 6 blades, $45^\circ$                           | Number of baffles = 4 |        |           |
| $D_i/D_T = 0.50$                               | $W_{BF}/D_T = 0.1$    |        |           |
| $W_B/D_i = 0.20$                               | $C_i/D_T = 0.25$      |        |           |
| <b>Pitched-blade turbine</b>                   | Flat-bottom tank      | 1.6    | [13, 15]  |
| Upward pumping                                 | $H_L/D_T = 1.0$       |        |           |
| 6 blades, $45^\circ$                           | Number of baffles = 4 |        |           |
| $D_i/D_T = 0.5$                                | $W_{BF}/D_T = 0.1$    |        |           |
| $W_B/D_i = 0.20$                               | $C_i/D_T = 0.25$      |        |           |
| <b>Curved-blade disc turbine (Scaba 6SRGT)</b> | Flat-bottom tank      | 1.5    | [9]       |
| 6 blades                                       | $H_L/D_T = 1.0$       |        |           |
| $D_i/D_T = 0.33$                               | Number of baffles = 4 |        |           |
| $W_B/D_i = 0.15$                               | $W_{BF}/D_T = 0.1$    |        |           |
| $L_B/D_i = 0.28$                               | $C_i/D_T = 0.25$      |        |           |
| <b>Hydrofoil (Lightnin A315)</b>               | Flat-bottom tank      | 0.84   | [16]      |
| Downward pumping                               | $H_L/D_T = 1.0$       |        |           |
| 4 blades                                       | Number of baffles = 4 |        |           |
| $D_i/D_T = 0.40$                               | $W_{BF}/D_T = 0.1$    |        |           |
|  | $C_i/D_T = 0.25$      |        |           |

|                              |                       |     |      |
|------------------------------|-----------------------|-----|------|
| Hydrofoil (Prochem Maxflo T) | Flat-bottom tank      | 1.6 | [17] |
| Downward pumping             | $H_L/D_T = 1.0$       |     |      |
| 6 blades                     | Number of baffles = 4 |     |      |
| $D_i/D_T = 0.35$             | $W_{BF}/D_T = 0.1$    |     |      |
|                              | $C_i/D_T = 0.45$      |     |      |

the impeller clearance from the bottom of the tank, and so on, are altered. For a Rushton turbine under fully turbulent conditions ( $Re_i > 10^4$ ),  $N'_P$  lies between about 1 and 7 depending on these parameters [19]. For axial-flow impellers, blade angle has a major influence on power requirements. For example,  $N'_P$  for a pitched-blade turbine with six blades set at an angle of  $60^\circ$  to the horizontal is more than fivefold that for the same impeller with blade angle  $30^\circ$  [20]. Impeller pitch has a similarly significant effect on the power number for propellers [19, 21]. Experimental studies have shown that blade thickness and vessel scale can also affect  $N'_P$  [13, 22].

## EXAMPLE 8.2 CALCULATION OF POWER REQUIREMENTS

A fermentation broth with viscosity  $10^{-2}$  Pa s and density  $1000 \text{ kg m}^{-3}$  is agitated in a  $50\text{-m}^3$  baffled tank using a marine propeller  $1.3\text{ m}$  in diameter. The tank geometry is as specified in Figure 8.29. Calculate the power required for a stirrer speed of  $4 \text{ s}^{-1}$ .

### Solution

From Eq. (7.2):

$$Re_i = \frac{4 \text{ s}^{-1} (1.3 \text{ m})^2 1000 \text{ kg m}^{-3}}{10^{-2} \text{ kg m}^{-1} \text{ s}^{-1}} = 6.76 \times 10^5$$

From Figure 8.29, flow at this  $Re_i$  is fully turbulent. From Table 8.1,  $N'_P$  is 0.35. Therefore, from Eq. (8.9):

$$P = (0.35) 1000 \text{ kg m}^{-3} (4 \text{ s}^{-1})^3 (1.3 \text{ m})^5 = 8.3 \times 10^4 \text{ kg m}^2 \text{ s}^{-3}$$

From Table A.8 in Appendix A,  $1 \text{ kg m}^2 \text{ s}^{-3} = 1 \text{ W}$ . Therefore:

$$P = 83 \text{ kW}$$

### 8.5.2 Ungassed Non-Newtonian Fluids

Estimation of the power requirements for non-Newtonian fluids is more difficult. It is often impossible with highly viscous fluids to achieve fully developed turbulence; under these conditions  $N_P$  is always dependent on  $Re_i$  and we cannot use the constant  $N'_P$  value in power calculations. In addition, because the viscosity of non-Newtonian liquids varies with shear conditions, the impeller Reynolds number used to correlate power

requirements must be redefined. Some power correlations have been developed using an impeller Reynolds number based on the apparent viscosity  $\mu_a$  (Section 7.5):

$$Re_i = \frac{N_i D_i^2 \rho}{\mu_a} \quad (8.10)$$

Therefore, from Eq. (7.12) for power-law fluids:

$$Re_i = \frac{N_i D_i^2 \rho}{K \dot{\gamma}^{n-1}} \quad (8.11)$$

where  $n$  is the flow behaviour index and  $K$  is the consistency index. A problem with application of Eq. (8.11) is the evaluation of  $\dot{\gamma}$ . For stirred tanks, an approximate relationship is often used:

$$\dot{\gamma} = k N_i \quad (7.15)$$

where the value of the constant  $k$  depends on the geometry of the impeller. The relationship of Eq. (7.15) is discussed further in Section 8.15; however, for turbine impellers  $k$  is about 10. Substituting Eq. (7.15) into Eq. (8.11) gives an appropriate Reynolds number for pseudoplastic fluids:

$$Re_i = \frac{N_i^{2-n} D_i^2 \rho}{K k^{n-1}} \quad (8.12)$$

The relationship between the Reynolds number  $Re_i$  and the power number  $N_p$  for a Rushton turbine in a baffled tank containing pseudoplastic fluid is shown in Figure 8.31. The upper line was measured using Newtonian fluids for which  $Re_i$  is defined by Eq. (7.2); this line corresponds to part of the curve already shown in Figure 8.29. The lower line gives the  $Re_i-N_p$  relationship for pseudoplastic fluids with  $Re_i$  defined by Eq. (8.12). The laminar region extends to higher Reynolds numbers in pseudoplastic fluids than in Newtonian systems. At  $Re_i$  below 10 and above 200, the results for Newtonian and

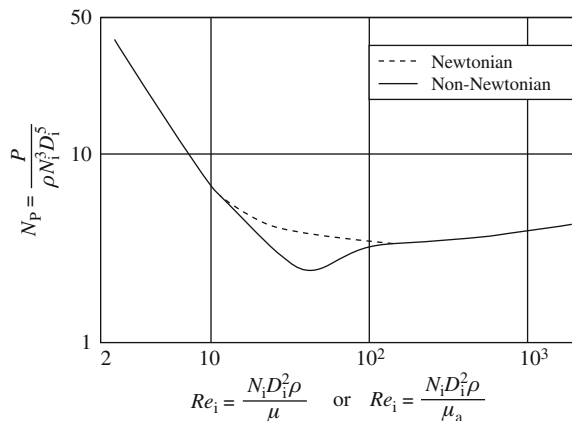


**FIGURE 8.31** The correlation between the Reynolds number and power number for a Rushton turbine in ungassed non-Newtonian fluid in a baffled tank.

From A.B. Metzner, R.H. Feehs, H. Lopez Ramos, R.E. Otto, and J.D. Tuthill, 1961, Agitation of viscous Newtonian and non-Newtonian fluids. AIChE J. 7, 3–9.

non-Newtonian fluids are essentially the same. In the intermediate range, pseudoplastic liquids require less power than Newtonian fluids to achieve the same Reynolds number.

There are several practical difficulties with application of Figure 8.31 to bioreactors. As discussed further in Section 8.15, flow patterns in pseudoplastic and Newtonian fluids differ significantly. Even if there is high turbulence near the impeller in pseudoplastic systems, the bulk liquid may be moving very slowly and consuming relatively little power. Another problem is that, as illustrated in Figure 7.11, the non-Newtonian parameters  $K$  and  $n$ , and therefore  $\mu_a$ , can vary substantially during the course of fermentation.

### 8.5.3 Gassed Fluids

Liquids into which gas is sparged have reduced power requirements for stirring. The presence of gas bubbles decreases the density of the fluid; however, the influence of density as expressed in Eq. (8.9) does not explain adequately all the power characteristics of gas–liquid systems. The main reason that gassing affects power consumption is that bubbles have a profound impact on the hydrodynamic behaviour of fluid around the impeller. As described for Rushton turbines and other impellers in Section 8.4, gas-filled cavities develop behind the stirrer blades in aerated liquids. These cavities decrease the drag forces generated at the impeller and significantly reduce the resistance to impeller rotation, thus causing a substantial drop in the power required to operate the stirrer compared with nonaerated conditions.

The relationship between the power drop with gassing and operating conditions such as the gas flow rate and stirrer speed is often represented using graphs such as those shown in Figure 8.32. In these graphs,  $P_g$  is the power required with gassing and  $P_0$  is the power required without gassing;  $P_0$  is the same as the power evaluated using the methods described in Sections 8.5.1 and 8.5.2. The operating conditions are represented by the dimensionless gas flow number  $Fl_g$  defined in Eq. (8.1). Figure 8.32 shows reductions in power as a function of the gas flow number for three different impellers in low-viscosity fluid. Each curve represents experimental data for a given impeller operated at constant stirrer speed (i.e., for each curve, the value of  $Fl_g$  changes only because of changes in the gas flow rate).

As indicated in Figure 8.32(a), power reductions of up to 70% can occur with Rushton turbines in low-viscosity fluids, although most practical operating conditions give a 40 to 50% loss of power. The rheological properties of the fluid exert a considerable influence: power losses of more than 80% occur with Rushton turbines in viscous or non-Newtonian fluids sparged with gas. The fall in power with increasing gas flow rate is due to the increased size and changes in structure of the ventilated cavities behind the blades of Rushton turbines as illustrated in Figure 8.21. The power demand at low gas flows (low  $Fl_g$ ) corresponding to the formation of vortex cavities differs little from that without gassing. With the formation of six clinging cavities at higher gas flow rates, the power requirement is reduced by at most 10% compared with ungassed conditions. Development of the ‘3–3’ cavity structure is associated with a significant reduction in power of up to 60% of the ungassed value. If the gas supply is extended beyond the gas-handling capacity

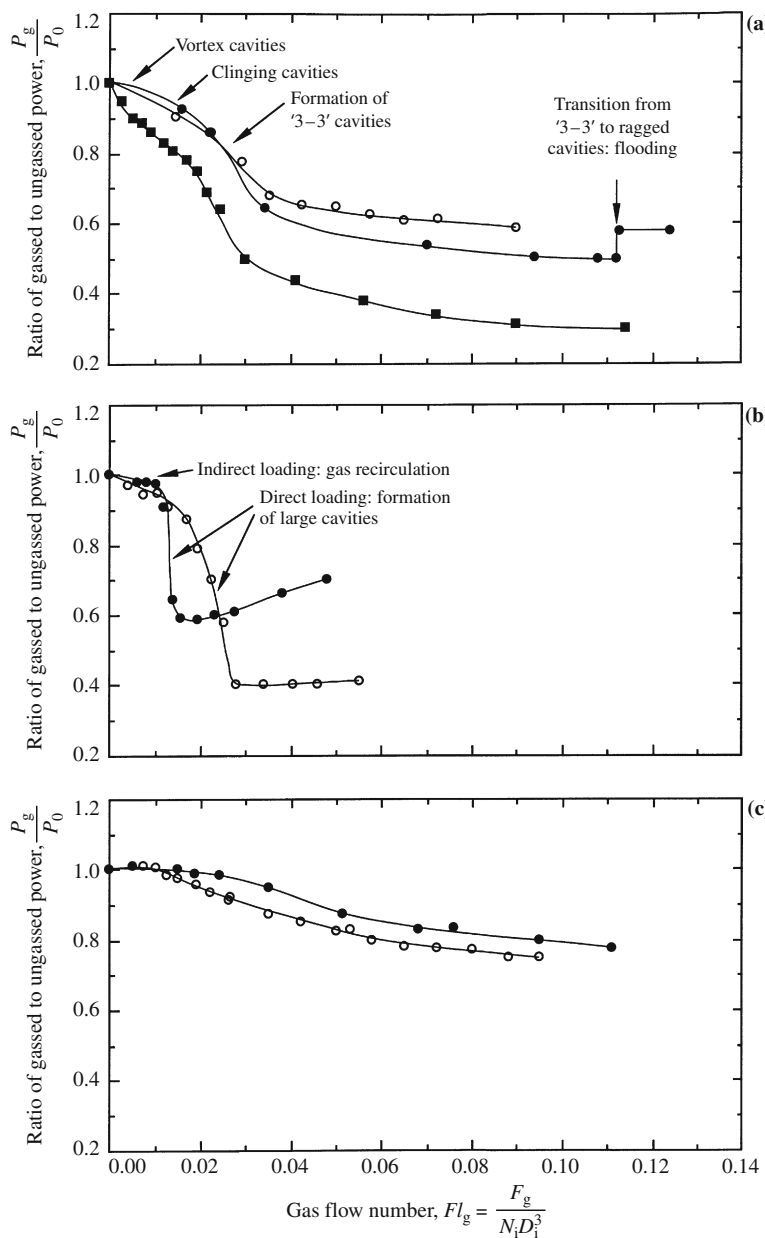


**FIGURE 8.32** Variation in power consumption with gassing  $P_g$  relative to ungassed power consumption  $P_0$  at constant stirrer speed.  $Fl_g$  is dimensionless gas flow number;  $F_g$  is volumetric gas flow rate;  $N_i$  is stirrer speed;  $D_i$  is impeller diameter.

(a) Rushton turbine: (○)  $N_i = 120$  rpm; (●)  $N_i = 150$  rpm; (■)  $N_i = 360$  rpm.

(b) Downward-pumping pitched-blade turbine, six blades are angled 45°: (●)  $N_i = 180$  rpm; (○)  $N_i = 300$  rpm.

(c) Upward-pumping pitched-blade turbine, six blades are angled 45°: (●)  $N_i = 190$  rpm; (○)  $N_i = 236$  rpm.

(a) Data from M.M.C.G. Warmoeskerken, J.M. Smith, and M. Konno, 1985, *On the flooding/loading transition and the complete dispersal condition in aerated vessels agitated by a Rushton-turbine*. In: *Mixing*, Proc. 5th Eur. Conf. on Mixing, pp. 143–154, The Fluid Engineering Centre; and M.M.C.G. Warmoeskerken, J. Feijen, and J.M. Smith, 1981, *Hydrodynamics and power consumption in stirred gas–liquid dispersions*. In: *Fluid Mixing*, IChemE Symp. Ser. 64, J1–J14.

(b) Data from M.M.C.G. Warmoeskerken, J. Speur, and J.M. Smith, 1984, *Gas–liquid dispersion with pitched blade turbines*. Chem. Eng. Commun. 25, 11–29.

(c) Data from W. Bujalski, M. Konno, and A.W. Nienow, 1988, *Scale-up of 45° pitch blade agitators for gas dispersion and solid suspension*. In: *Mixing*, Proc. 6th Eur. Conf. on Mixing, pp. 389–398, The Fluid Engineering Centre.

of the impeller, the formation of six ragged cavities coincides with impeller flooding and a rise in power consumption as indicated in [Figure 8.32\(a\)](#).

Changes in power consumption with gassing for a downward-pumping pitched-blade turbine are shown in [Figure 8.32\(b\)](#). At low gas flow rates corresponding to the indirect loading regime (Section 8.4.3, Downward Pumping subsection), gas flow to the impeller relies on gas recirculation. Under these conditions, the loss of power is relatively small at  $\leq 10\%$ . Depending on the stirrer speed, at higher gas flows there may be a transition to direct loading; this coincides with a sharp decrease in power consumption as large ventilated cavities form behind the impeller blades. The power drawn by downward-pumping pitched-blade turbines can be reduced to as little as 30 to 40% of the power requirements without gassing.

Whereas the power consumption by ungassed upward-pumping pitched-blade turbines is similar to that for downward-pumping turbines of the same geometry ([Table 8.2](#)), as indicated in [Figure 8.32\(c\)](#) there is a much smaller reduction in power with aeration for upward-pumping impellers. Power consumption is reduced by a maximum of only about 20% during upward-pumping operation, even though ventilated cavities form behind the impeller blades.

Power characteristics with aeration have also been measured for the impellers described in [Section 8.4.4](#). When the curved-blade disc turbine shown in [Figure 8.25](#) is rotated clockwise with the concave sides of the blades forward, the curvature of the blades ensures that no large ventilated cavities can form on the convex surfaces. As a consequence, in low-viscosity fluids the power consumption with gassing remains close to that without gassing until impeller flooding occurs. In non-Newtonian or viscous fluids, power losses may be greater at up to about 20% [9]. For the hydrofoil impellers shown in [Figure 8.26](#) operated for downward pumping, depending on the stirrer speed, abrupt reductions in power can accompany the transition from indirect to direct loading as large cavities form behind the blades. However, this drop in power is usually less than that with Rushton turbines under similar conditions [7]. In contrast, for upward-pumping hydrofoils, there is virtually no reduction in power draw with aeration over a wide range of gas flow rates [23].

As indicated in [Figure 8.32](#), there is a strong correlation between the power consumption in gassed liquids and changes in the structure of the ventilated cavities behind the impeller blades. However, although data such as those shown in [Figure 8.32](#) have been measured for different impellers and illustrate how aeration affects power consumption, these graphs cannot be used to predict impeller power requirements with gassing. This limitation is related to the inadequacy of the gas flow number  $Fl_g$  to fully define the hydrodynamic conditions affecting the development of ventilated cavities. Whereas the value of  $Fl_g$  reflects the flow rate of gas from the sparger, the amount of gas actually entering the impeller region depends also on gas recirculation within the fluid. As shown in [Figure 8.32](#), the size of the cavities and therefore the power draw vary with stirrer speed at constant  $Fl_g$ . This indicates that the results for  $P_g/P_0$  are sensitive to aspects of the mixing system not represented by  $Fl_g$ . The exact extent to which power requirements are reduced by sparging is a complex function of the stirrer speed, air flow rate, vessel size, fluid properties, and the geometry of the impeller and tank including the impeller off-bottom clearance and sparger size. Because all of the changes in hydrodynamic behaviour due to gassing are not completely understood, prediction of the power requirements in aerated systems remains difficult and cannot yet be achieved with accuracy.

Although the power requirements in aerated systems depend strongly on the size of the ventilated cavities behind the impeller blades, differences in the power draw with gassing between coalescing and noncoalescing liquids (Section 10.6.2) are small, both for Rushton turbines and for axial-flow impellers such as hydrofoils [2, 24].

Reduction in stirrer power consumption with gassing may seem a desirable feature because of the potential for energy and cost savings during operation of the impeller. However, when all the relevant factors are considered, stirrers with power requirements that are relatively insensitive to gassing are preferred. In the design of fermentation equipment, the stirrer motor is usually sized to allow operation under nonaerated conditions. This is necessary to prevent motor burn-out if there is a failure of air supply during operation of the fermenter: the stirrer motor must be large enough to provide sufficient power during any abrupt change from gassed to ungassed conditions. In addition, medium in fermenters is often mixed without aeration during the heating and cooling cycles of *in situ* batch sterilisation (Section 14.6.1). Therefore, the decrease in impeller power consumption with gassing represents an under-utilisation of the capacity of the stirrer motor. As outlined in Chapter 10 (Section 10.9), the rate of oxygen transfer from gas to liquid in aerated systems depends on the power input to the fluid; therefore, any reduction in power diminishes the effectiveness of mass transfer in the system with potential deleterious consequences for culture performance. Power losses may also reduce the ability of the stirrer to maintain complete suspension of solids. For example, the sudden reductions in power shown in [Figure 8.32\(a\)](#) and [\(b\)](#) can result in severe loss of suspension capacity, with the result that cells begin to settle out on the vessel floor. An additional problem with stirrers that lose power with aeration is our inability to predict the exact extent of the power loss and the conditions under which it will occur. This creates some degree of uncertainty in the operation of gassed stirrer systems. All of these factors have promoted interest in the development of impellers such as the curved-blade disc turbine and upward-pumping hydrofoils, for which there is minimal reduction in power draw with gassing.

## 8.6 POWER INPUT BY GASSING

In addition to mechanical stirring, gas sparging itself contributes to the total power input to bioreactors during operation under aerated conditions. The power input from sparging,  $P_v$ , can be calculated using the equation:

$$P_v = F_g \rho g H_L \quad (8.13)$$

where  $F_g$  is the volumetric flow rate of gas at the temperature and average pressure of the liquid in the tank,  $\rho$  is the liquid density,  $g$  is gravitational acceleration, and  $H_L$  is the liquid height. For aerated vessels stirred with an impeller,  $P_v$  is usually only a small fraction of the total power input and is often neglected. However, if high gas flow rates are used at low stirrer speeds, for example in reactors that rely mainly on gas sparging for mixing with the stirrer playing a relatively minor role, the contribution of  $P_v$  to the total power input can be more substantial.

## 8.7 IMPELLER PUMPING CAPACITY

Fluid is pumped by the blades of rotating impellers. The volumetric flow rate of fluid leaving the blades varies with operating parameters such as the stirrer speed and size of the impeller, but is also a characteristic of the impeller type or design. The effectiveness of impellers for pumping fluid is represented by a dimensionless number called the *flow number*:

$$Fl = \frac{Q}{N_i D_i^3} \quad (8.14)$$

where  $Fl$  is the flow number,  $Q$  is the volumetric flow rate of fluid leaving the impeller blades,  $N_i$  is the stirrer speed, and  $D_i$  is the impeller diameter. The flow number is a measure of the ability of the impeller to generate strong circulatory flows, such as those necessary for blending operations and solids suspension.

The value of  $Q$  during impeller operation can be obtained by measuring local fluid velocities near the impeller blades using techniques such as laser Doppler velocimetry (Section 7.9.3). Typical fluid discharge velocity profiles for radial- and axial-flow turbines are shown in Figure 8.33. For radial-flow impellers, the mean discharge velocity is maximum at the centre line of the blade and decays above and below the centre line to form a bell-shaped curve, as illustrated in Figure 8.33(a). As well as fluid leaving the edge of the blade directly, from which  $Q$  is evaluated, there is also significant additional flow of entrained fluid above and below the blade that is swept along by the direct discharge stream. The total discharge flow from the impeller region including the entrained fluid can be several times greater than  $Q$ . The discharge velocity profile for an axial-flow turbine is shown in Figure 8.33(b). In this case,  $Q$  is the volumetric flow rate of fluid leaving directly from the lower edges of the blades, excluding entrained flow from the surrounding region.

Values of the flow number  $Fl$  for several impellers operating in the turbulent regime in low-viscosity fluids without gassing are listed in Table 8.3.  $Fl$  is dependent on the vessel and blade geometry; however this dependence and the variation of  $Fl$  between impeller types is not as great as for the turbulent power number  $N'_P$ .

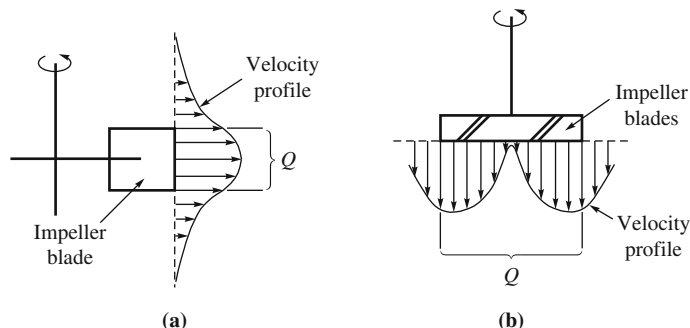


FIGURE 8.33 Graphic of discharge velocity profiles from the blades of: (a) a radial-flow impeller and (b) an axial-flow impeller.

**TABLE 8.3** Values of the Turbulent Ungassed Flow Number  $Fl$  for a Selection of Different Impellers in Baffled Tanks Containing Low-Viscosity Fluid

| Impeller  | $Fl$ | Reference |
|---|------|-----------|
| Rushton turbine   | 0.78 | [25]      |
| Propeller<br>3 blades   | 0.73 | [26]      |
| Pitched-blade turbine<br>Downward pumping<br>4 blades, $45^\circ$ | 0.75 | [4]       |
| Pitched-blade turbine<br>Downward pumping<br>6 blades, $45^\circ$ | 0.81 | [27]      |
| Hydrofoil (Lightnin A315)<br>Downward pumping<br>4 blades         | 0.74 | [27]      |
| Hydrofoil (Prochem Maxflo T)<br>Downward pumping<br>6 blades      | 0.82 | [17]      |

The effectiveness of different impellers for generating flow can be compared relative to their power requirements. Combination of Eqs. (8.14) and (8.9) yields an expression for the impeller discharge flow rate per unit power consumed:

$$\frac{Q}{P} = \frac{Fl}{N'_P \rho N_i^2 D_i^2} \quad (8.15)$$

Therefore, if two different impellers of the same size are operated in the same fluid at the same stirrer speed, their pumping efficiencies can be compared using the ratio:

$$\frac{\left(\frac{Q}{P}\right)_{\text{impeller 1}}}{\left(\frac{Q}{P}\right)_{\text{impeller 2}}} = \frac{\left(\frac{Fl}{N'_P}\right)_{\text{impeller 1}}}{\left(\frac{Fl}{N'_P}\right)_{\text{impeller 2}}} \quad (8.16)$$

We can compare the pumping efficiencies of Rushton and pitched-blade turbines using Eq. (8.16) and values of  $N'_P$  and  $Fl$  from Tables 8.2 and 8.3. For a Rushton turbine with  $D_i/D_T = 0.50$ ,  $N'_P = 5.9$  and  $Fl = 0.78$ . For a six-blade downward-pumping pitched-blade turbine of the same size,  $N'_P = 1.6$  and  $Fl = 0.81$ . Therefore:

$$\frac{\left(\frac{Q}{P}\right)_{\text{pitched-blade}}}{\left(\frac{Q}{P}\right)_{\text{Rushton}}} = \frac{\left(\frac{0.81}{1.6}\right)}{\left(\frac{0.78}{5.9}\right)} = 3.8 \quad (8.17)$$

This result indicates that pitched-blade turbines produce almost four times the flow for the same power input as Rushton turbines. The analysis provides an explanation for why Rushton turbines are considered to have relatively low pumping efficiency (Section 8.4.1, Without Gassing subsection), while pitched-blade turbines are recognised for their high pumping capacity and effectiveness for blending operations (Section 8.4.3). A comparison of Rushton turbines with hydrofoil impellers yields similar results. The analysis applies only for ungassed liquids; the effect of gassing on liquid pumping rates and power consumption varies considerably between different impellers.

## 8.8 SUSPENSION OF SOLIDS

Bioreactors used for cell culture contain biomass solids of varying size. Microorganisms such as single-cell bacteria and yeast are small and finely divided; other cells such as mycelia and plant cells form macroscopic aggregates or clumps depending on the culture conditions. Because cells contain a high percentage of water, the difference in density between the solid phase and the suspending liquid is generally very small. However, in some bioprocesses, cells are immobilised on or in solid matrices of varying material density. These systems include anchorage-dependent animal cells cultured on microcarrier beads, and bacteria attached to sand grains for waste water treatment.

One of the functions of mixing in stirred fermenters is to maintain the cells in suspension. Accumulation of biomass at the bottom of the vessel is highly undesirable, as cells within settled layers have poor access to nutrients and oxygen and can become starved of these components. It is important, therefore, to know what operating conditions are required to completely suspend solids in stirred tanks.

### 8.8.1 Without Gassing

A common criterion used to define complete suspension of solids is that no particle should remain motionless on the bottom of the vessel for more than 1 to 2 seconds. Applying this criterion, the Zwietering equation [28]:

$$N_{JS} = \frac{S \nu_L^{0.1} D_p^{0.2} \left[ g(\rho_p - \rho_L)/\rho_L \right]^{0.45} X^{0.13}}{D_i^{0.85}} \quad (8.18)$$

is generally accepted as the best correlation for  $N_{JS}$ , the stirrer speed required for just complete suspension of solids in the absence of gassing. In Eq. (8.18),  $S$  is a dimensionless parameter dependent on the impeller and tank geometry,  $\nu_L$  is the liquid kinematic viscosity (Section 7.3),  $D_p$  is the diameter of the solid particles,  $g$  is gravitational acceleration,  $\rho_p$  is the particle density,  $\rho_L$  is the liquid density,  $X$  is the weight percentage of particles in the suspension, and  $D_i$  is the impeller diameter.

Zwietering's equation has been subjected to extensive testing over many years using a wide range of system properties. The exponents in Eq. (8.18) are independent of the tank size, impeller type, impeller-to-tank diameter ratio, and impeller off-bottom clearance;

TABLE 8.4 Values of the Geometric Parameter S in Eq. (8.18) for Flat-Bottom Tanks

| Impeller                        | $D_i/D_T$ | $C_i/D_T$ | S    | Reference |
|---------------------------------|-----------|-----------|------|-----------|
| Rushton                         | 0.25      | 0.25      | 12   | [12]      |
|                                 | 0.33      | 0.17      | 5.8  | [12]      |
|                                 | 0.33      | 0.25      | 6.7  | [12]      |
|                                 | 0.33      | 0.50      | 8.0  | [12]      |
|                                 | 0.50      | 0.25      | 4.25 | [12]      |
|                                 | 0.50      | 0.17      | 3.9  | [29]      |
| Propeller                       | 0.33      | 0.25      | 6.6  | [29]      |
| Pitched-blade turbine           | 0.33      | 0.20      | 5.7  | [30]      |
| Downward pumping, 4 blades, 45° | 0.33      | 0.25      | 6.2  | [30]      |
|                                 | 0.33      | 0.33      | 6.8  | [30]      |
|                                 | 0.33      | 0.50      | 11.5 | [30]      |
|                                 | 0.50      | 0.25      | 5.8  | [12]      |
| Pitched-blade turbine           | 0.50      | 0.25      | 5.7  | [29]      |
| Downward pumping, 6 blades, 45° |           |           |      |           |
| Pitched-blade turbine           | 0.50      | 0.25      | 6.9  | [31]      |
| Upward pumping, 6 blades, 45°   |           |           |      |           |

these geometric factors are reflected in the value of  $S$ . Table 8.4 lists some values of  $S$  for different impeller geometries; these data were obtained using flat-bottomed cylindrical vessels with four baffles of width 1/10 the tank diameter and liquid height equal to the tank diameter.

$N_{JS}$  decreases significantly as the size of the impeller increases, not only because of the direct effect of  $D_i$  in Eq. (8.18) but also because the  $D_i/D_T$  ratio changes the value of  $S$ . For a fixed impeller off-bottom clearance, a general relationship is:

$$S \propto \left(\frac{D_T}{D_i}\right)^\alpha \quad (8.19)$$

where  $\alpha$  is approximately 1.5 for Rushton turbines and 0.82 for propellers [28]. For many impellers,  $S$  is sensitive to the impeller off-bottom clearance ratio  $C_i/D_T$ . As shown in Table 8.4 for Rushton and pitched-blade turbines,  $S$  at constant  $D_i/D_T$  decreases as the impeller clearance is reduced, so that lower stirrer speeds are required for complete suspension. The shape of the base of the vessel (Figure 8.2) also influences the efficiency of solids suspension, with dished, contoured, and cone-and-fillet bases offering advantages in some cases for reducing  $S$ . The extent of this effect depends, however, on the type of flow pattern generated by the impeller [14, 29, 32]. The presence of obstructions near the vessel floor, such as large sparger pipes or the bearing and seal housing for bottom-entry stirrers, can significantly impede solids suspension. Under these conditions, application of Eq. (8.18) will result in substantial underestimation of  $N_{JS}$ .

Even if a stirrer is operated at speeds equal to or above  $N_{JS}$  to obtain complete particle suspension, this does not guarantee that the suspension is homogeneous throughout the tank. Although, in general, speeds considerably higher than  $N_{JS}$  are required to achieve uniform particle concentration, for small particles such as dispersed cells with density similar to that of the suspending liquid, a reasonable degree of homogeneity can be expected at  $N_{JS}$ . In some respects, the criterion of complete solids suspension is a severe one, as suspension of the final few particles can require a disproportionately large increase in power—for example, as much as 100% [6]. In some systems, an adequate level of solids suspension may be achieved at stirrer speeds lower than  $N_{JS}$ .

### EXAMPLE 8.3 SOLIDS SUSPENSION

Clump-forming fungal cells are cultured in a flat-bottomed 10-m<sup>3</sup> fermenter of diameter 2.4 m equipped with a Rushton turbine of diameter 1.2 m operated at 50 rpm. The impeller off-bottom clearance is 0.6 m. The density of the fermentation medium is 1000 kg m<sup>-3</sup> and the viscosity is 0.055 Pa s. The density and diameter of the cell clumps are 1035 kg m<sup>-3</sup> and 600 μm, respectively. The concentration of cells in the fermenter reaches 40% w/w. Are the cells suspended under these conditions?

#### Solution

$D_i/D_T = 0.50$  and  $C_i/D_T = 0.25$ . Therefore, from Table 8.4,  $S = 4.25$ . From Eq. (2.16),  $g = 9.81 \text{ m s}^{-2}$ . From Table A.9 in Appendix A,  $1 \text{ Pa s} = 1 \text{ kg m}^{-1} \text{ s}^{-1}$ . Therefore, using Eq. (7.9) to calculate the kinematic viscosity:

$$\nu_L = \frac{0.055 \text{ kg m}^{-1} \text{ s}^{-1}}{1000 \text{ kg m}^{-3}} = 5.5 \times 10^{-5} \text{ m}^2 \text{ s}^{-1}$$

Substituting values into Eq. (8.18) gives:

$$N_{JS} = \frac{4.25 (5.5 \times 10^{-5} \text{ m}^2 \text{ s}^{-1})^{0.1} (600 \times 10^{-6} \text{ m})^{0.2} \left( 9.81 \text{ m s}^{-2} \frac{(1035 - 1000) \text{ kg m}^{-3}}{1000 \text{ kg m}^{-3}} \right)^{0.45} 40^{0.13}}{(1.2 \text{ m})^{0.85}}$$

$$N_{JS} = 0.31 \text{ s}^{-1} = 18.6 \text{ rpm}$$

The operating stirrer speed of 50 rpm is well above the stirrer speed required for solids suspension. The cells are therefore completely suspended.

As illustrated in Example 8.3, complete suspension of cells and small cell clumps is generally achieved at low to moderate stirrer speeds. This is due mainly to the small size and almost neutral density (i.e., density close to that of the suspending liquid) of the cells.

### 8.8.2 With Gassing

The formation of ventilated cavities behind impeller blades reduces the power draw and liquid pumping capacity of the impeller, with the result that higher stirrer speeds are often required for solids suspension in aerated systems. If the fall in power with gassing is severe—for example, as shown in [Figure 8.32\(b\)](#) for downward-pumping pitched-blade turbines—there may be a corresponding sudden loss of solids suspension capacity.

Equations relating  $N_{JSg}$ , the stirrer speed required for just complete suspension of solids in the presence of gassing, to  $N_{JS}$  have been developed for various impellers [3, 31]. For Rushton turbines of two different sizes with an impeller off-bottom clearance of one-quarter the tank diameter [3]:

$$N_{JSg} = N_{JS} + 2.4 F_{gv} \quad \text{for } D_i/D_T = 0.33 \quad (8.20)$$

$$N_{JSg} = N_{JS} + 0.94 F_{gv} \quad \text{for } D_i/D_T = 0.50 \quad (8.21)$$

where  $F_{gv}$  is the gas flow rate in units of vvm or volume of gas per volume of liquid per minute, and  $N_{JS}$  and  $N_{JSg}$  both have units of  $s^{-1}$ . The above equations apply when the impeller is not flooded; however, they may not apply for suspension of low-density particles with  $(\rho_p - \rho_L)$  less than about  $50 \text{ kg m}^{-3}$  [33], or at very low gas flow rates [34]. In both these cases, gassing has been shown to aid rather than hinder suspension. Solids suspension in aerated systems is sensitive to several aspects of tank geometry such as the impeller off-bottom clearance and the impeller–sparger separation [3, 14].

## 8.9 MECHANISMS OF MIXING

In this section we consider the mechanisms controlling the rate of mixing in stirred tanks containing a single liquid phase. As illustrated schematically in [Figures 8.7 and 8.8](#), large liquid circulation loops develop in stirred vessels. For mixing to be effective, the velocity of fluid leaving the impeller must be sufficient to carry material into the most remote regions of the tank; fluid circulated by the impeller must also sweep the entire vessel in a reasonable time. In addition, turbulence must be developed in the fluid as mixing is certain to be poor unless flow is turbulent. All these factors are important in mixing, which can be described as a combination of three physical processes:

- Distribution
- Dispersion
- Diffusion

Distribution is sometimes called *macromixing*; diffusion is also called *micromixing*. Dispersion can be classified as either micro- or macromixing depending on the scale of fluid motion.

The pattern of bulk fluid flow in a baffled vessel stirred by a centrally located radial-flow impeller is shown in detail in [Figure 8.34](#). Due to the periodic pumping action of the impeller, the contents of the vessel are recirculated through the mixing zone in a very regular manner. Near the impeller there is a zone of intense turbulence where fluid currents converge and exchange material. However, as fluid moves away from the impeller, flow

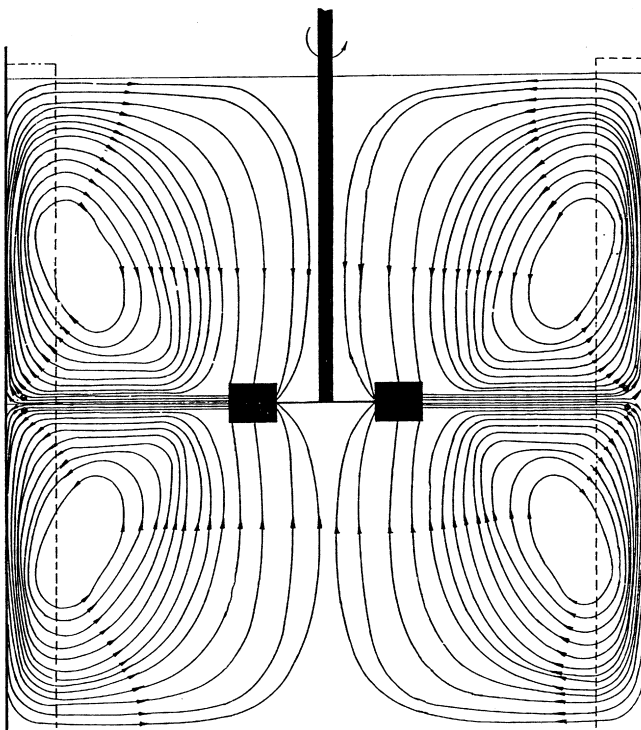


**FIGURE 8.34** Flow pattern developed by a centrally located radial-flow impeller. From R.M. Voncken, J.W. Rotte, and A.Th. ten Houten, 1965, *Circulation model for continuous-flow, turbine-stirred, baffled tanks*. In: Mixing—Theory Related to Practice, Proc. Symp. 10, AIChE–IChemE Joint Meeting, London.

becomes progressively slower and less turbulent. In large tanks, streamline or laminar flow may develop in these local regions. Under these conditions, because fluid elements move mostly parallel to each other in streamline flow (Section 7.2.1), mixing is not very effective away from the impeller zone.

Let us consider what happens when a small amount of liquid dye is dropped onto the top of the fluid in Figure 8.34. First, the dye is swept by circulating currents down to the impeller. At the impeller there is vigorous and turbulent motion of fluid; the dye is mechanically dispersed into smaller volumes and distributed between the large circulation loops. These smaller parcels of dye are then carried around the tank, dispersing all the while into those parts of the system not yet containing dye. Returning again to the impeller, the dye aliquots are broken up into even smaller volumes for further distribution. After a time, dye is homogeneously distributed throughout the tank and achieves a uniform concentration.

The process whereby dye is transported to all regions of the vessel by bulk circulation currents is called *distribution*. Distribution is an important process in mixing but can be relatively slow. In large tanks, the size of the circulation paths is large and the time taken to traverse them is long; this, together with the regularity of fluid pumping at the impeller, inhibits rapid mixing. Accordingly, *distribution is often the slowest step in the mixing process*. If the stirrer speed is sufficiently high, superimposed on the distribution process is turbulence. In turbulent flow, the fluid no longer travels along streamlines but moves erratically in the form of cross-currents; this enhances the mixing process at scales much smaller than

the scale of bulk circulation. As described in Section 7.9.1 (Eddies and Scales of Turbulence subsection), the kinetic energy of turbulent fluid is directed into regions of rotational flow called *eddies*; masses of eddies of various size coexist in turbulent flow. Large eddies are continuously formed from the bulk flow generated by the stirrer; these break down into small eddies that produce even smaller eddies. Eddies, like spinning tops, possess kinetic energy that is transferred to eddies of decreasing size. When the eddies become very small they can no longer sustain rotational motion and their kinetic energy is dissipated as heat. At steady state in a mixed tank, most of the energy from the stirrer is dissipated through the eddies as heat; energy lost in other processes (e.g., fluid collision with the tank walls) is generally negligible.

The process of breaking up the bulk flow into smaller and smaller eddies is called *dispersion*. Dispersion facilitates rapid transfer of material throughout the vessel. The degree of homogeneity possible as a result of dispersion is limited by the size of the smallest eddies that may be formed in a particular fluid. This size is given approximately as the *Kolmogorov scale of mixing or scale of turbulence*,  $\lambda$ , defined in Eq. (7.36) as:

$$\lambda = \left( \frac{\nu^3}{\varepsilon} \right)^{1/4} \quad (7.36)$$

where  $\lambda$  is the characteristic dimension of the smallest eddies,  $\nu$  is the kinematic viscosity of the fluid (Section 7.3), and  $\varepsilon$  is the local rate of turbulence energy dissipation per unit mass of fluid. At steady state, the average rate of energy dissipation by turbulence over the entire tank is equal to the power input to the fluid by the impeller; this power input is the same as that estimated using the methods of [Section 8.5](#). According to Eq. (7.36), the greater the power input to the fluid, the smaller are the eddies.  $\lambda$  is also dependent on viscosity: at a given power input, smaller eddies are produced in low-viscosity fluids. For low-viscosity liquids such as water,  $\lambda$  is usually in the range 30 to 100  $\mu\text{m}$ . For such fluids, this is the smallest scale of mixing achievable by dispersion.

Within eddies, flow of fluid is rotational and occurs in streamlines. Because streamline flow does not facilitate mixing, to achieve mixing on a scale smaller than the Kolmogorov scale, we must rely on *diffusion*. Molecular diffusion is generally regarded as a slow process; however, over small distances it can be accomplished quite rapidly. Within eddies of diameter 30 to 100  $\mu\text{m}$ , homogeneity is achieved in about 1 s for low-viscosity fluids. Consequently, if the power input to a stirred vessel produces eddies of this dimension, mixing on a molecular scale is accomplished virtually simultaneously.

## 8.10 ASSESSING MIXING EFFECTIVENESS

As explained in the last section, to achieve rapid mixing in a stirred tank, the agitator must provide good bulk circulation or macromixing. Micromixing at or near the molecular scale is also important, but occurs relatively quickly compared with macromixing. Mixing effectiveness is therefore usually a reflection of the rate of bulk flow.

*Mixing time* is a useful parameter for assessing the overall speed of mixing in stirred vessels. The mixing time  $t_m$  is the time required to achieve a given degree of homogeneity

starting from the completely segregated state. It can be measured by injecting a tracer into the vessel and following its concentration at a fixed point in the tank. Tracers in common use include acids, bases, and concentrated salt solutions; corresponding detectors are pH probes and conductivity cells. Mixing time can also be determined by measuring the temperature response after addition of a small quantity of heated liquid.

Let us assume that a small pulse of tracer is added to fluid in a stirred tank already containing tracer material at concentration  $C_i$ . When flow in the system is circulatory, the tracer concentration measured at some fixed point in the tank can be expected to follow a pattern similar to that shown in Figure 8.35. Before mixing is complete, a relatively high concentration will be detected every time the bulk flow brings tracer to the measurement point. The peaks in concentration will be separated by a period approximately equal to the average time required for fluid to traverse one bulk circulation loop. In stirred vessels this period is called the *circulation time*,  $t_c$ . After several circulations the desired degree of homogeneity is reached.

Definition of the mixing time  $t_m$  depends on the degree of homogeneity required. Usually, mixing time is defined as the time after which the concentration of tracer differs from the final concentration  $C_f$  by less than 10% of the total concentration difference ( $C_f - C_i$ ). However, there is no single, universally applied definition of mixing time; sometimes deviations greater or less than 10% are specified. Nevertheless, at  $t_m$  the tracer concentration is relatively steady and the fluid composition approaches uniformity. Industrial-scale stirred vessels with working volumes between 1 and 100 m<sup>3</sup> have mixing times between about 30 and 120 s, depending on conditions. For rapid and effective mixing,  $t_m$  should be as small as possible.

Intuitively, we can predict that the mixing time in stirred tanks will depend on variables such as the size of the tank and impeller, the fluid properties, and the stirrer speed. The relationship between mixing time and several of these variables has been determined experimentally for different impellers: results for a Rushton turbine in a baffled tank are shown in Figure 8.36. The dimensionless product  $N_i t_m$ , which is also known as the *homogenisation number* or *dimensionless mixing time*, is plotted as a function of the impeller

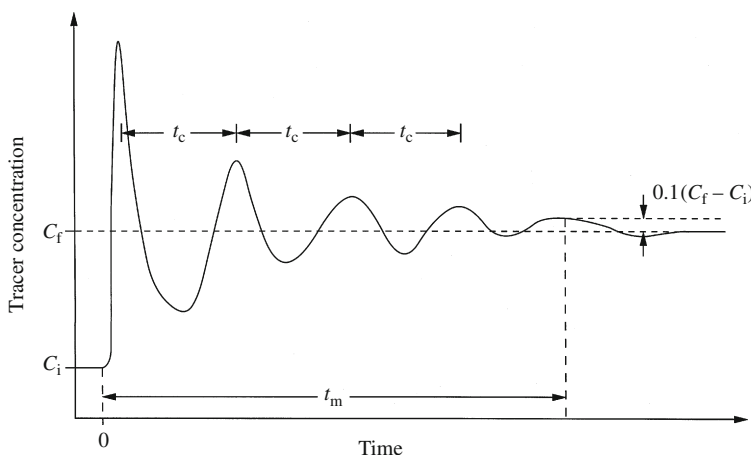


**FIGURE 8.35** Concentration response after dye is injected into a stirred tank.

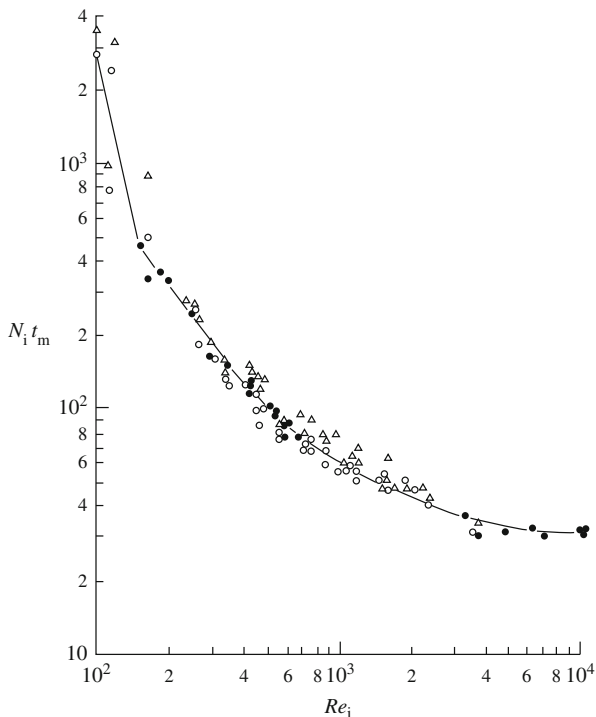


**FIGURE 8.36** Variation of mixing time with Reynolds number for a Rushton turbine in a baffled tank. The impeller is located one-third the tank diameter off the floor of the vessel, the impeller diameter is one-third the tank diameter, the liquid height is equal to the tank diameter, and the tank has four baffles of width one-tenth the tank diameter. Several measurement techniques and tank sizes were used: (●) thermal method, vessel diameter 1.8 m; (○) thermal method, vessel diameter 0.24 m; (Δ) decolouration method, vessel diameter 0.24 m.

Reprinted from C.J. Hoogendoorn and A.P. den Hartog, Model studies on mixers in the viscous flow region, Chem. Eng. Sci. 22, 1689–1699. Copyright 1967, with permission from Pergamon Press Ltd, Oxford.

Reynolds number  $Re_i$ ;  $t_m$  is the mixing time based on a 10% deviation from the total change in conditions, and  $N_i$  is the rotational speed of the stirrer. Conceptually,  $N_i t_m$  represents the number of stirrer rotations required to homogenise the liquid after addition of a small pulse of tracer. At relatively low Reynolds numbers in the laminar–transition regime,  $N_i t_m$  increases significantly with decreasing  $Re_i$ . However, as the Reynolds number is increased,  $N_i t_m$  approaches a constant value that persists into the turbulent regime at  $Re_i$  above about  $5 \times 10^3$ . The relationship between  $N_i t_m$  and  $Re_i$  for most other impellers is qualitatively similar to that shown in Figure 8.36 [10]; in practice, therefore, we can assume that  $N_i t_m$  reaches a constant value in turbulent flow. With  $N_i t_m$  constant, mixing time reduces in direct proportion to increase in stirrer speed.

An equation has been developed for estimating the mixing time in stirred vessels under turbulent flow conditions. This expression for  $t_m$  can be applied irrespective of the type of impeller used [35, 36]:

$$t_m = 5.9 D_T^{2/3} \left( \frac{\rho V_L}{P} \right)^{1/3} \left( \frac{D_T}{D_i} \right)^{1/3} \quad (8.22)$$

where  $t_m$  is the mixing time,  $D_T$  is the tank diameter,  $\rho$  is the liquid density,  $V_L$  is the liquid volume,  $P$  is the power input, and  $D_i$  is the impeller diameter. Equation (8.22) applies to baffled vessels stirred with a single impeller and with liquid height equal to the tank diameter. The relationship has been verified using a range of different impellers with

$0.2 \leq D_i/D_T \leq 0.7$  in vessels of diameter up to 2.7 m. The equation is also valid under aerated conditions provided the impeller disperses the gas effectively (i.e., is not flooded) and  $P$  is the power drawn with gassing [36]. As Eq. (8.22) does not depend on the type of impeller, we can deduce that all impellers are equally energy efficient with respect to mixing time. Equation (8.22) indicates that, for a tank of fixed diameter and liquid volume, mixing time is reduced if we use a large impeller and a high power input.

For a cylindrical tank with liquid height equal to the tank diameter, the geometric formula for the volume of a cylinder is:

$$V_L = \frac{\pi}{4} D_T^3 \quad (8.23)$$

Also, as Eq. (8.22) applies under turbulent conditions, we can express  $P$  in terms of the turbulent power number  $N'_P$  using Eq. (8.9). Substituting Eqs. (8.9) and (8.23) into Eq. (8.22) gives:

$$t_m = \frac{5.4}{N_i} \left( \frac{1}{N'_P} \right)^{1/3} \left( \frac{D_T}{D_i} \right)^2 \quad (8.24)$$

Equation (8.24) indicates that mixing time reduces in direct proportion to stirrer speed. This is the same as saying that  $N_i t_m$  for a given impeller and tank geometry is constant for turbulent flow, as discussed earlier with reference to Figure 8.36. At constant  $N_i$ ,  $t_m$  is directly proportional to  $(D_T/D_i)^2$ , showing that mixing times can be reduced significantly using impellers with large  $D_i/D_T$  ratio. However, because of the strong influence of impeller diameter on power requirements (Section 8.5.1), increasing  $D_i$  also raises the power consumption, so there will be a cost associated with using this strategy to improve mixing.

#### EXAMPLE 8.4 ESTIMATION OF MIXING TIME

A baffled fermenter with tank diameter and liquid height equal to 1.2 m is stirred using a six-blade downward-pumping Prochem Maxflo T hydrofoil impeller. The impeller diameter is 0.42 m and the stirrer speed is  $1.5 \text{ s}^{-1}$ . The viscosity of the fermentation broth is  $10^{-2} \text{ Pa s}$  and the density is  $1000 \text{ kg m}^{-3}$ . Estimate the mixing time under nonaerated conditions.

##### Solution

From Eq. (7.2):

$$Re_i = \frac{1.5 \text{ s}^{-1} (0.42 \text{ m})^2 1000 \text{ kg m}^{-3}}{10^{-2} \text{ kg m}^{-1} \text{ s}^{-1}} = 2.6 \times 10^4$$

Flow is turbulent for remote-clearance impellers at this Reynolds number; therefore Eq. (8.24) can be used to calculate  $t_m$ . From Table 8.2,  $N'_P$  for this hydrofoil impeller is equal to 1.6. Therefore:

$$t_m = \frac{5.4}{1.5 \text{ s}^{-1}} \left( \frac{1}{1.6} \right)^{1/3} \left( \frac{1.2 \text{ m}}{0.42 \text{ m}} \right)^2 = 25.1 \text{ s}$$

The mixing time is 25 s.

Because the parameters affecting mixing efficiency also affect stirrer power requirements, it is not always possible to achieve small mixing times without consuming enormous amounts of energy, especially in large vessels. Relationships between power requirements, mixing time, and tank size are explored further in the following section.

## 8.11 SCALE-UP OF MIXING SYSTEMS

Design of industrial-scale bioprocesses is usually based on the performance of small-scale prototypes. It is always better to know whether a particular process will work properly before it is constructed in full size: determining optimum operating conditions at production scale is expensive and time-consuming. Ideally, scale-up should be carried out so that conditions in the large vessel are as close as possible to those producing good results at the smaller scale. As mixing is of critical importance in bioreactors, it would seem desirable to keep the mixing time constant on scale-up. Unfortunately, as explained in this section, the relationship between mixing time and power consumption makes this rarely possible in practice.

Suppose a cylindrical 1-m<sup>3</sup> pilot-scale stirred tank is scaled up to 100 m<sup>3</sup>. Let us consider the power required to maintain the same mixing time in the large and small vessels. From Eq. (8.22), equating  $t_m$  values gives:

$$5.9 D_{T1}^{2/3} \left( \frac{\rho_1 V_{L1}}{P_1} \right)^{1/3} \left( \frac{D_{T1}}{D_{i1}} \right)^{1/3} = 5.9 D_{T2}^{2/3} \left( \frac{\rho_2 V_{L2}}{P_2} \right)^{1/3} \left( \frac{D_{T2}}{D_{i2}} \right)^{1/3} \quad (8.25)$$

where subscript 1 refers to the small-scale system and subscript 2 refers to the large-scale system. If the tanks are geometrically similar, the ratio  $D_T/D_i$  is the same at both scales. Similarly, the fluid density will be the same before and after scale-up, and we can also cancel the constant multiplier from both sides. Therefore, Eq. (8.25) reduces to:

$$D_{T1}^{2/3} \left( \frac{V_{L1}}{P_1} \right)^{1/3} = D_{T2}^{2/3} \left( \frac{V_{L2}}{P_2} \right)^{1/3} \quad (8.26)$$

Cubing both sides of Eq. (8.26) and rearranging gives:

$$P_2 = P_1 \left( \frac{D_{T2}}{D_{T1}} \right)^2 \frac{V_{L2}}{V_{L1}} \quad (8.27)$$

The geometric relationship between  $V_L$  and  $D_T$  is given by Eq. (8.23) for cylindrical tanks with liquid height equal to the tank diameter. Solving Eq. (8.23) for  $D_T$  gives:

$$D_T = \left( \frac{4V_L}{\pi} \right)^{1/3} \quad (8.28)$$

Substituting this expression into Eq. (8.27) for both scales gives:

$$P_2 = P_1 \left( \frac{V_{L2}}{V_{L1}} \right)^{5/3} \quad (8.29)$$

In our example of scale-up from  $1\text{ m}^3$  to  $100\text{ m}^3$ ,  $V_{L2} = 100 V_{L1}$ . Therefore, the result from Eq. (8.29) is that  $P_2 = \sim 2000 P_1$ ; that is, the power required to achieve equal mixing time in the  $100\text{-m}^3$  tank is  $\sim 2000$  times greater than in the  $1\text{-m}^3$  vessel. This represents an extremely large increase in power, much greater than is economically or technically feasible with most equipment used for stirring. This example illustrates why the criterion of constant mixing time can hardly ever be applied for scale-up. Because the implications for power consumption are impractical, it is inevitable that mixing times increase with scale.

Reduced culture performance and productivity often accompany scale-up of bioreactors as a result of lower mixing efficiencies and consequent alteration of the physical environment. One way to improve the design procedure is to use *scale-down methods*. The general idea behind scale-down is that small-scale experiments to determine operating parameters are carried out under conditions that can actually be realised, physically and economically, at the production scale. For example, if we decide that power input to a large-scale vessel cannot exceed a certain limit, we can calculate the corresponding mixing time in the larger vessel, then use an appropriate power input to a small-scale reactor to simulate the mixing conditions that are in the large-scale system. Using this approach, as long as the flow regime (e.g., turbulent flow) is the same in the small- and large-scale fermenters, there is a better chance that the results achieved in the small-scale unit will be reproducible in the larger system.

## 8.12 IMPROVING MIXING IN FERMENTERS

Because of the limitations outlined in the previous section, longer mixing times are often unavoidable when stirred vessels are scaled up in size. In these circumstances, it is not possible to reduce mixing times sufficiently by simply raising the power input to the stirrer. In this section we consider methods for improving mixing in stirred tanks that do not involve consumption of significantly greater amounts of energy.

### 8.12.1 Impeller and Vessel Geometry

Mixing can sometimes be improved by changing the system's physical configuration.

- Baffles should be installed; this is routine for stirred fermenters and produces greater turbulence.
- For efficient mixing, the impeller should be mounted below the geometric centre of the vessel. For example, mixing by radial impellers such as Rushton turbines is facilitated when the circulation currents below the impeller are smaller than those above (as shown in Figure 8.7), as this makes the upper and lower circulation loops asynchronous. Under these conditions, fluid particles leaving the impeller at the same instant but entering different circulation paths take different periods of time to return and exchange material. The rate of distribution throughout the vessel is increased when the same fluid particles from different circulation loops do not meet each other every time they return to the impeller region.

- For two- and three-phase mixing (i.e., in gas–liquid and gas–liquid–solid systems), good mixing includes achieving complete gas dispersion and solids suspension. These stirrer functions are sensitive to various aspects of tank geometry, including the impeller off-bottom clearance, type of sparger, clearance between the sparger and the impeller, and base profile of the tank. Optimisation of these features of the system can yield considerable improvements in mixing effectiveness without necessarily requiring large amounts of extra power.
- Although installation of multiple impellers on the same stirrer shaft may seem a solution to problems of poor mixing, as discussed further in [Section 8.13](#), the power required increases substantially when extra impellers are fitted. Furthermore, depending on the impeller design and the separation allowed between the impellers, mixing efficiency can actually be lower with multiple impellers than in single-impeller systems.

### 8.12.2 Feed Points

Severe mixing problems can occur in industrial-scale fermenters when material is fed into the vessel during operation. Concentrated acid or alkali and antifoam agents are often pumped automatically into the broth for pH and foam control; fermenters operated with continuous flow or in fed-batch mode also have fresh medium and nutrients added during the culture. If mixing and bulk distribution are slow, very high local concentrations of added material develop near the feed point. This problem has been observed in many types of culture but is particularly acute during large-scale production of single-cell protein from methanol. Because high levels of methanol are toxic to cells, biomass yields decrease significantly when mixing of feed material into the broth is slow. Such problems can be alleviated by installing multiple injection points to aid the distribution of substrate throughout the vessel. It is much less expensive to do this than to increase the stirrer speed and power input.

Location of the feed point (or feed points) is also important. In most commercial operations, material is fed into bioreactors using a single inlet delivering to the top surface of the liquid. However, mixing can be improved substantially by feeding directly into the impeller zone. This ensures rapid distribution and dispersion as convective currents and turbulence are strongest in this region. In many respects, use of surface-entry feeding represents the worst choice of feed-point location; as illustrated in [Figures 8.14 and 8.27](#), fluid velocities in the upper reaches of stirred vessels can be very weak. Under these conditions, flow may be virtually stagnant in the regions where feeding is taking place, resulting in very poor rates of blending.

## 8.13 MULTIPLE IMPELLERS

Typical bioreactors used for aerobic fermentations do not conform to the standard configuration for stirred tanks illustrated in [Figure 8.1](#), where the liquid height is approximately equal to the tank diameter. Instead, aerobic cultures are carried out in tall vessels

with liquid heights 2 to 5 times the tank diameter, an aspect ratio of 3:1 being common. The reasons for using this geometry are that relatively high hydrostatic pressures are produced in tall vessels filled with liquid, thus increasing the solubility of oxygen, while rising air bubbles have longer contact time with the liquid, thus improving oxygen transfer from the gas phase.

Mixing in tall fermenters is carried out using more than one impeller mounted on the stirrer shaft. Each impeller generates its own circulation currents, but interaction between the fluid streams from different impellers can produce very complex flow patterns. An important parameter affecting the performance of multiple impellers is the spacing between them.

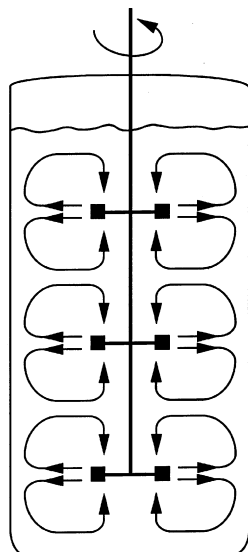
### 8.13.1 Multiple Rushton Turbines without Gassing

Because Rushton turbines have been the standard impeller in the bioprocessing industry for many years, the agitation system in many fermentation vessels consists of multiple Rushton turbines. In low-viscosity fluids, if Rushton turbines are spaced adequately apart, they each produce a radial discharge stream and generate independent large-scale circulation loops as illustrated in [Figure 8.37](#). In this case, a vessel equipped with three Rushton turbines is mixed as if three separate stirred tanks were stacked one on top of the other. Under these conditions without gassing, the power required by multiple impellers can be estimated using the following equation:

$$(P)_n = n (P)_1 \quad (8.30)$$

where  $(P)_n$  is the power required by  $n$  impellers and  $(P)_1$  is the power required by a single impeller. The minimum spacing between the impellers for the flow pattern of [Figure 8.37](#)

**FIGURE 8.37** Independent circulation loops generated by multiple Rushton turbines in a tall fermenter when the spacing between the impellers is relatively large.



to occur, and for Eq. (8.30) to be valid, is not well defined, being reported variously as one to three impeller diameters or one tank diameter [37]. Equation (8.30) indicates that, at this spacing, each impeller draws the same power as if it were operating alone.

An important drawback associated with operation of multiple Rushton turbines is compartmentation of the fluid. As indicated in Figure 8.37, the radial flow pattern generated by Rushton turbines creates separate circulation currents above and below each impeller, providing little opportunity for interaction between the fluid streams emanating from different impellers. The resulting segregation creates a strong barrier to axial flow and top-to-bottom mixing of the contents of the tank over the entire height of the vessel. As a consequence, at a fixed stirrer speed, the overall rate of mixing is lower with multiple Rushton turbines than in a standard single-impeller system. In other words, installation of two Rushton impellers in a vessel with liquid height twice the tank diameter does not achieve the same mixing time as one Rushton impeller in liquid with height equal to the tank diameter. This result reflects the slow speed of fluid exchange between the separate circulation loops induced by multiple Rushton turbines compared with the rate of convective flow developed by a single impeller. In multiple impeller systems, *the rate of exchange flow between the fluid compartments generated by each impeller determines the rate of overall mixing in the vessel*. Therefore, improving the exchange between compartments has a high priority in mixing operations using multiple impellers.

When material is added to fermenters with multiple Rushton turbines, the location of the feed point has a significant effect on mixing time. This is illustrated in Figure 8.38, in which mixing time is plotted as a function of the height of the injection point in a vessel stirred with dual Rushton turbines. In this experiment, the clearance between the impellers was two times the impeller diameter or one tank diameter. The mixing time was lowest when the tracer was injected at the height where the circulation loops from the upper and lower impellers came together. Using this strategy, the barriers to mixing between the circulation loops were minimised as tracer became available to both impellers relatively quickly. The mixing time under these conditions was less than half that when material

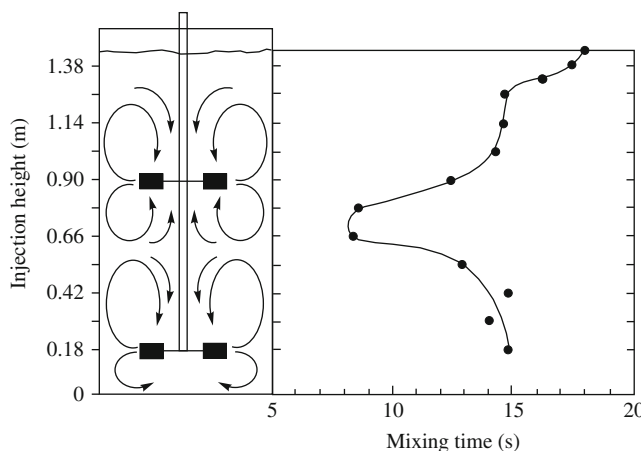


**FIGURE 8.38** Variation in mixing time with height of the tracer injection point for dual Rushton turbines with clearance between the impellers equal to the tank diameter.

From D.G. Cronin, A.W. Nienow, and G.W. Moody, 1994, *An experimental study of mixing in a proto-fermenter agitated by dual Rushton turbines*. Trans. IChemE 72C, 35–40.

was fed to the top surface of the liquid. If more than two impellers are present, similar advantage could be obtained by injecting feed material separately into each impeller zone.

Impeller spacings other than those giving the flow conditions illustrated in Figure 8.37 have also been tested [38]. If the impellers are moved further apart, the chances of material being exchanged between the circulation loops is reduced further, resulting in poorer overall mixing. On the other hand, if the impellers are moved closer together, the circulation loops from each impeller impinge on each other, allowing better fluid interchange. However, depending on the liquid height and the position of the impellers within the tank, placing impellers close together may leave large volumes of liquid in the upper or lower regions of the vessel less well mixed. Therefore, although inter-impeller mixing is improved, overall mixing is reduced. Additional impellers could be installed to overcome this problem but this would require a substantial increase in the total power input to the system.

### 8.13.2 Other Impeller Combinations without Gassing

Various combinations of impellers, including Rushton turbines, curved-blade disc turbines, propellers, and pitched-blade and hydrofoil impellers in both downward-pumping and upward-pumping modes, have been tested for multiple-impeller mixing. Combining radial- and axial-flow impellers, or combining different axial-flow turbines, significantly reduces fluid compartmentation and enhances mixing compared with multiple Rushton turbines. However, the flow patterns generated can be complex and show strong sensitivity to impeller geometry, diameter, and clearance.

A typical mean velocity vector plot for a dual-impeller system comprising a Rushton turbine in the lower position and a downward-pumping pitched-blade turbine above is shown in Figure 8.39. The upper impeller generates strong downward flow that enters the lower impeller axially from the top. The lower Rushton turbine generates an outward

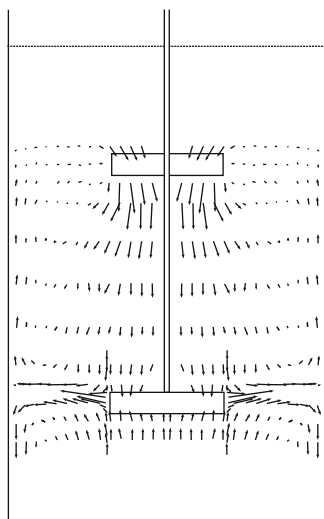


**FIGURE 8.39** Mean velocity vector plot for a dual-impeller combination of a Rushton turbine in the lower position and a downward-pumping pitched-blade turbine above. The velocities were measured using laser Doppler velocimetry.

From V.P. Mishra and J.B. Joshi, 1994, *Flow generated by a disc turbine. Part IV: Multiple impellers*. Trans. IChemE 72A, 657–668.

radial jet, which divides into two streams near the wall. The fluid flowing downwards at the wall forms a large-scale circulation loop below the Rushton impeller, while the fluid flowing upwards joins the major circulation current generated by the pitched-blade turbine. In this way, in contrast to the independent circulation loops developed by multiple Rushton turbines illustrated in [Figure 8.37](#), the radial-flow–axial-flow combination in [Figure 8.39](#) allows a greater degree of interaction between the fluid currents originating from each impeller. Only two major fluid compartments are generated, in contrast to the four separate circulation loops (i.e., one above and one below each impeller) that would be created with dual Rushton turbines. Generally, the smaller the number of separate large-scale flow loops in the vessel, the better is the mixing.

As discussed in [Section 8.10](#), for single impellers under turbulent flow conditions, the mixing time  $t_m$  for a given power input is independent of impeller type. Therefore, [Eqs. \(8.22\)](#) and [\(8.24\)](#) can be applied irrespective of the impeller design. In contrast, in multiple impeller systems, the mixing time depends strongly on the type (or types) of impeller used. This is because the extent of interaction between the flow currents generated by each impeller, which has a significant effect on overall mixing, varies with impeller design.

For operation without gassing and with individual impellers spaced at least one impeller diameter apart, [Eq. \(8.30\)](#) provides a reasonable basis for estimating the power required by combinations of radial- and axial-flow impellers or multiple axial-flow turbines [\[39, 40\]](#). The total power for the multiple impeller system is approximately equal to the sum of the individual power requirements for each impeller.

### 8.13.3 Multiple-Phase Operation

When gassing is required in vessels with multiple impellers, Rushton or curved-blade disc turbines are often used in the lowest position closest to the sparger because of their superior ability to handle gas compared with axial-flow turbines. Combining hydrofoil or pitched-blade impellers above a Rushton turbine is very effective in aerated systems: the lower impeller breaks up the gas flow while the upper, high-flow impeller/s distribute the dispersed gas throughout the tank.

With gassing, the power relationship for multiple impellers is not as simple as that in [Eq. \(8.30\)](#). The main reason is that the power required by the individual impellers may be affected by the presence of gas, but each impeller is not affected to the same extent. At the lowest impeller, the formation of ventilated cavities at the impeller blades reduces the power drawn as described in [Section 8.5.3](#). However, as the quantity of gas passing through the upper impellers is much smaller than that handled by the lowest impeller, the reduction in power at the upper impellers is less significant. The effect of gassing on the power required by the upper impellers depends on the distance of the impeller from the sparger and the level of gas recirculation in the system. Although the lower impeller can be flooded if the gas flow rate is too high relative to the stirrer speed, the upper impellers are rarely flooded and continue to pump liquid effectively.

Solids suspension in multiple impeller systems has been studied comparatively little. In general, irrespective of the liquid height, there appears to be no advantage associated with

using more than one impeller to suspend solids, with respect to either the stirrer speed or power required. At the same time, however, the use of multiple impellers may improve the uniformity of particle concentration throughout the tank [3, 41].

## 8.14 RETROFITTING

It is sometimes necessary or desirable to change the type of impeller used in existing fermentation vessels. For many years, Rushton turbines with diameter one-third the tank diameter were used almost exclusively for bioprocessing applications, and most fermentation facilities were constructed for operation with this impeller geometry. However, with increasing recognition of the importance of mixing in bioprocesses, and as modern impellers with improved features are being developed, the idea of replacing Rushton turbines with new impellers in retrofitting operations is now being pursued.

An important requirement for retrofitting is that neither the agitator drive nor the drive assembly be modified. This is because the expense associated with replacing the shaft, seals, bearings, gearbox, and possibly also the motor itself adds considerably to the overall cost. Therefore, ideally, retrofitting is carried out so that the power draw and torque in the new stirrer system are the same as for the old stirrer. From Eq. (8.5), maintaining the same power and torque implies that the operating stirrer speed  $N_i$  will also be the same.

For operation in the turbulent regime, we can calculate the size of the new impeller using Eq. (8.9). If the new and old impellers consume the same power, from Eq. (8.9):

$$(N'_P \rho N_i^3 D_i^5)_{\text{new}} = (N'_P \rho N_i^3 D_i^5)_{\text{old}} \quad (8.31)$$

As the liquid density and stirrer speed will be the same:

$$(D_i)_{\text{new}}^5 = \frac{(N'_P)_{\text{old}}}{(N'_P)_{\text{new}}} (D_i)_{\text{old}}^5 \quad (8.32)$$

or

$$(D_i)_{\text{new}} = \left( \frac{(N'_P)_{\text{old}}}{(N'_P)_{\text{new}}} \right)^{1/5} (D_i)_{\text{old}} \quad (8.33)$$

Because Rushton turbines have a relatively high turbulent power number  $N'_P$ , if a Rushton turbine is replaced with a low- $N'_P$  impeller such as a hydrofoil or curved-blade disc turbine, Eq. (8.33) indicates that the diameter of the new impeller will be larger than the old. This has implications especially for improved gas handling and dispersion, as discussed in Section 8.4.1 (With Gassing subsection). Additional benefits may also apply: for example, if a curved-blade disc turbine is chosen as the replacement impeller, the loss of power with aeration will be much smaller compared with a Rushton turbine, thus allowing improved rates of oxygen transfer. In multiple impeller systems, replacing upper Rushton turbines with larger-diameter upward- or downward-pumping axial-flow turbines significantly reduces fluid compartmentation and enhances bulk mixing.

While there are advantages associated with retrofitting, there are also potential difficulties. Because of the different directions of fluid discharge from radial- and axial-flow impellers, different stresses are exerted by these types of impeller on the stirrer shaft, gear drive, and tank. The vessel and stirrer assembly must be able to withstand any change in external load after retrofitting. Mechanical as well as hydrodynamic instabilities, including increased vessel vibration, may occur in gassed systems after retrofitting of downward-pumping axial-flow impellers [42]; these problems are largely absent with Rushton turbines. Other factors may also affect retrofitting of larger-diameter impellers: for example, the presence of cooling coils and other fittings inside the vessel could limit the extent to which the impeller size can be increased, or the stirrer assembly may not be capable of supporting the increased impeller weight.

## 8.15 EFFECT OF RHEOLOGICAL PROPERTIES ON MIXING

As discussed in Sections 7.7 and 7.8, many fermentation broths have high viscosity or exhibit non-Newtonian flow behaviour. These properties have a profound influence on mixing, making it more difficult to achieve small mixing times and homogeneous broth composition. The principal deleterious effects of high fluid viscosity and non-Newtonian rheology are reduced turbulence and the formation of stagnant zones in the vessel.

For effective mixing, flow must be turbulent. As described in [Section 8.9](#), turbulence is responsible for dispersing material at the scale of the smallest eddies. The existence of turbulence is indicated by the value of the impeller Reynolds number  $Re_i$ . Turbulence is damped at  $Re_i$  below about  $10^4$  for remote-clearance impellers; as a consequence, mixing times increase significantly as shown in [Figure 8.36](#).  $Re_i$  as defined in Eq. (7.2) is inversely proportional to viscosity. Accordingly, nonturbulent flow and poor mixing are likely to occur during agitation of highly viscous fluids. Increasing the power input is an obvious solution; however, raising the power sufficiently to achieve turbulence is often impractical.

Most non-Newtonian fluids in bioprocessing are pseudoplastic. Because the apparent viscosity of these fluids depends on the shear rate, their rheological behaviour varies with the shear conditions in the fermenter. Metzner and Otto [43] proposed that the average shear rate  $\dot{\gamma}_{av}$  in a stirred vessel is a linear function of the stirrer speed  $N_i$ :

$$\dot{\gamma}_{av} = k N_i \quad (8.34)$$

where  $k$  is a constant dependent on the type of impeller. Experimentally determined values of  $k$  are listed in [Table 8.5](#). The validity of [Eq. \(8.34\)](#) was established in studies by Metzner et al. [44]. However, like other properties such as fluid velocity and turbulence kinetic energy, the shear rate in stirred vessels is far from uniform, being strongly dependent on distance from the impeller. [Figure 8.40](#) shows estimated values of the shear rate in a pseudoplastic fluid as a function of radial distance from the tip of a Rushton turbine. The maximum shear rate close to the impeller is much higher than the average calculated using [Eq. \(8.34\)](#).

Pseudoplastic fluids are shear-thinning; that is, their apparent viscosity decreases with increasing shear. Accordingly, in stirred vessels, pseudoplastic fluids have relatively low

TABLE 8.5 Observed Values of  $k$  in Eq. (8.34)

| Impeller type   | $k$   |
|-----------------|-------|
| Rushton turbine | 10–13 |
| Propeller       | 10    |
| Anchor          | 20–25 |
| Helical ribbon  | 30    |

From S. Nagata, 1975, Mixing: Principles and Applications, Kodansha, Tokyo.

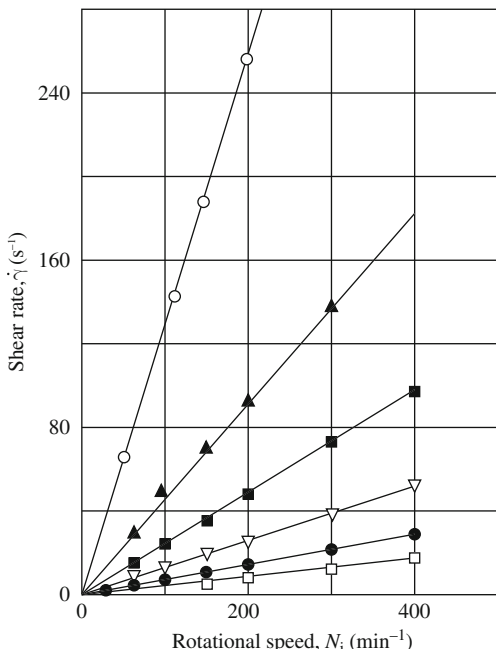
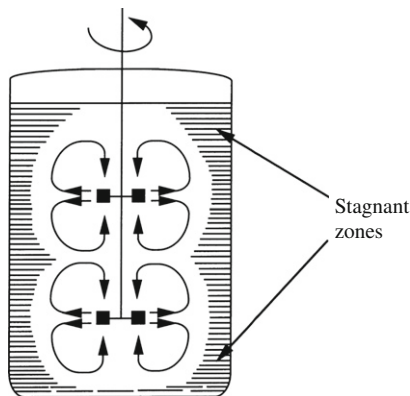


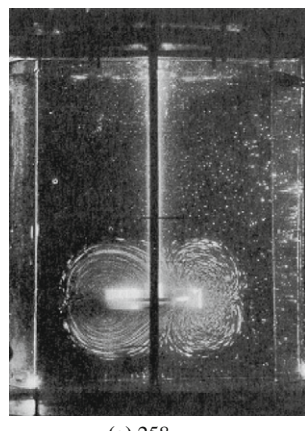
FIGURE 8.40 Shear rates in a pseudoplastic fluid as a function of the stirrer speed and radial distance from the impeller: (○) impeller tip; (▲) 0.10 in.; (■) 0.20 in.; (▽) 0.34 in.; (●) 0.50 in.; (□) 1.00 in.

From A.B. Metzner and J.S. Taylor, 1960, Flow patterns in agitated vessels. AIChE J. 6, 109–114.

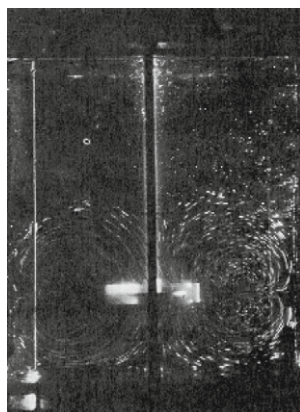
apparent viscosity in the high-shear zone near the impeller, and relatively high apparent viscosity away from the impeller. As a result, flow patterns similar to that shown in Figure 8.41 can develop. Highly shear-thinning fluids with flow behaviour index  $n$  (Section 7.5.1) less than 0.2 to 0.3 form *caverns* when subjected to agitation. Caverns are circulating pools of fluid surrounding the impeller; outside the caverns, the bulk liquid scarcely moves at all. Caverns also develop in liquids that exhibit a yield stress (Section 7.5.1); in this case, fluid remains stagnant in regions away from the impeller where the yield stress is not exceeded. Mixing inside caverns is intense, but there is very little exchange of material between the cavern and the rest of the tank. The effect of stirrer speed on cavern size is shown in Figure 8.42. Although the cavern expands as a proportion of the tank volume with increasing stirrer speed, dead zones persist in the peripheral



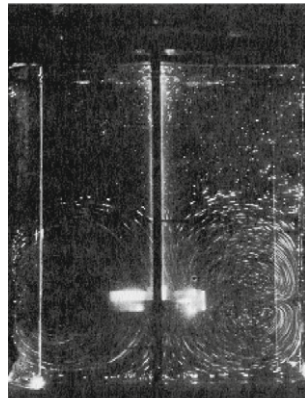
**FIGURE 8.41** Mixing pattern for pseudoplastic fluid in a stirred fermenter.



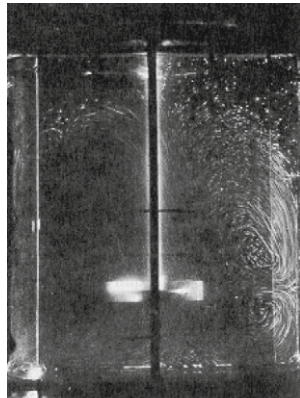
(a) 258 rpm



(b) 468 rpm



(c) 600 rpm



(d) 1020 rpm

**FIGURE 8.42** Effect of stirrer speed on cavern size in non-Newtonian, shear-thinning fluid with a yield stress.

From J. Solomon, T.P. Elson, A.W. Nienow, and G.C. Pace, 1981, Cavern sizes in agitated fluids with a yield stress. Chem. Eng. Commun. 11, 143–164. Reproduced with permission from Taylor & Francis.

regions of the vessel even with vigorous agitation and high power input. Therefore, in fermenters containing highly non-Newtonian broths (e.g., for production of biological gums such as xanthan) stagnant zones are very likely to develop in regions of the vessel away from the impeller caverns.

The effects of local fluid thinning in pseudoplastic fluids can be countered by modifying the geometry of the system and/or the impeller design. The use of multiple impellers, even when the liquid height is no greater than the tank diameter, improves the mixing of pseudoplastic fluids significantly. The combination of a Rushton turbine in the lower position and downward-pumping pitched-blade turbines above is particularly effective. Because the size of the caverns increases with impeller diameter, large impellers with diameters greater than one-half the tank diameter are also recommended. Different impeller designs that sweep the entire volume of the vessel may also be beneficial. As discussed in [Section 8.4](#), the most common impellers used for viscous mixing are gate, anchor, and helical stirrers mounted with small clearance between the impeller and tank wall. However, application of these impellers in fermenters is only possible when the culture oxygen demand is low. Although small-clearance impellers operating at relatively slow speed give superior bulk mixing in viscous fluids, high-shear systems with high-speed, remote-clearance impellers are preferable for breaking up gas bubbles and promoting oxygen transfer to the liquid.

## 8.16 ROLE OF SHEAR IN STIRRED FERMENTERS

As outlined in [Section 7.2.2](#), the development of shear stresses in fluids is related to the presence of velocity gradients. In turbulent flow, unsteady velocity components associated with eddies give rise to additional fluctuating velocity gradients that are superimposed on the mean flow. As a consequence, turbulent shear stresses are much greater than those developed in laminar flow ([Section 7.9.2](#), Reynolds Stresses subsection). Turbulent shear stress also varies considerably with time and position in the fluid.

Mixing in bioreactors used for aerobic cell culture must provide the shear conditions necessary to disperse gas bubbles and, if appropriate, break up liquid droplets or cell flocs. The dispersion of gas bubbles by impellers involves a balance between opposing forces. The interaction of bubbles with turbulent velocity fluctuations in the fluid causes the bubbles to stretch and deform. Bubble break-up occurs if the induced stresses exceed the stabilising forces due to surface tension at the gas–liquid interface, which tend to restore the bubble to its spherical shape. For droplets, the droplet viscosity is an additional stabilising influence opposing break-up. In the case of solid material such as cells or aggregates, break-up occurs if the stresses induced by the turbulent velocity gradients are greater than the mechanical strength of the particles.

Whereas bubble break-up is required in fermenters to facilitate oxygen transfer, disruption of individual cells is undesirable. As indicated in [Table 8.6](#), different cell types have different susceptibilities to damage in the bioreactor environment. This susceptibility is usually referred to as *shear sensitivity*, although the damage observed may not arise necessarily from the effects of fluid velocity gradients. In this context, the term ‘shear’ is used

TABLE 8.6 Cell Shear Sensitivity

| Cell type                     | Size                 | Shear sensitivity |
|-------------------------------|----------------------|-------------------|
| Microbial cells               | 1–10 $\mu\text{m}$   | Low               |
| Microbial pellets/clumps      | Up to 1 cm           | Moderate          |
| Plant cells                   | 100 $\mu\text{m}$    | Moderate/high     |
| Plant cell aggregates         | Up to 1–2 cm         | High              |
| Animal cells                  | 20 $\mu\text{m}$     | High              |
| Animal cells on microcarriers | 80–200 $\mu\text{m}$ | Very high         |

imprecisely to mean any mechanism dependent on the hydrodynamic conditions in the vessel that results in cell damage.

Because of their relatively small size, bacteria and yeast are considered generally not to be shear sensitive. The main effect of agitation on filamentous fungi and actinomycetes is a change in morphology between pelleted and dispersed forms; the mean size of cell clumps also varies with hydrodynamic conditions. Insect, mammalian, and plant cells are considered to be particularly sensitive to hydrodynamic forces. Bioreactors used for culture of these cells must take this sensitivity into account while still providing adequate mixing and oxygen transfer. At the present time, the effects of hydrodynamic forces on cells are not understood completely. Cell disruption is an obvious outcome; however more subtle *sublytic effects* such as slower growth or product synthesis, denaturation of extracellular proteins, and thickening of the cell walls may also occur. In some cases, cellular metabolism is stimulated by exposure to hydrodynamic forces. Because there are many gaps in our knowledge of how cells are affected, it is not possible in most cases to predict with confidence what bioreactor operating conditions will or will not damage shear-sensitive organisms. Some of the findings from research into various culture systems, and some of the mechanisms postulated to explain cell damage in bioreactors, are outlined next.

### 8.16.1 Studies with Animal Cell Cultures

Studies of cell damage in fermenters have been carried out mostly with animal cells. As animal cells lack a protective cell wall, cell injury and loss are significant problems in large-scale culture. Some types of animal cell such as insect, hybridoma, and blood cells grow readily when freely suspended in liquid medium. However, many transformed animal cell lines are *anchorage dependent*: this means that the cells must be attached to a solid surface for survival. In bioreactors, the surface area required for cell attachment is often provided by *microcarrier beads*, which are plastic or polymer beads of diameter 80 to 200  $\mu\text{m}$ . As shown in Figure 8.43, the animal cells cover the surface of the beads, which are then suspended in nutrient medium. Many benefits are associated with the use of microcarriers; however, a disadvantage is that the cells cannot change position or rotate

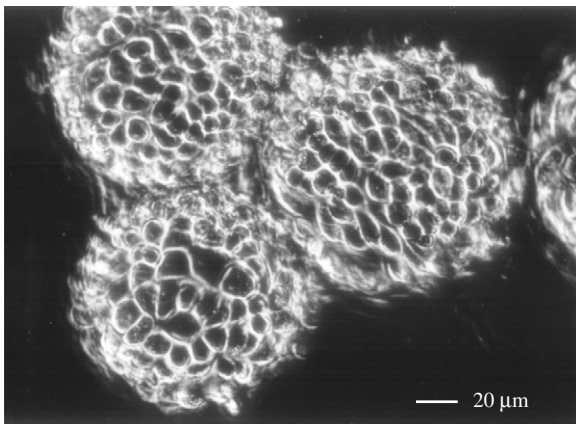


**FIGURE 8.43** Chinese hamster ovary (CHO) cells attached to microcarrier beads.  
Photograph courtesy of J. Crowley.

easily in response to hydrodynamic forces in the fluid. This makes animal cells on microcarriers particularly susceptible to shear damage.

Several mechanisms have been postulated to cause cell damage in bioreactors:

- Interaction between cells and turbulent eddies
- Collisions between cells or between microcarrier beads, collision of cells with the impeller, and collision of cells with stationary surfaces in the vessel
- Interaction between cells and shear forces in the boundary layers and wakes near solid objects in the reactor, especially the impeller
- Interaction between cells and the mechanical forces associated with formation of bubbles at the sparger and bubble rise through the liquid
- Interaction between cells and bursting bubbles at the liquid surface

Investigation of these effects has so far resulted in only a partial understanding of animal cell damage in bioreactors. Industrial practice in this area is based largely on assumptions and 'rules of thumb' rather than theoretical or scientific principles. For cells attached to microcarrier beads, bead-bead interactions and interactions between the microcarriers and small turbulent eddies are considered most likely to damage cells. However, it has also been established that if the vessel is sparged with air, severe damage of suspended cells can occur during gas bubble burst at the surface of the liquid.

### ***Interaction between Microcarriers and Turbulent Eddies***

Interactions between microcarriers and eddies in turbulent flow have the potential to cause mechanical damage to cells. The intensity of the forces associated with these interactions is dependent on the size of the eddies relative to the microcarrier particles. If the particles are small, they tend to be captured or entrained in the eddies as shown in Figure 8.44(a). As fluid motion within eddies is laminar, if the density of the microcarriers is about the same as the suspending fluid, there is little relative motion of the particles. Accordingly, the velocity difference between the fluid streamlines and the microcarriers is small, except for brief periods of acceleration when the bead enters a new eddy. On

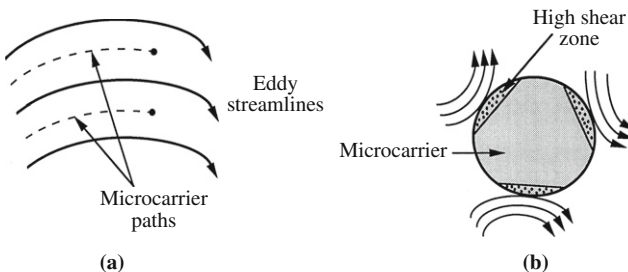


**FIGURE 8.44** Eddy–microcarrier interactions. (a) Microcarriers are captured in large eddies and move within the streamline flow. (b) When several small eddies with opposing rotation interact with the microcarrier simultaneously, high levels of shear develop on the bead surface.

From R.S. Cherry and E.T. Papoutsakis, 1986, *Hydrodynamic effects on cells in agitated tissue culture reactors*. Bioprocess Eng. 1, 29–41.

average, therefore, if the particles are smaller than the eddies, the shear effects of eddy–cell interactions are minimal.

If the stirrer speed is increased and the average eddy size reduced, interactions between eddies and microcarriers can occur in two possible ways. A single eddy that cannot fully engulf the particle may act on part of its surface and cause the particle to rotate in the fluid; this will result in a relatively low level of shear at the surface of the bead. However, much higher shear stresses develop when several eddies with opposing rotation interact with the particle and dissipate their energies on its surface simultaneously, as illustrated in Figure 8.44(b).

Experimental data for cell damage on microcarriers has been correlated by comparing the microcarrier diameter with the eddy size represented by the Kolmogorov scale as defined in Eq. (7.36):

$$\lambda = \left( \frac{\nu^3}{\varepsilon} \right)^{1/4} \quad (7.36)$$

In this equation,  $\lambda$  is the characteristic size of eddies in the dissipative range of the turbulence spectrum,  $\nu$  is the kinematic viscosity of the fluid, and  $\varepsilon$  is the local rate of dissipation of turbulence kinetic energy per unit mass of fluid. For  $\varepsilon$  calculated as the average rate of energy dissipation over the entire tank volume, it has been found that cells on microcarriers suffer detrimental effects when the Kolmogorov scale drops below  $2/3$  to  $1/2$  the diameter of the microcarrier beads [45, 46]. Under these conditions, excessive agitation is considered to generate eddies of small enough size but sufficient energy to cause damage to the cells. The recommendation, therefore, is to operate the bioreactor so that the Kolmogorov scale remains greater than the microcarrier diameter.

As indicated in Eq. (7.36), if the viscosity of the fluid is increased, the size of the smallest eddies also increases. Raising the fluid viscosity should, therefore, reduce cell damage in bioreactors. This effect has been demonstrated by adding thickening agents to animal cell culture medium: Moderate increases in viscosity led to significant reductions in turbulent cell death [46].

Although this approach to predicting turbulent cell damage has been found to apply reasonably well in small-scale vessels, its broader application at larger scales raises several difficulties. Conceptually, the method is based on comparing the size of the microcarriers to the size of the dissipative eddies in the fluid. However, determining the size of the

dissipative eddies can be problematical. As discussed in Section 7.9.2 (Isotropic Turbulence subsection), Kolmogorov's theories about scales of turbulence apply only to isotropic turbulence, which does not exist within the entire volume of bioreactors and may not exist even in the region of most intense turbulence near the impeller. Moreover, Kolmogorov's equation gives only an order-of-magnitude estimate of the size of eddies in the dissipative range. On a practical level, the value of  $\lambda$  estimated using Eq. (7.36) is dependent directly on the volume used to evaluate the rate of turbulence energy dissipation per unit mass of fluid,  $\varepsilon$ . One approach is to assume that the power input by the impeller is dissipated uniformly over the entire tank volume. In this case:

$$\varepsilon = \frac{P}{\rho V_L} \quad (8.35)$$

where  $P$  is the power input,  $\rho$  is the fluid density, and  $V_L$  is the volume of fluid in the vessel. Yet, this is clearly an inaccurate method for estimating  $\varepsilon$ : as illustrated in Figure 8.17, the rate of turbulence kinetic energy dissipation is far from uniformly distributed in stirred tanks, being much greater near the impeller than in the remainder of the fluid. Therefore, use of the total liquid volume to evaluate  $\varepsilon$  is questionable and becomes increasingly so at large scales where rates of energy dissipation in most parts of the tank are very low. Application of Eq. (8.35) gives relatively high values of  $\lambda$  for a given power input, thus potentially underestimating the damaging effects of eddies. In contrast, if we assume that the power is dissipated mostly in the region of intense turbulence around the impeller, an alternative expression for  $\varepsilon$  is [47]:

$$\varepsilon = \frac{P}{\rho D_i^3} \quad (8.36)$$

where  $D_i$  is the impeller diameter and  $D_i^3$  represents the approximate volume near the impeller where most of the energy dissipation occurs. Compared with Eq. (8.35), the calculated value of  $\lambda$  is smaller if Eq. (8.36) is used to estimate  $\varepsilon$ , so that damaging effects will appear more likely. In practice, it is very difficult to know the precise distribution of energy dissipation rates under particular operating conditions, and this affects accurate estimation of  $\varepsilon$  and thus the size of the dissipative eddies.

### **Cell Damage from Bursting Bubbles**

Because of the much smaller size of individual animal cells ( $\sim 20 \mu\text{m}$ ) compared with microcarriers ( $80\text{--}200 \mu\text{m}$ ), individual animal cells in suspension are relatively insensitive to the hydrodynamic forces generated by turbulence unless the agitation intensity is extremely high. However, when liquid containing shear-sensitive cells is sparged with gas, damaging mechanisms other than those associated with turbulence come into play. From research carried out so far, damage of suspended animal cells in bioreactors appears to be caused mainly by bubbles bursting as they disengage from the liquid at the surface of the culture. If the same cells are grown in the absence of air sparging, and the stirrer is prevented from entraining gas from the atmosphere, very high agitation rates can be tolerated without significant cell damage [48, 49].

Figure 8.45 shows the sequence of events associated with rupture of a bubble at a gas–liquid surface. The rising bubble just below the surface pushes liquid at the interface into a hemispherical film cap of thickness 1 to 10  $\mu\text{m}$ . The cap drains under gravity until a critical thickness (typically  $< 0.1 \mu\text{m}$ ) is reached, then ruptures at the thinnest point at the apex. The hole formed expands rapidly in size as the liquid drains away and flows underneath the bubble cavity. When this flow from all sides meets at the bottom of the cavity, if the bubbles are small enough, the resulting fluid pressure creates an upward jet that rises above the surface before disintegrating into droplets and disappearing back into the liquid.

Very high levels of energy dissipation are associated with bubble rupture. The liquid draining back from the film cap reaches velocities of 1 to 50  $\text{m s}^{-1}$ , generating shear forces several orders of magnitude greater than known tolerance levels for animal cells. To make matters worse, in typical animal cell cultures, cells attach to rising bubbles and are retained in the thin film of the liquid cap [50], thus being present at the most damaging location as the bubbles burst. After bubble rupture, the cells are subjected to high liquid velocities within the draining film and, as a consequence, suffer severe damage. Measurements with insect cells have shown that, for each 3.5-mm bubble ruptured at the culture

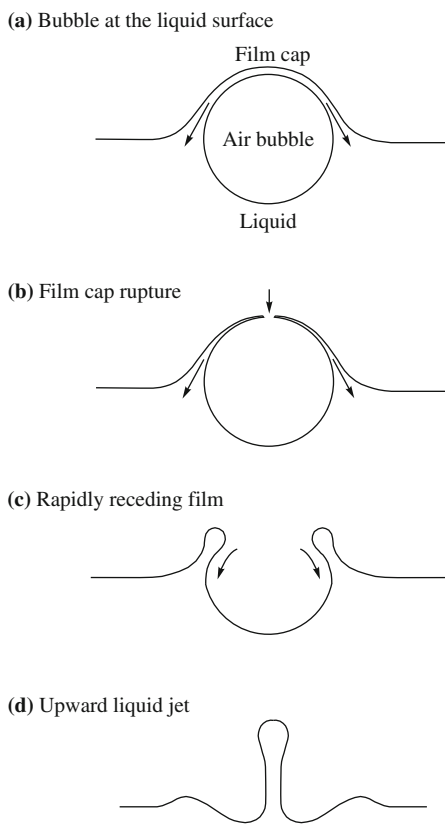


**FIGURE 8.45** Sequence of events when a bubble bursts at a gas–liquid interface.

surface, about  $10^3$  cells are killed from a suspension initially containing approximately  $10^6$  cells  $\text{ml}^{-1}$  [51]. At this rate, most of the cells in an average bioreactor would be killed in only a few hours.

The severe damaging effects of bursting bubbles on suspended animal cells can be attenuated by adding protective agents to the medium. Additives such as Pluronic F-68 lower the gas–liquid interfacial tension significantly and prevent the attachment of cells to bubbles, thus removing cells from the damaging zone at the time of bubble rupture. Stable foam layers on the surface of animal cell cultures have also been found to offer some protection from bursting bubbles [52].

### 8.16.2 Other Studies and Approaches

A common concept in studies of cell damage is that the potential for damage or the extent to which it occurs is related to the rate of dissipation of turbulence kinetic energy in the fluid. For dissipation of a given amount of power, cell damage is likely to depend on whether the power is dissipated within a small volume, in which case the damaging effects will probably be severe, or whether it is dissipated more uniformly within a larger volume at a lower turbulence intensity. The way in which turbulence kinetic energy and rates of energy dissipation are distributed in stirred vessels depends largely on the type of impeller used. Therefore, if the *distribution* of energy dissipation in the tank is important in addition to the overall *rate* of energy dissipated (i.e., the power), we can predict that different degrees of cell damage will occur using different impellers, even if each impeller is dissipating the same amount of power.

The turbulence measurement techniques described in Section 7.9.3 can be used to characterise the performance of impellers in terms of turbulence generation and the distribution of energy dissipation rates. To date, however, mainly because of the practical difficulties associated with evaluating rates of energy dissipation as outlined in Section 7.9.2 (Rate of Dissipation of Turbulence Kinetic Energy subsection) we do not have an unambiguous picture of how different impellers utilise and distribute the power supplied to them. Nevertheless, some success in predicting cell damage has been achieved using empirical correlations derived from our broader understanding of impeller function. In work with fungal hyphae in stirred fermenters, damage measured as a reduction in total hyphal length or cell clump size depended not only on the power input, but also on the size of the impeller, the number of trailing vortices generated per impeller blade, and the frequency with which different impellers circulated fluid through the impeller region [53]. By taking all these factors into account, the extent of damage could be predicted irrespective of the type of impeller used. In these experiments, Rushton turbines were found to be less damaging than pitched-blade turbines, and cell damage increased as the ratio of impeller diameter to tank diameter was reduced. An implication from this work is that the potential for cell damage decreases with scale-up of mixing systems. Although successful with fungal cultures, the applicability of this approach to other cell types remains to be tested.

It is possible that the response of cells to hydrodynamic conditions depends not only on the intensity of the damaging forces generated by turbulent flow, but also on their duration. The cumulative amount of energy dissipated on cells has been used to correlate the

damaging effects of turbulence in fungal and plant cell cultures [54–57]. The cumulative energy dissipated on the cells per unit volume can be calculated as:

$$E = \frac{1}{V} \int P\phi dt \quad (8.37)$$

where  $E$  is the cumulative energy dissipation per unit volume,  $V$  is the culture volume,  $P$  is the power input,  $\phi$  is the fraction of the culture volume occupied by the cells, and  $t$  is time. Under steady-state conditions, for example, during continuous fermentations, Eq. (8.37) reduces to:

$$E = \frac{P\phi\tau}{V} \quad (8.38)$$

where  $\tau$  is the average residence time in the vessel. In experiments with plant cells, several properties have been measured as indicators of sublytic damage, including cell viability, growth, membrane integrity, cell chain length, protein release into the medium, and cell aggregate size. Depending on the species, cell damage was found at cumulative energy dissipation levels of  $10^5$  to  $10^9$  J m<sup>-3</sup>. The implication of this result is that no damage will occur if cumulative energy dissipation is limited to less than these threshold values.

Another view of the damaging effects of hydrodynamic conditions on cells is related to the fine-scale intermittency of turbulence and the fluctuations in instantaneous velocity, energy dissipation rate, and other properties that are characteristic of turbulent flow. Rather than the average properties of turbulent flow causing cell damage, as is assumed in most other approaches to this problem, it is possible that rare, rapid, and very violent events in turbulence are responsible for rupturing cells and aggregates. Although it has been shown theoretically that strong bursts of energy dissipation have the potential to control cell damage in bioreactors [58], practical application to cell cultures has not yet been demonstrated.

## SUMMARY OF CHAPTER 8

---

This chapter covers various topics related to mixing and cell damage in bioreactors. At the end of Chapter 8 you should:

- Be familiar with the broad range of equipment used for mixing in stirred vessels, including different impeller designs, their operating characteristics, and their suitability for particular mixing applications
- Be able to describe *rotational*-, *radial*-, and *axial-flow* patterns in stirred tanks and the types of impeller that induce them
- Be able to describe the different two-phase flow patterns in stirred vessels with gassing, using terms such as *impeller flooding*, *impeller loading*, *complete gas dispersion*, and *gas recirculation*
- Understand the role of *trailing vortices* and *ventilated cavities* in impeller operation
- Know how impeller size, stirrer speed, tank geometry, liquid properties, and gas sparging affect power consumption in stirred vessels

- Be able to determine the stirrer operating conditions for complete solids suspension
- Understand the mechanisms of mixing
- Know what is meant by *mixing time* and how it is measured
- Be able to describe the effects of scale-up on mixing, and options for improving mixing without the input of extra power
- Understand the factors affecting the performance of multiple-impeller systems
- Know the problems associated with mixing highly pseudoplastic or yield-stress fluids
- Understand how cells can be damaged in stirred and aerated fermenters

---

## PROBLEMS

### 8.1. Impeller loading and gas dispersion

An aerated bioreactor of diameter 1.2 m is used for batch culture of *Brevibacterium flavum*. The reactor is stirred using a Rushton turbine of diameter 0.4 m. At the beginning of the culture when the cell concentration and culture oxygen requirements are relatively small, the stirrer operating speed of 110 rpm is just sufficient to completely disperse the air bubbles. Towards the end of the culture when the cell density is high, it is decided to double the volumetric flow rate of air to supply more oxygen.

- (a) Will the impeller be flooded or loaded under these conditions?
- (b) What stirrer speed is needed to achieve complete gas dispersion at the new aeration rate?

### 8.2. Hydrodynamic conditions for animal cell culture

Mouse hybridoma cells are grown in suspension culture in a stirred tank of diameter 1 m and liquid volume 0.8 m<sup>3</sup>. The stirrer speed is 1.5 rps. The vessel has four 10% baffles and is sparged with air at a flow rate of 0.3 vvm (volume of gas per volume of liquid per minute). Pluronic F-68 is added to the medium to protect the cells against the effects of bursting bubbles. The density of the medium is 1000 kg m<sup>-3</sup> and the viscosity is 1.4 cP. The impeller is a Rushton turbine of diameter 0.4 m.

- (a) Is the air dispersed effectively in this system?
- (b) Is the flow turbulent?
- (c) What proportion of the power input is from sparging?

### 8.3. Gas dispersion and power requirements

A stirred, baffled fermenter is used to culture *Streptomyces cinnamonensis* for production of monensin. The tank diameter and liquid height are both 1.1 m. The broth density is 1000 kg m<sup>-3</sup> and the viscosity is 15 cP. The fermenter is mixed using a Rushton turbine of diameter one-half the tank diameter. The air flow rate is 0.66 vvm (volume of gas per volume of liquid per minute).

- (a) What stirrer speed is required for complete gas dispersion?
- (b) What are the power requirements for complete gas dispersion? Assume the power draw with gassing is 50% of that without gassing.

### 8.4. Electrical power required for mixing

Laboratory-scale fermenters are usually mixed using small stirrers with electric motors rated between 100 and 500 W. One such motor is used to drive a 7-cm Rushton turbine in a small reactor containing fluid with the properties of water. The stirrer speed is 900 rpm. Estimate the power requirements for this process. How do you explain the difference

between the amount of electrical power consumed by the motor and the power required by the stirrer?

#### 8.5. Effect of viscosity on power requirements

A cylindrical bioreactor of diameter 3 m has four baffles. A Rushton turbine mounted in the reactor has a diameter of one-third the tank diameter. The liquid height is equal to the tank diameter and the density of the fluid is approximately  $1 \text{ g cm}^{-3}$ . The reactor is used to culture an anaerobic organism that does not require gas sparging. The broth can be assumed Newtonian. As the cells grow, the viscosity of the broth increases.

- (a) The stirrer is operated at a constant speed of 90 rpm. Compare the power requirements when the viscosity is:
- (i) Approximately that of water
  - (ii) 100 times greater than water
  - (iii)  $2 \times 10^5$  times greater than water
- (b) The viscosity reaches a value 1000 times greater than water.
- (i) What stirrer speed is required to achieve turbulence?
  - (ii) Estimate the power required to achieve turbulence.
  - (iii) What power per unit volume is required for turbulence? Is it reasonable to expect to be able to provide this amount of power? Why or why not?

#### 8.6. Power and scale-up

A pilot-scale fermenter of diameter and liquid height 0.5 m is fitted with four baffles of width one-tenth the tank diameter. Stirring is provided using a Scaba 6SRGT curved-blade disc turbine with diameter one-third the tank diameter. The density of the culture broth is  $1000 \text{ kg m}^{-3}$  and the viscosity is 5 cP. Optimum culture conditions are provided in the pilot-scale fermenter when the stirrer speed is 185 rpm. Following completion of the pilot studies, a larger production-scale fermenter is constructed. The large fermenter has a capacity of  $6 \text{ m}^3$ , is geometrically similar to the pilot-scale vessel, and is also equipped with a Scaba 6SRGT impeller of diameter one-third the tank diameter.

- (a) What is the power consumption in the pilot-scale fermenter?
- (b) If the production-scale fermenter is operated so that the power consumed per unit volume is the same as in the pilot-scale vessel, what is the power requirement after scale-up?
- (c) For the conditions in (b), what is the stirrer speed after scale-up?
- (d) If, instead of (b) and (c), the impeller tip speed ( $= \pi N_i D_i$ ) is kept the same in the pilot- and production-scale fermenters, what is the stirrer speed after scale-up?
- (e) For the conditions in (d), what power is required after scale-up?

#### 8.7. Particle suspension and gas dispersion

Bacteria immobilised on particles of gravel are being studied for bioremediation of polychlorinated biphenyls (PCBs). The cells are cultured in an aqueous solution of density  $1000 \text{ kg m}^{-3}$  and viscosity  $0.8 \text{ mPa s}$  in a 400-litre bioreactor of diameter 0.8 m. The reactor is stirred with a Rushton turbine of diameter one-third the tank diameter positioned with an impeller off-bottom clearance of a one-quarter the tank diameter. The average particle diameter is  $250 \mu\text{m}$ , the density of gravel is  $1.9 \text{ g cm}^{-3}$ , and the particle concentration is 15% by weight. The bioreactor is supplied with air at a flow rate of 0.5 vvm (volume of gas

per volume of liquid per minute). If the stirrer speed is set so that the solids are just completely suspended in the solution, will the gas be completely dispersed?

#### 8.8. Impeller flooding and power requirements

You are asked to purchase a new Rushton turbine and drive assembly for a fermenter of diameter 2 m equipped with four 10% baffles and with liquid height equal to the tank diameter. The fermenter is used to culture organisms that require an air flow rate of 1.5 vvm (volume of gas per volume of liquid per minute). The broth density is close to  $1.0 \text{ g cm}^{-3}$  and the viscosity is 0.9 mPa s. Your colleagues have suggested that you design the system for an impeller of diameter one-third the tank diameter, as this is standard company practice. However, after inspecting the vessel internals, you find that an impeller diameter of one-half the tank diameter is also a possibility.

(a) What stirrer speed is required to prevent impeller flooding with  $D_i = 1/3 D_T$ ?

(b) What stirrer speed is required to prevent impeller flooding with  $D_i = 1/2 D_T$ ?

Your supervisor is worried about the operating costs associated with the new impeller, and suggests you use the smaller impeller with  $D_i = 1/3 D_T$  to reduce the factory power bill.

(c) Under the operating conditions determined in (a) and (b) to avoid impeller flooding, which impeller consumes the least power? Assume that the % drop in power with gassing is the same for both impellers. Which of the two impellers would you recommend?

#### 8.9. Stirrer effectiveness with sparging

A baffled cylindrical tank of diameter and liquid height 1.15 m is stirred using a four-blade pitched-blade turbine of diameter 0.36 m operated at 200 rpm. The vessel is sparged with air at a volumetric flow rate of  $0.036 \text{ m}^3 \text{ s}^{-1}$ . Under these conditions, the turbulent power number for the impeller with gassing is about 1.0. The liquid in the tank has a density of  $1 \text{ g cm}^{-3}$  and viscosity 1 cP.

(a) Is the impeller likely to be flooded or loaded? What assumptions are involved in your answer?

(b) What is the rate of energy input by the impeller?

(c) What is the rate of energy input by gassing?

(d) In your opinion, is this stirring system effective for mixing and gas dispersion?

#### 8.10. Cell suspension and power requirements

A fermentation broth contains 40 wt% cells of average dimension  $10 \mu\text{m}$  and density  $1.04 \text{ g cm}^{-3}$ . A marine propeller of diameter 30 cm is used for mixing. The density and viscosity of the medium are approximately the same as water. The fermentation is carried out without gas sparging.

(a) Estimate the stirrer speed required to just completely suspend the cells.

(b) What power is required for cell suspension?

You plan to improve this fermentation process by using a new cell strain immobilised in porous plastic beads of diameter 2 mm and density  $1.75 \text{ g cm}^{-3}$ . The particle concentration required for comparable rates of fermentation is 10% by weight.

(c) How does changing over to the immobilised cell system affect the stirrer speed and power required for particle suspension?

**8.11. Particle suspension and scale-up**

Bacteria attached to particles of clinker are being tested for treatment of industrial waste. In the laboratory, the process is carried out under anaerobic conditions in a stirred bioreactor with liquid height equal to the tank diameter. The system is then scaled up to a geometrically similar vessel of volume 90 times that of the laboratory reactor. The suspending fluid and the particle size, density, and concentration remain the same as in the smaller vessel. The type of impeller is also unchanged, as is the impeller-to-tank diameter ratio.

- (a) How does the stirrer speed required for suspension of the particles change after scale-up?
- (b) Assuming operation in the turbulent regime for both vessels, what effect does scale-up have on:
  - (i) The power required for particle suspension?
  - (ii) The power per unit volume required for particle suspension?

**8.12. Impeller diameter, mixing, and power requirements**

Solids suspension and gas dispersion can both be achieved at lower stirrer speeds if the impeller diameter is increased. However, the power requirements for stirring increase with impeller size. In this exercise, the energy efficiencies of small and large impellers are compared for solids suspension and gas dispersion.

- (a) For ungassed Rushton turbines operating in the turbulent regime, how does the power required for complete solids suspension vary with impeller diameter if all other properties of the system remain unchanged?
- (b) Using the result from (a), compare the power requirements for complete solids suspension using Rushton turbines of diameters one-third and one-half the tank diameter.
- (c) All else being equal, how does the power required for complete gas dispersion by Rushton turbines vary with impeller diameter under turbulent flow conditions?
- (d) Compare the power requirements for complete gas dispersion using Rushton turbines of diameters one-third and one-half the tank diameter.

**8.13. Efficiency of different impellers for solids suspension**

Compared with a Rushton turbine of diameter one-half the tank diameter, what are the power requirements for solids suspension by a downward-pumping, six-blade pitched-blade turbine of the same size?

**8.14. Power and mixing time with aeration**

A cylindrical stirred bioreactor of diameter and liquid height 2 m is equipped with a Rushton turbine of diameter one-third the tank diameter. The bioreactor contains Newtonian culture broth with the same density as water and viscosity 4 cP.

- (a) If the specific power consumption must not exceed  $1.5 \text{ kW m}^{-3}$ , determine the maximum allowable stirrer speed.
- (b) What is the mixing time at the stirrer speed determined in (a)?
- (c) The tank is now aerated. In the presence of gas bubbles, the approximate relationship between the ungassed turbulent power number ( $N'_P$ )<sub>0</sub> and the gassed turbulent power number ( $N'_P$ )<sub>g</sub> is:  $(N'_P)_g = 0.5 (N'_P)_0$ . What maximum stirrer speed is now possible in the sparged reactor?
- (d) What is the mixing time with aeration at the stirrer speed determined in (c)?

**8.15. Scale-up of mixing system**

To ensure turbulent conditions during agitation with a turbine impeller, the Reynolds number must be at least  $10^4$ .

- (a) A laboratory fermenter of diameter and liquid height 15 cm is equipped with a 5-cm-diameter Rushton turbine operated at 800 rpm. If the density of the broth is close to that of water, what is the upper limit for the broth viscosity if turbulence is to be achieved?
- (b) Estimate the mixing time in the laboratory fermenter.
- (c) The fermenter is scaled up so the tank and impeller are 15 times the diameter of the laboratory equipment. The stirrer in the large vessel is operated at the same impeller tip speed ( $= \pi N_i D_i$ ) as in the laboratory apparatus. How does scale-up affect the maximum viscosity allowable for maintenance of turbulent conditions?
- (d) What effect does scale-up have on the mixing time?

**8.16. Effect on mixing of scale-up at constant power per unit volume**

A baffled pilot-scale fermenter with liquid height equal to the vessel diameter is scaled up to a geometrically similar production vessel. The working volume of the production fermenter is 50 times greater than that at the pilot scale. If the agitation system is scaled up using the basis of constant power per unit volume, what effect will scale-up have on the mixing time?

**8.17. Alternative impellers**

*Escherichia coli* cells are cultured in an industrial-scale fermenter for production of supercoiled plasmid DNA used in gene therapy.

- (a) A fermenter of diameter 2.3 m and working volume  $10\text{ m}^3$  is equipped with a Rushton turbine of diameter one-third the tank diameter. The impeller is operated at 60 rpm and the vessel is sparged with air. The density and viscosity of the fermentation fluid are close to those of water, that is,  $1000\text{ kg m}^{-3}$  and 1 cP, respectively. The power with gassing is about 60% of the ungassed power.
  - (i) Calculate the power draw.
  - (ii) Estimate the mixing time.
- (b) To satisfy the burgeoning demand for gene therapy vectors and DNA vaccines, the fermentation factory is being expanded. Two new  $10\text{-m}^3$  fermenters are being designed and constructed. It is decided to investigate the use of different impellers in an effort to reduce the power required but still achieve the same mixing time as that obtained with the Rushton turbine described in (a).
  - (i) Compared with the Rushton turbine of diameter one-third the tank diameter, what power savings can be made using a Rushton turbine of diameter one-half the tank diameter?
  - (ii) Compared with the Rushton turbine of diameter one-third the tank diameter, what power savings can be made using a Lightnin A315 hydrofoil impeller of diameter 0.4 times the tank diameter?
  - (iii) The power with gassing is about 50% of the ungassed power for both the larger Rushton turbine and the A315 hydrofoil. What stirrer speeds are required with these impellers to achieve the same mixing time as that determined in (a) (ii)?

**8.18. Retrofitting**

A 1.8-m-diameter cylindrical fermenter with four baffles of width one-tenth the tank diameter and working volume  $4.6 \text{ m}^3$  is used to produce amylose. The density of the culture broth is  $1000 \text{ kg m}^{-3}$  and the viscosity is 20 cP. The vessel is equipped with a 0.6-m Rushton turbine. Under these conditions, the motor delivers a maximum stirrer speed of 150 rpm. A sales representative from the local impeller manufacturing company has suggested that better culture performance might be achieved by replacing the Rushton turbine with a more modern impeller design. On offer at discounted prices are curved-blade disc turbines and a downward-pumping hydrofoil with characteristics similar to those of the Lightnin A315.

- (a) Estimate the impeller diameters appropriate for retrofitting of the alternative agitators. What assumptions are involved in your answer?
- (b) Compare the mixing times expected after retrofitting each of the alternative impellers with the mixing time delivered by the existing Rushton impeller. Considering mixing time only, do you think that the cost of retrofitting a new impeller is justified? Why or why not?
- (c) Which of the three impellers would you recommend for use in future fermentations:
  - (i) Under nonaerated conditions?
  - (ii) With aeration?

Explain your decision in each case.

**8.19. Retrofitting multiple impellers**

An industrial fermentation vessel with diameter 1.9 m and aspect ratio 3:1 is used for production of leucine by aerobic cultures of *Serratia marcescens*. At present, the fermenter is fitted with three Rushton turbines of diameter one-third the tank diameter. The impellers are spaced far enough apart so there is no significant interaction between their flow currents. The stirrer motor is rated for a maximum stirrer speed of 1.2 rps. It is proposed to carry out an impeller retrofitting operation to improve the performance of the culture. Although the culture is aerobic, the new stirring system will be designed for operation under nonaerated conditions as a safety precaution against accidental blockage of the air supply. It is decided to replace the two upper Rushton turbines with two identical downward-pumping hydrofoil impellers. The turbulent power number for the hydrofoil impellers is around 0.9. If the bottom Rushton impeller is replaced by a curved-blade disc turbine of diameter one-third the tank diameter, what size hydrofoil impellers are required? What assumptions are involved in your answer?

**8.20. Impeller viscometer**

An impeller viscometer is being developed to measure the rheological properties of pseudoplastic fermentation broths. The broth density is  $1000 \text{ kg m}^{-3}$ . Typical rheological parameters for the broth are flow behaviour index  $n = 0.2$  and consistency index  $K = 0.05 \text{ N s}^n \text{ m}^{-2}$ . As outlined in Section 7.6.3, impeller viscometers must be operated under laminar flow conditions.

- (a) If a Rushton turbine of diameter 4 cm is used at speeds between 2.5 and 10 rpm, is the flow laminar?
- (b) What shear rate range does operation with the Rushton turbine provide?
- (c) Approximately what range of shear stresses is induced in the Rushton turbine viscometer?

- (d) If the Rushton turbine is replaced by a close-clearance helical ribbon impeller of diameter 7.5 cm, what maximum stirrer speed can be used under laminar flow conditions?
- (e) If the minimum practical stirrer speed with the helical ribbon impeller is 2.5 rpm, what ranges of shear rates and shear stresses can be investigated using this viscometer? What advantages, if any, does the helical ribbon viscometer offer over the Rushton turbine viscometer?

#### 8.21. Turbulent shear damage

Microcarrier beads 120  $\mu\text{m}$  in diameter are used to culture recombinant CHO cells for production of growth hormone. It is proposed to use a 20-cm Rushton turbine to mix the culture in a 200-litre bioreactor. Oxygen and carbon dioxide are supplied by gas flow through the reactor headspace. The microcarrier suspension has a density of approximately 1010  $\text{kg m}^{-3}$  and a viscosity of  $10^{-3}$  Pa s.

- (a) Assuming that the power input by the stirrer is dissipated uniformly in the vessel, estimate the maximum allowable stirrer speed that avoids turbulent shear damage of the cells.
- (b) How is your estimate affected if the stirrer power is dissipated close to the impeller, within a volume equal to the impeller diameter cubed?

#### 8.22. Avoiding cell damage

Suspended plant cell cultures derived from lemon trees are being used to produce citrus oil for the cosmetic industry. The cells are known to be sensitive to agitation conditions: cell damage occurs and oil production is detrimentally affected if the cumulative energy dissipation level exceeds  $10^5 \text{ J m}^{-3}$ . The cells are grown in a bioreactor with continuous feeding of nutrient medium and withdrawal of culture broth. At the operating flow rate, the average residence time in the bioreactor is 2.9 days. The diameter of the vessel is 0.73 m, the liquid height is equal to the tank diameter, four 10% baffles are fitted, and stirring is carried out using a 25-cm curved-blade disc turbine with six blades. The vessel is aerated but the effect of gassing on the impeller power draw is negligible. At steady state, the cell concentration is 0.24 v/v, the broth density is 1  $\text{g cm}^{-3}$ , and the viscosity is 3.3 mPa s. What is the maximum stirrer speed that can be used without damaging the cells?

## References

- [1] A.W. Nienow, M.M.C.G. Warmoeskerken, J.M. Smith, M. Konno, On the flooding/loading transition and the complete dispersal condition in aerated vessels agitated by a Rushton-turbine, in: Mixing, Proc. 5th Eur. Conf. on Mixing, Würzburg, Germany, 1985, pp. 143–154; BHRA: The Fluid Engineering Centre, Cranfield, U.K.
- [2] W. Bruijn, K. van't Riet, J.M. Smith, Power consumption with aerated Rushton turbines, Trans. IChemE 52 (1974) 88–104.
- [3] C.M. Chapman, A.W. Nienow, M. Cooke, J.C. Middleton, Particle–gas–liquid mixing in stirred vessels. Part III: Three phase mixing, Chem. Eng. Res. Des. 61 (1983) 167–181.
- [4] S.M. Kresta, P.E. Wood, The mean flow field produced by a 45° pitched blade turbine: changes in the circulation pattern due to off bottom clearance, Can. J. Chem. Eng. 71 (1993) 42–53.
- [5] K.J. Bittorf, S.M. Kresta, Active volume of mean circulation for stirred tanks agitated with axial impellers, Chem. Eng. Sci. 55 (2000) 1325–1335.

- [6] J.J. Frijlink, M. Kolijn, J.M. Smith, Suspension of solids with aerated pitched blade turbines, in: Fluid Mixing II, IChemE Symp. Ser. 89, U.K. Institution of Chemical Engineers, 1984, pp. 49–58.
- [7] A.W. Nienow, Gas dispersion performance in fermenter operation, *Chem. Eng. Prog.* 86 (2) (1990) 61–71.
- [8] A.W. Nienow, M. Konno, W. Bujalski, Studies on three-phase mixing: a review and recent results, *Chem. Eng. Res. Des.* 64 (1986) 35–42.
- [9] F. Saito, A.W. Nienow, S. Chatwin, I.P.T. Moore, Power, gas dispersion and homogenisation characteristics of Scaba SRGT and Rushton turbine impellers, *J. Chem. Eng. Japan* 25 (1992) 281–287.
- [10] M. Zlokarnik, H. Judat, Stirring, in: W. Gerhartz (Ed.), Ullmann's Encyclopedia of Industrial Chemistry, fifth ed., vol. B2, VCH, 1988, pp. 25-1–25-33.
- [11] R.L. Bates, P.L. Fondy, R.R. Corpstein, An examination of some geometric parameters of impeller power, *Ind. Eng. Chem. Process Des. Dev.* 2 (1963) 310–314.
- [12] C.M. Chapman, A.W. Nienow, M. Cooke, J.C. Middleton, Particle–gas–liquid mixing in stirred vessels. Part I: Particle–liquid mixing, *Chem. Eng. Res. Des.* 61 (1983) 71–81.
- [13] W. Bujalski, A.W. Nienow, S. Chatwin, M. Cooke, The dependency on scale and material thickness of power numbers of different impeller types, in: Proc. Int. Conf. on Mechanical Agitation, Toulouse, France, ENS Association pour la Promotion du Genie Chimique, 1986, pp. 1-37–1-46.
- [14] J.J. Frijlink, A. Bakker, J.M. Smith, Suspension of solid particles with gassed impellers, *Chem. Eng. Sci.* 45 (1990) 1703–1718.
- [15] S. Ibrahim, A.W. Nienow, Power curves and flow patterns for a range of impellers in Newtonian fluids:  $40 < Re < 5 \times 10^5$ , *Trans. IChemE* 73A (1995) 485–491.
- [16] C.M. McFarlane, X.-M. Zhao, A.W. Nienow, Studies of high solidity ratio hydrofoil impellers for aerated bioreactors. 2. Air–water studies, *Biotechnol. Prog.* 11 (1995) 608–618.
- [17] Z. Jaworski, A.W. Nienow, K.N. Dyster, An LDA study of the turbulent flow field in a baffled vessel agitated by an axial, down-pumping hydrofoil impeller, *Can. J. Chem. Eng.* 74 (1996) 3–15.
- [18] J.H. Rushton, E.W. Costich, H.J. Everett, Power characteristics of mixing impellers, Part I. *Chem. Eng. Prog.* 46 (1950) 395–404.
- [19] J.H. Rushton, E.W. Costich, H.J. Everett, Power characteristics of mixing impellers. Part II, *Chem. Eng. Prog.* 46 (1950) 467–476.
- [20] M.M.C.G. Warmoeskerken, J. Speur, J.M. Smith, Gas–liquid dispersion with pitched blade turbines, *Chem. Eng. Commun.* 25 (1984) 11–29.
- [21] R.L. Bates, P.L. Fondy, J.G. Fenic, Impeller characteristics and power, in: V.W. Uhl, J.B. Gray (Eds.), *Mixing: Theory and Practice*, vol. 1, Academic Press, 1966, pp. 111–178.
- [22] K. Rutherford, S.M.S. Mahmoudi, K.C. Lee, M. Yianneskis, The influence of Rushton impeller blade and disk thickness on the mixing characteristics of stirred vessels, *Trans. IChemE* 74A (1996) 369–378.
- [23] A.W. Nienow, Gas–liquid mixing studies: a comparison of Rushton turbines with some modern impellers, *Trans. IChemE* 74A (1996) 417–423.
- [24] C.M. McFarlane, A.W. Nienow, Studies of high solidity ratio hydrofoil impellers for aerated bioreactors. 3. Fluids of enhanced viscosity and exhibiting coalescence repression, *Biotechnol. Prog.* 12 (1996) 1–8.
- [25] K.N. Dyster, E. Koutsakos, Z. Jaworski, A.W. Nienow, An LDA study of the radial discharge velocities generated by a Rushton turbine: Newtonian fluids,  $Re \geq 5$ , *Trans. IChemE* 71A (1993) 11–23.
- [26] V.P. Mishra, K.N. Dyster, Z. Jaworski, A.W. Nienow, J. McKemmie, A study of an up- and a down-pumping wide blade hydrofoil impeller: Part I. LDA measurements, *Can. J. Chem. Eng.* 76 (1998) 577–588.
- [27] A. Bakker, H.E.A. van den Akker, A computational model for the gas–liquid flow in stirred reactors, *Trans. IChemE* 72A (1994) 594–606.
- [28] Th.N. Zwietering, Suspending of solid particles in liquid by agitators, *Chem. Eng. Sci.* 8 (1958) 244–253.
- [29] A.W. Nienow, The suspension of solid particles, in: N. Harnby, M.F. Edwards, A.W. Nienow (Eds.), *Mixing in the Process Industries*, second ed., Butterworth-Heinemann, 1992, pp. 364–393.
- [30] C.W. Wong, J.P. Wang, S.T. Huang, Investigations of fluid dynamics in mechanically stirred aerated slurry reactors, *Can. J. Chem. Eng.* 65 (1987) 412–419.
- [31] W. Bujalski, M. Konno, A.W. Nienow, Scale-up of 45° pitch blade agitators for gas dispersion and solid suspension, in: *Mixing*, Proc. 6th Eur. Conf. on Mixing, Pavia, Italy, 1988, pp. 389–398, BHRA The Fluid Engineering Centre, Cranfield, U.K.

- [32] S. Ibrahim, A.W. Nienow, Particle suspension in the turbulent regime: the effect of impeller type and impeller/vessel configuration, *Trans. IChemE* 74A (1996) 679–688.
- [33] C.M. Chapman, A.W. Nienow, J.C. Middleton, Particle suspension in a gas sparged Rushton-turbine agitated vessel, *Trans. IChemE* 59 (1981) 134–137.
- [34] M.M.C.G. Warmoeskerken, M.C. van Houwelingen, J.J. Frijlink, J.M. Smith, Role of cavity formation in stirred gas–liquid–solid reactors, *Chem. Eng. Res. Des.* 62 (1984) 197–200.
- [35] S. Ruszkowski, A rational method for measuring blending performance, and comparison of different impeller types, in: *Mixing, Proc. 8th Eur. Conf. on Mixing*, Cambridge, U.K., IChemE Symp. Ser. 136, Institution of Chemical Engineers, 1994, pp. 283–291.
- [36] A.W. Nienow, On impeller circulation and mixing effectiveness in the turbulent flow regime, *Chem. Eng. Sci.* 52 (1997) 2557–2565.
- [37] V. Hudcova, V. Machon, A.W. Nienow, Gas–liquid dispersion with dual Rushton turbine impellers, *Biotechnol. Bioeng.* 34 (1989) 617–628.
- [38] D.G. Cronin, A.W. Nienow, G.W. Moody, An experimental study of mixing in a proto-fermenter agitated by dual Rushton turbines, *Trans. IChemE* 72C (1994) 35–40.
- [39] R. Kuboi, A.W. Nienow, The power drawn by dual impeller systems under gassed and ungassed conditions, in: *Mixing, Proc. 4th Eur. Conf. on Mixing*, Noordwijkerhout, The Netherlands, 1982, pp. 247–261, BHRA Fluid Engineering, Cranfield, U.K.
- [40] D. Hari-Prajitno, V.P. Mishra, K. Takenaka, W. Bujalski, A.W. Nienow, J. McKemmie, Gas–liquid mixing studies with multiple up- and down-pumping hydrofoil impellers: power characteristics and mixing time, *Can. J. Chem. Eng.* 76 (1998) 1056–1068.
- [41] A.T.C. Mak, S. Ruszkowski, Solids suspension with multiple impellers. *Proc. 1993 IChemE Research Event*, Birmingham, U.K., 1993, pp. 756–758, Institution of Chemical Engineers, Rugby, U.K.
- [42] A.W. Nienow, G. Hunt, B.C. Buckland, A fluid dynamic study of the retrofitting of large agitated bioreactors: turbulent flow, *Biotechnol. Bioeng.* 44 (1994) 1177–1185.
- [43] A.B. Metzner, R.E. Otto, Agitation of non-Newtonian fluids, *AIChE J.* 3 (1957) 3–10.
- [44] A.B. Metzner, R.H. Feehs, H. Lopez Ramos, R.E. Otto, J.D. Tuthill, Agitation of viscous Newtonian and non-Newtonian fluids, *AIChE J.* 7 (1961) 3–9.
- [45] M.S. Croughan, J.-F. Hamel, D.I.C. Wang, Hydrodynamic effects on animal cells grown in microcarrier cultures, *Biotechnol. Bioeng.* 29 (1987) 130–141.
- [46] M.S. Croughan, E.S. Sayre, D.I.C. Wang, Viscous reduction of turbulent damage in animal cell culture, *Biotechnol. Bioeng.* 33 (1989) 862–872.
- [47] R.S. Cherry, E.T. Papoutsakis, Physical mechanisms of cell damage in microcarrier cell culture bioreactors, *Biotechnol. Bioeng.* 32 (1988) 1001–1014.
- [48] K.T. Kunas, E.T. Papoutsakis, Damage mechanisms of suspended animal cells in agitated bioreactors with and without bubble entrainment, *Biotechnol. Bioeng.* 36 (1990) 476–483.
- [49] S.K.W. Oh, A.W. Nienow, M. Al-Rubeai, A.N. Emery, The effects of agitation intensity with and without continuous sparging on the growth and antibody production of hybridoma cells, *J. Biotechnol.* 12 (1989) 45–62.
- [50] J.J. Chalmers, F. Bavarian, Microscopic visualization of insect cell–bubble interactions. II. The bubble film and bubble rupture, *Biotechnol. Prog.* 7 (1991) 151–158.
- [51] K. Trinh, M. Garcia-Briones, F. Hink, J.J. Chalmers, Quantification of damage to suspended insect cells as a result of bubble rupture, *Biotechnol. Bioeng.* 43 (1994) 37–45.
- [52] J.D. Michaels, J.E. Nowak, A.K. Mallik, K. Koczo, D.T. Wasan, E.T. Papoutsakis, Interfacial properties of cell culture media with cell-protecting additives, *Biotechnol. Bioeng.* 47 (1995) 420–430.
- [53] P. Jüsten, G.C. Paul, A.W. Nienow, C.R. Thomas, Dependence of mycelial morphology on impeller type and agitation intensity, *Biotechnol. Bioeng.* 52 (1996) 672–684.
- [54] M. Reuß, Influence of mechanical stress on the growth of *Rhizopus nigricans* in stirred bioreactors, *Chem. Eng. Technol.* 11 (1988) 178–187.
- [55] E.H. Dunlop, P.K. Namdev, M.Z. Rosenberg, Effect of fluid shear forces on plant cell suspensions, *Chem. Eng. Sci.* 49 (1994) 2263–2276.
- [56] R. Wongsamuth, P.M. Doran, The filtration properties of *Atropa belladonna* plant cell suspensions; effects of hydrodynamic shear and elevated carbon dioxide levels on culture and filtration parameters, *J. Chem. Tech. Biotechnol.* 69 (1997) 15–26.

- [57] P.F. MacLoughlin, D.M. Malone, J.T. Murtagh, P.M. Kieran, The effects of turbulent jet flows on plant cell suspension cultures, *Biotechnol. Bioeng.* 58 (1998) 595–604.
- [58] J. Bałdyga, J.R. Bourne, Interpretation of turbulent mixing using fractals and multifractals, *Chem. Eng. Sci.* 50 (1995) 381–400.

## Suggestions for Further Reading

### **Mixing Equipment**

Oldshue, J. Y. (1983). *Fluid Mixing Technology*. McGraw-Hill.

### **Power Requirements and Hydrodynamics in Stirred Vessels**

See also references 7 and 10.

- Harnby, N., Edwards, M. F., & Nienow, A. W. (Eds.), (1992). *Mixing in the Process Industries* (2nd ed.). Butterworth-Heinemann.
- McFarlane, C. M., & Nienow, A. W. (1995, 1996). Studies of high solidity ratio hydrofoil impellers for aerated bioreactors: Parts 1–4. *Biotechnol. Prog.*, 11, 601–607, 608–618; 12, 1–8, 9–15.
- Nienow, A. W. (1998). Hydrodynamics of stirred bioreactors. *Appl. Mech. Rev.*, 51, 3–32.
- Tatterson, G. B. (1991). *Fluid Mixing and Gas Dispersion in Agitated Tanks*. McGraw-Hill.
- Tatterson, G. B. (1994). *Scaleup and Design of Industrial Mixing Processes*. McGraw-Hill.

### **Multiple Impeller Systems**

- Gogate, P. R., Beenackers, A.A.C.M., & Pandit, A. B. (2000). Multiple-impeller systems with a special emphasis on bioreactors: a critical review. *Biochem. Eng. J.*, 6, 109–144.

### **Cell Damage in Fermenters**

- Chalmers, J. (2000). Animal cell culture, effects of agitation and aeration on cell adaptation. In R. E. Spier (Ed.), *Encyclopedia of Cell Technology* (vol. 1, pp. 41–51). John Wiley.
- Namdev, P. K., & Dunlop, E. H. (1995). Shear sensitivity of plant cells in suspensions. *Appl. Biochem. Biotechnol.*, 54, 109–131.
- Papoutsakis, E. T. (1991). Fluid-mechanical damage of animal cells in bioreactors. *Trends in Biotechnol.*, 9, 427–437.
- Thomas, C. R., & Zhang, Z. (1998). The effect of hydrodynamics on biological materials. In E. Galindo & O. T. Ramírez (Eds.), *Advances in Bioprocess Engineering II* (pp. 137–170). Kluwer Academic.
- Wu, J. (1995). Mechanisms of animal cell damage associated with gas bubbles and cell protection by medium additives. *J. Biotechnol.*, 43, 81–94.